Cold atmospheric plasma interactions with biofilm cells and the extracellular matrix

Binbin Xia

THE UNIVERSITY OF SYDNEY

School of Chemical and Biomolecular Engineering

The University of Sydney

2025

A thesis submitted in fulfillment of the requirements for the degree of Doctor of Philosophy

Statement of Originality

This is to certify that to the best of my knowledge, the content of this thesis is my own work. This thesis has not been submitted for any degree or other purposes. I certify that the intellectual content of this thesis is the product of my own work and contains no materials previously published or written by another person, except where the due reference has been made in the text.

Binbin Xia

2025

Author Attribution Statement

Chapter 3 of this thesis has been published in the *Environmental Chemical Engineering Journal:*

Binbin Xia, Heema Kumari Nilesh Vyas, Renwu Zhou, Tianqi Zhang, Jungmi Hong, Joanna G Rothwell, Scott A Rice, Dee Carter, Kostya Ken Ostrikov, Patrick J Cullen, Anne Mai-Prochnow. 2023 The importance of superoxide anion for Escherichia coli biofilm removal using plasma-activated water

Candidate contributions: first author, experimental design, performing all of the experiment, analysis, writing and editing the manuscript

Chapter 4 of this thesis has been submitted and accepted in the special edition of *Biofilm Journal*:

Binbin Xia, Heema KN Vyas, Scott A Rice, Timothy P Newsome, Patrick J Cullen, Anne Mai-Prochnow. 2025, Antimicrobial mechanism of in-situ plasma activated water treatment of pathogenic Escherichia coli and Staphylococcus aureus biofilms

Candidate contributions: first and corresponding author, experimental design, performing all of the experiment, analysis, writing and editing the manuscript

	Authorship attribution	Percentage
Chapter 2	Writing, experimental design and performing (Cell viability assay, RONS species measurement, stability testing of PAW)	100%
Chapter 3	Writing, experimental design and performing (Cell viability, IV measurement, RONS measurement, OES, Confocal microscope, scavenger assay)	90%
Chapter 4	Writing, experimental design and performing (Cell viability, biomass assay, EPS assay, confocal microscope, Membrane assay, Intracellular ROS assay)	90%
Chapter 5	Writing, experimental design and performing (Cell viability, protein quantification, SDS-page, LCMS analysis)	90%

In addition to the statements above, in cases where I am not the corresponding author of a published item, permission to include the published material has been granted by the corresponding author.

Binbin Xia

2025

As supervisor for the candidature upon which this thesis is based, I can confirm that the authorship attribution statements above are correct.

Patrick J. Cullen

2025

Gen AI Tools Statement

During the preparation of this thesis, ChatGTP4 was used for the purposes of text enhancement, including sentence structure and paraphrasing in Chapter 1. Where any text was modified by generative AI, the author then reviewed the resulting content for any errors, inaccuracies or biases, and modified it as required. The author takes full responsibility for the submitted thesis and ensures the work is their own and has used generative AI within the parameters of use, see University of Sydney generative AI guide for researchers.

Binbin Xia

2025

Conference presentations

Talk title: **Importance of superoxide anion for Escherichia coli biofilm removal using plasma-activated water: antibiofilm mechanism investigation**

EuroBiofilm Conference, Copenhagen, Denmark, June 2024, 15 minute presentation and 5 minute panel for a Q+A

Talk title: **Physicochemical mechanisms study of plasma-activated water on Escherichia coli biofilm removal**

Biofilm SIG Conference, Sydney, Australia, October 2023, 10 minute presentation and 5 minute panel for a Q+A

Talk title: **Plasma activated water on bacterial biofilm removal**

JAMS student special Conference, Sydney, Australia, July 2023, 10 minute presentation and 5 minute panel for a Q+A

Talk title: **Importance of superoxide anion for Escherichia coli biofilm removal using plasma-activated water**

ISPC25 Conference, Kyoto, Japan, June 2023, 30 minute presentation and 5 minute panel for a Q+A

Poster title: **Superoxide anion radical in plasma activated water**

NZI2022 Net Zero and Circular Economy Conference, Sydney, Australia, October 2022

Poster title: **Plasma activated water on bacterial biofilm removal**

JAMS11 Symposium Conference, Sydney, Australia, September 2022

Poster title: **In situ flow cell plasma activated water generation**

Gaseous Electronics Meeting (GEM)2022 Hybrid Conference, Sydney, Australia, February 2022

Acknowledgements

First and foremost, I would like to express my deepest gratitude to my advisor, Dr. Anne Mai-Prochnow, Prof. Patrick J. Cullen, Dr. Heema Vyas, and A/Prof. Timothy Peter, for their exceptional guidance, unwavering support, and valuable insights throughout my research. Their patience, encouragement, and expertise have been instrumental in shaping this thesis and my academic growth.

I would like to acknowledge the Faculty of Engineering Scholarship and Discovery Project from Australian Research Council for their financial support, which allowed me to conduct my research and complete this thesis.

I am immensely grateful to students, staff, and researchers of the School of Chemical and Biomolecular Engineering whose camaraderie, discussions, and collaboration have made my academic journey both enjoyable and rewarding. Special thanks to Dr. Heema Vyas, A/Prof. Renwu Zhou, Dr.Jungmi Hong for their guide and support with SEM imaging, OES measurement, and COMSOL simulation experiments.

A heartfelt thank you goes to my family, whose love and encouragement have been a constant source of strength. To my spouse Xi Cao and my three cats, Mellow, Brookie, and Cyan, I am truly grateful for your unwavering support and company with me, even during the most challenging times.

Lastly, I would like to thank everyone else who has contributed in any way to the completion of this thesis. Your support, no matter how big or small, has made a significant impact on my work and my journey.

Abstract

Microbial biofilms are a major source of contamination in various environments, such as pipelines, filtration systems, membranes, and food processing facilities. These biofilms represent a significant threat to human health and contribute to substantial costs associated with cleaning and maintenance. Cold plasma, a partially ionized gas, along with plasma-activated water (PAW), has shown potent antimicrobial properties. However, the ideal conditions for generating PAW and the mechanisms by which it exerts its antimicrobial effects remain poorly understood. This study aims to advance PAW as an innovative disinfectant for tackling microbial biofilm contamination. In this work, PAWs were produced using different gases in a plasma bubble spark discharge (BSD) reactor, and their effectiveness in biofilm removal was evaluated under both direct and indirect PAW treatments. The stability of PAWs was assessed through storage experiments. Results revealed that direct PAW treatment was more effective in eradicating biofilms, with further optimization achieved by altering the activated gases used. The physical and chemical properties of various PAWs were systematically optimized, and the underlying antimicrobial mechanisms were explored at both the intracellular and extracellular levels. A key finding was the significant increase in intracellular reactive oxygen species (ROS) levels in *Escherichia coli* (*E. coli*) ATCC 25922 biofilms treated with PAW generated with oxygen gas, where superoxide anion radicals ($\bullet O_2^-$) were identified as crucial contributors to biofilm inactivation. Confocal microscopy analysis confirmed the removal of the majority of biofilm cells from the surface, leaving only a small fraction of dead cells behind. Additionally, the study revealed that PAW effectively targets both the extracellular matrix and bacterial cells in biofilms from both Gram-negative *E. coli* UTI 89 and Gram-positive *Staphylococcus aureus* (*S. aureus*) NCTC 8325 bacteria. A proteomic analysis further elucidated the response of *E. coli* and *S. aureus* biofilms to PAW-induced stress. Overall, the findings presented in this thesis demonstrate the potential of PAW as a novel solution for addressing biofilm-related contamination and its implications for public health improvement.

Table of Contents

List of Figures

List of Tables

List of abbreviations

PAW plasma-activated water

BSD bubble spark discharge

RONS reactive oxygen and nitrogen species

ROS reactive oxygen species

RNS reactive nitrogen species

OES optical emission spectroscopy

PAW-O_2 PAW generated using oxygen

E. coli Escherichia coli

•O_2^- superoxide anion radical

OES optical emission spectra

EPR electron paramagnetic resonance spectrometry

CAP cold atmospheric plasma

OH hydroxyl radical

O atomic oxygen

ONOO- peroxynitrite anion

O_3 ozone

H_2O_2 hydrogen peroxide

NOx nitrogen oxides

pH potential of hydrogen

ORP oxidation-reduction potential

EC electrical conductivity

TSA tryptic soy agar

TSB tryptic soy broth

slm standard liter per minute

Ar argon

N_2 nitrogen

O_2 oxygen

PBS phosphate buffered saline

CFU colony forming units

NO_3- nitrate

NO_2- nitrite

$TiOSO_4$ titanium oxysulphate

DMPO 5,5-dimethylpyrroline-N-oxide

Ex/Em Excitation/Emission

DCFDA 2',7'-dichlorofluorescin diacetate

$\mu \pm \sigma$ mean ± standard deviation

D-value Decimal value

DNA deoxyribonucleic acid

UV ultraviolet

SPS second positive system

FNS first negative system

FPS first positive system

UA uric acid

DCF dichlorofluorescein

V-I voltage and current

NAC N-Acetyl-L-cysteine

SP sodium pyruvate

BOLSIG+ Boltzmann equation solver

E/N electric field

EPS extracellular polymer substances

LB Luria-Bertani

SDS sodium dodecyl sulfate

Con A Concanavalin A

eDNA extracellular DNA

SEM Scanning electron microscopy

CTAB cetyltrimethylammonium bromide

NPN N-phenyl-1-naphthylamine

S. aureus Staphylococcus aureus

CV crystal violet

DiSC3(5) 3,3'-diethylthiadicarbocyanine iodides

DAF-FM 4,5-diaminofluorescein diacetate

Gram+ gram positive

Gram- gram negative

1 Chapter 1 General introduction

1.1 Background of plasma

Plasma is the fourth phase of matter in addition to solid, liquid, and gas. In 1928, it was first introduced as the term of “plasma” by Irving Langmuir to describe an ionized or charged particle (Tonks & Langmuir, 1929). The high energy input can lead to the ionization of gas molecule, and further form ions, photons, free electrons, excited atoms and etc (H. Tresp et al., 2013). When the temperature of the output plasma is <60 °C, plasma is generally referred to as non-thermal plasma or cold plasma (Xiao et al., 2014).

Cold atmospheric pressure plasma (CAPP) is produced by applying an electrical discharge to a gas at room temperature and atmospheric pressure, resulting in the ionization, dissociation, and excitation of the gas's constituent atoms and molecules. This plasma consists of a variety of components, including electrons, both positive and negative ions, free radicals, as well as excited and non-excited atoms and molecules, along with ultraviolet photons. Furthermore, CAPP generates reactive oxygen and nitrogen species (ROS and RNS, or collectively RONS), such as ozone, superoxide, hydrogen peroxide, hydroxyl and peroxyl radicals, singlet oxygen, atomic oxygen, nitric oxide, and nitrogen dioxide (Gilmore et al., 2018).

The reactive oxygen and nitrogen species (RONS) produced by cold atmospheric pressure plasma (CAPP) have demonstrated significant potential in effectively inactivating microorganisms (Brun et al., 2018; Delben et al., 2016). In addition to its cost-effectiveness, rapid treatment time, operational safety, and non-thermal nature, CAPP is regarded as an environmentally friendly antimicrobial method. It also offers the ability to enhance the microbiological quality of food and serves as an efficient means for decontaminating food packaging materials and surfaces that come into contact with food. (López et al., 2019).

1.1.1 Generation of PAW

The exposure of water to the action of plasma leads to the production of the plasma-activated water (PAW). There are two types of ways to form PAW, which including indirect contact of water with

plasma and direct contact of water with plasma (Mai-Prochnow et al., 2021). The principal reactor classes used in the literature are: (1) plasma jets (including atmospheric pressure plasma jets), (2) dielectric barrier discharge (DBD) systems (surface/air DBDs and submerged DBDs), and (3) corona or gliding arc discharges. Reactor geometry, feed gas composition (air, O_2, N_2, He, Ar), power, treatment time, distance/immersion mode (direct submerged discharge/indirect non-contact exposure), and water chemistry (pH, conductivity, dissolved organics) strongly influence the RONS spectrum and PAW properties (pH, ORP, H_2O_2, NO_2^-/NO_3^-, transient radicals) (Wong et al., 2023; Zhou et al., 2020b).

The relevant antimicrobial properties of PAW can persist for long periods of time, which is most likely due to the ability of the RONS generated in the plasma to diffuse and interact with each other or with water molecules, promoting the formation of new chemicals species. It is noteworthy that PAW provides a series of additional advantages when compared to the direct treatment of CAPP, including its straightforward generation and application, as well as its aptitude to be stored. This is leading to an increase of research around the world who are developing innovations related to the application of PAW in the food industry, antimicrobial development, and water treatment (López et al., 2019).

1.1.2 Reactive species in PAW

The antimicrobial activity is mainly attributed to the formation of reactive oxygen and nitrogen species (RONS) (Chen et al., 2018; D. Guo et al., 2021; Thirumdas et al., 2018; Zhao et al., 2022). RONS encompasses both transient species, such as hydroxyl radical (OH), atomic oxygen (O), peroxynitrite anion (ONOO-), and superoxide anion (O_2^-), which have been shown to have a half-life of just a few seconds, or even less than one second, as well as more stable species like ozone (O_3), hydrogen peroxide (H_2O_2), and nitrogen oxides (NO_x), which can persist for several minutes, days, or even years (Zhou et al., 2020b).

While plasma is generally effective, the optimal generating conditions and mode of action are still unclear. Diverse PAW production methods have been explored, including plasma discharge above the water surface, plasma discharges in bubbles dissolved in the water, and direct plasma discharges in

the water (Gao et al., 2022; Kaushik et al., 2018; Zhou et al., 2020b). The design and operating conditions significantly affect the plasma composition (Bălan et al., 2018; Man et al., 2022; Thirumdas et al., 2018; Wang et al., 2018; Zhou et al., 2020b). Not surprisingly, the use of different operating gases leads to the generation of different cocktails of active species, which determine the antimicrobial efficacy (Rathore et al., 2021a; Yahaya et al., 2021). While CAP can be generated using a range of gases or gas mixtures, different gases lead to the formation of unique combinations of reactive species. Air, argon, nitrogen and oxygen are frequently used as working gases (Cullen et al., 2018; Li et al., 2022b; Muhammad et al., 2018; Stapelmann et al., 2008; Wang et al., 2021), and in particular, the addition of oxygen leads to the generation of ROS with strong antibacterial effects (Yahaya et al., 2021).

1.2 Biofilms

Biofilms are a complex 3D-sturcture communities, often consisting of several interacting species. The aggregating biofilms can flourish on either abiotic or biotic surfaces, such as medical devices, bathtubs, unbrushed teeth, and skin tissues. There might be some beneficial microbes biofilm on the gut, however, most of the biofilms are problematic. It was estimated that in Australia the annual cost of pathogens-associated public health burden was in excess of A$2.44 billion (Kolbe et al., 2024).

Contamination of surfaces in contact with biofilm-forming bacteria is a major problem for drinking water supplies, industrial water processing systems, membranes, filters, and food processing stainless-steel units (Dula et al., 2021; Lu et al., 2013; Wan et al., 2021). Biofilms are particularly hard to eradicate because of their higher resistance to antimicrobials and disinfectants compared to planktonic cells (Chakraborty et al., 2021; Costerton et al., 1999). Such contamination can lead to equipment failure, energy losses, product contamination, and environmental pollution, resulting in adverse human health outcomes and significant costs to industries (Cámara et al., 2022). Therefore, it is important to understand biofilm formation mechanisms, and a new decontamination method is

critically needed that can effectively decontaminate resistant biofilms, whilst also avoiding damage to the surface of the treated material or leaving toxic chemical residues.

1.2.1 Biofilms formation

In contrast to the free-living or planktonic bacteria commonly studies in the lab, most prokaryotes in natures settle down in a complex biofilm community. Bacterial communities form when free swimming bacteria reversibly or irreversibly attach to a surface. At high cell densities, many species trigger processes involved in microcolony biofilm formation, including production of extracellular polymer substances (EPS) matrix. The EPS is a sticky mixture of polysaccharides, protein and eDNA that adheres to bacteria to the surface and provides a protection shield from predators and antibiotics. As the biofilm matures, bacteria specialize into performing different tasks within the biofilm. Some individuals focus on reproduction to expand the colony, while others specialize in construction, forming polysaccharides and proteins that make up the EPS matrix. Other bacteria defend the community, enhancing biofilm structure that against competitors with toxins. When the biofilm community needs change, a subset of cells sprouts flagella and disperses from the community to colonize new surfaces.

Biofilm formation including five stages: reversible attachment, irreversible attachment, microcolony adhesion, maturation of biofilm (Figure 1.1): quorum sensing and biofilm biomass formation, and biofilm dispersal due to environmental stress (Toyofuku et al., 2016). Bacteria cells initiate and adherent on the surfaces by some bacterial structures; such as type 1 fimbria and curli(Shineh et al., 2023). The adherent cells start to accumulate through quorum sensing (QS) which is a regulatory system of cell-to-cell communication (Dula et al., 2021). Understanding the genetic factors of biofilm formation is essential for developing strategies to control biofilm-related infections and improve industrial processes such as wastewater treatment and biofilm-based bioremediation.

Reversible attachment

Biofilm formation is a sequential process that begins with the adhesion of cells to surfaces (Saharan et al., 2024). The first contact between planktonic forces (van der Waals, electrostatic and hydrophobic interactions) and by cell appendages (flagella, pili) that mediate surface exploration and initial tethering. At this stage, cells can readily detach and return to the planktonic phase. However, surface sensing mechanisms can trigger regulatory changes that commit cells to a sessile lifestyle (Sauer et al., 2022).

Irreversible attachment

Irreversible attachment follows when adhesins, fimbriae, or secreted polymers form stable bonds with the surface and with neighboring cells, accompanied by transcriptional shits that upregulate matrix components and downregulate motility. Production of early EPS components, such as exopolysaccharides, proteins, and extracellular DNA, to stabilise the attached monolayer and prevents easy detachment, marking a point of no return for many cells (Campoccia et al., 2021; Sauer et al., 2022).

Microcolony formation

Attached cells proliferate and recruit additional cells to form microcolonies which is a three-dimensional cluster. Intercellular signalling (notably QS), metabolic interactions and localized EPS deposition coordinate microcolony architecture. Microcolonies establish nascent channels and heterogeneity in nutrient and oxygen availability, laying the groundwork for larger-scale biofilm structure (Luo et al., 2022; Saharan et al., 2024).

Biofilm Maturation

Once microcolonies are established and the EPS matrix is well developed, the biofilm matures into a three-dimensional architecture. Key features include water channels (for nutrient and waste transport), differentiated microenvironments (e.g., oxygen and nutrient gradients), metabolic heterogeneity, higher biomass and often increased resistance to antimicrobials and environmental stress (Sauer et al.,

2022). A recent study discusses how in *Enterococcus spp.* The maturation stage depends on capsule production, surface adhesins, and QS to maintain biofilm size and stability (Ruhal et al., 2024).

Dispersal/Detachment

Dispersal is the stage by which cells or aggregates leave the biofilm to colonize new sites. It can be active (regulated by genetic programs, enzymatic degradation of EPS, changes in nutrient or oxygen levels, quorum sensing signals) or passive (due to shear or physical disruption). Ma et al. (2023) examines how dispersal contributes not only to colonization of fresh sites but to disease dissemination in hosts. They show that dispersal is not just a simple detachment, but involves population dynamics that affect which subpopulations spread. Also, another work reveals a specific molecular trigger (a toxin-antitoxin system) for dispersal in thermophilic archaea, indicating that dispersal regulation is widespread and can be highly specialized (Lewis et al., 2023). Therefore, dispersal is essential for spread, survival under stress, and rejuvenation of biofilm life cycles.

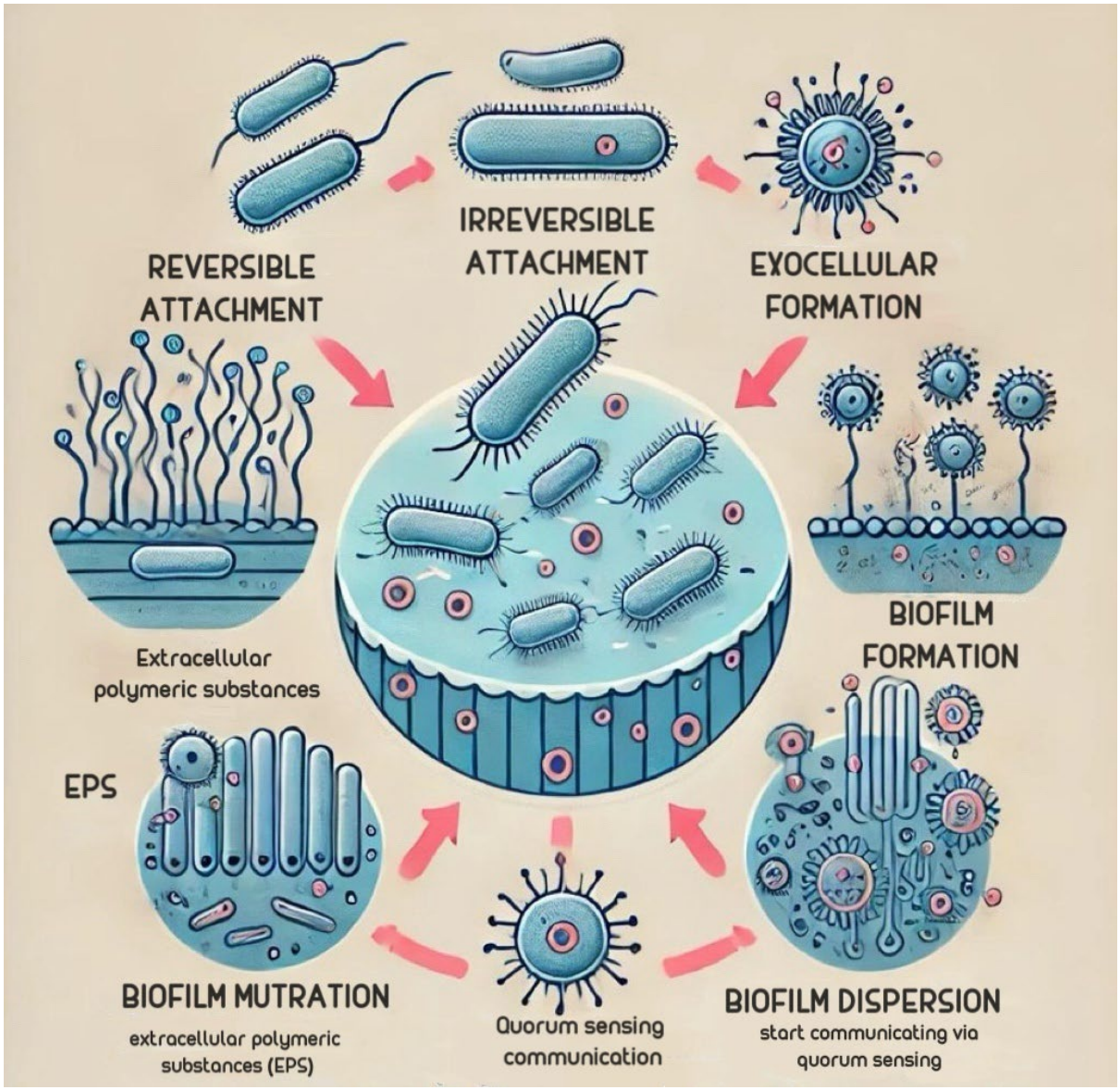

Figure 1.1. The biofilm life cycle

1.2.2 Biofilm EPS matrix

There is no clear high-resolution image of the internal structure of biofilms. It was generally believed that it is consisted of tolerant cells, resistant cells, perister cells, viable but nonculturable cells, matrix exopolysaccharides, extracellular DNA, and functional proteins (Karygianni et al., 2020). McConnell observed a meandering network through the interior of *Escherichia coli* biofilm colony. These conduits were suggested to transport nutrients, oxygen and other resources into the biofilm core, and might be exploited to maneuver antibiotics into the center of the biofilm (McConnell et al., 2016).

Extracellular nucleic acids (eDNA)

eDNA is now recognized as a ubiquitous and multifunctional constituent of the EPS. Far from being a passive residue, eDNA contributes mechanically to matrix cohesion, mediates adhesion to surfaces, binds divalent cations and extracellular proteins, and can act as a scaffold for other EPS polymers (Panlilio & Rice, 2021). In many species, eDNA is released via regulated autolysis, membrane vesicles, or active secretion and is essential during initial attachment and for the structural integrity of mature biofilms, enzymatic degradation of eDNA (e.g., DNase I) frequently weakens biofilm architecture and increases susceptibility to antimicrobials. Beyond mechanical roles, eDNA can act as a source of nucleotides and as a signaling or damage-associated molecular patten (DAMP) influencing community behavior (Sharma & Rajpurohit, 2024).

Polysaccharides

Polysaccharides composited predominately to the biofilm matrix (Flemming & Wingender, 2010). One prominent exopolysaccharide is N-acetylglucosamine polymer found in the biofilms of *E. coli, S. aureus*, and *S. epidermidis* (Nguyen et al., 2020; Wang et al., 2004), with the ability of forming a capsule on the cell surface, serving not only to bind cells to surfaces but also as an adhesin to stabilize the biofilm structure (Flemming & Wingender, 2010; Sharma et al., 2016).

The inhibition of biofilm formation can be achieved by either interference with the QS mechanism, adhesion mechanism, or disruption of EPS. The antimicrobial mechanism of cold plasma has been studied via planktonic *Pseudomonas aeruginosa* (Liu et al., 2022), and *E. coli* (Wang et al., 2023) via planktonic bacteria cells perspective.

Proteins

Proteins are essential for the impenetrable core of antibiotics sneaking into the biofilm. For example, pyocyanin, a type of phenozine which is a group of metabolites expressed as the beginning of *P. aeruginosa* biofilm clumping, was found to encourage bacterial cells to interact. Destroying procyanin using the enzyme PodA made biofilms more vulnerable to antibiotics, but PodA is unstable and synthesized naturally in minute quantities (Costa et al., 2017).

1.2.3 Redox gradients and microenvironmental heterogeneity of biofilms

Biofilms are microscale chemical landscape: steep gradients of oxygen, redox potential, pH and nutrients develop over tens to hundreds of micrometres, creating functionally distinct strata (Jo et al., 2022). Cells in oxic surface layers differ markedly in physiology from anoxic core populations, which drives spatial division of labour (aerobic respiration and fermentation/anaerobic metabolisms), differential gene expression, and phenotypic heterogeneity (persister formation). These gradients determine local metabolic fluxes and modulate EPS composition and function (Sies et al., 2024). Notably, redox stratification also alters susceptibility to oxidant-based disinfectants and shapes electron transfer pathways in electroactive biofilms (Yates et al., 2018).

A growing number of works emphasize the ecological and physiological importance of redox-active metabolites, such as phenazines (e.g., pyocyanin), flavins, quinones and other secondary metabolites (Abdelaziz et al., 2023; Thalhammer & Newman, 2023). Redox-active small molecules (RAMs) can shuttle electrons across redox gradients, enabling cells in hypoxic zones to dispose of reducing equivalents to more oxidised niches or to extracellular acceptors; this electron shuttling facilitates metabolic coupling and can expand the viable habitat within thick biofilms (Ciemniecki & Newman, 2020). RAMs also function as intercellular signals and competitive weapons by modulating biofilms morphology, promoting dispersal or suppression of competitors, and generating localized oxidative stress that affects both producers and surrounding cells (Thalhammer & Newman, 2023).

1.2.4 Beneficial and ecosystem services provided by biofilms

While much attention focuses on deleterious biofilms (infections, biofouling), biofilms perform indispensable ecological and biotechnological roles (Philipp et al., 2024). Environmental biofilms drive nutrient cycling (carbon, nitrogen, sulfur), catalyse biogeochemical transformations, stabilize soils, and support primary colonization on surfaces that seed successional communities (Ünal Turhan et al., 2019). In engineered systems, biofilms are harnessed for wastewater treatment, bioenergy production (microbial fuel cells), bioremediation of organic pollutants and metal recovery (Qureshi, 2009). The above studies emphasize the potential to harness beneficial biofilms for pollutant

degradation, plant growth promotion, and resilient microbial consortia. However, recognition of controlling undesirable spread or gene transfer is needed.

1.3 Current studies of PAW on biofilm inactivation

Recent methodological advances of PAW might vary in different PAW generators. *In-situ* submerged discharges and surfaces DBDs that create PAW with high RONS concentrations rapidly (Rathore et al., 2022). There are also some comparative studies show different RONS profiles and antimicrobial efficacies depending on DBD configuration (Rathore et al., 2021a). Moreover, portable, recirculating PAW reactors and industrial-scale prototypes (plasma jet-based and RF-driven jets) that increase throughput and RONS yield, moving the technology beyond benchtop experiments (Agus et al., 2024). These prototypes often focus on adjustable power, gas flow, and water recirculation to maximize RONS generation while managing energy use. Notably, hybrid approaches such as plasma bubble discharge (BSD) to enhance retention and delivery of reactive species, and combinations with additives (e.g., iodide) to potentiate antimicrobial action (McClenaghan et al., 2025; Tiwari et al., 2025). Such hybrids aim to improve PAW stability and mass transfer into biofilms.

1.3.1 Inactivation kinetics of PAW on bacterial biofilms

Quantitative inactivation results for biofilms vary with microbial species, biofilm age/thickness, surface/material, PAW composition, and exposure protocol (direct PAW contact vs. plasma post-exposure). Several recent experimental reports document multi-log reduction (often 3-7 $\log_{10}$) of culturable cells in model mono-species biofilms (e.g., *E. coli, L, innocua, L. monocytogenes, Salmonella*) after sufficient long PAW exposure (Rothwell et al., 2022; Rothwell et al., 2023; Vyas et al., 2023). A small but growing body of work reports D-values for biofilm cell exposed to PAW; these D-values can differ substantially by species and by which RONS dominate (e.g., superoxide importance highlighted for *E. coli* ATCC25922 biofilms) (Wang et al., 2023; Xia et al., 2023). Moreover, Gram-negative versus Gram-positive differences are commonly observed (differences in outer membrane, EPS composition and biofilm architecture affect susceptibility), and thicker/older

biofilms generally require longer exposures or stronger PAW (higher RONS) to achieve the same log reduction (Mai-Prochnow et al., 2021; Zhao et al., 2021).

1.3.2 Interaction of PAW with biofilms

Contemporary mechanistic work indicates that PAW exerts anti-biofilm action through multiple and complementary pathways, including RONS-mediated oxidative attack, membrane lipid peroxidation & permeability increase, intracellular macromolecular damage, physical dispersal and EPS degradation, and synergistic/indirect effects. Long-lived species in PAW (H_2O_2, NO_2^-/NO_3^-, peroxynitrite precursors) and short-lived radicals (•OH, O_2^-, ONOOH) oxidise EPS components and bacterial biomolecules (Mai-Prochnow et al., 2021; Xia et al., 2023). Oxidation of polysaccharides and proteins in the EPS weakens the matrix, facilitating detachment and improving penetration of antimicrobials (Chen et al., 2017). RONS could also cause damage to cell envelopes (lipid peroxidation, protein oxidation), compromising membrane integrity and leading to leakage, loss of membrane potential and cell death (Wang et al., 2023; Zhao et al., 2025). Oxidative lesions to proteins and nucleic acids, and interferences with metabolic processes, are reported in transcriptomic and biochemical analyses after PAW exposure (Vyas et al., 2025). Beyond killing, PAW can promote detachment/dispersion of biofilm fragments by degrading EPS; this dispersal effect can be beneficial in biofilm removal but may transiently release cells into bulk fluid if not coupled with downstream inactivation (Mai-Prochnow et al., 2021). PAW often acts synergistically with conventional disinfectants, enzymes (EPS-degrading), or phages: EPS weakening increases access for other agents, and combinations can reduce required doses or exposure times (McClenaghan et al., 2025).

1.3.3 Translational studies of PAW and limitations

Researchers are actively investigating the applications of PAW in real-world use, such as food industry sanitation, healthcare (wound care, device decontamination), water/wastewater and membrane cleaning, biofouling, agriculture and postharvest disinfection, and etc (Moreno-Couranjou et al., 2018; Soni et al., 2021; Wang & Salvi, 2021; Zhao et al., 2021). Promising lab and pilot studies investigated PAW as a wash or surface sanitizer to reduce pathogen loads on produce, equipment, and

food contact surfaces (Basiri et al., 2023; Zhao et al., 2021), but scale-up, contact times, and regulatory approvals remain further investigation. PAW and plasma-treated liquids are being tested for wound disinfections and for reducing device biofilms (Abdo et al., 2025; Vyas et al., 2023). An *in-vivo* PAW generation model has shown potent biofilm reduction in model systems, through clinical translation demands safety and biocompatibility data (Zhou et al., 2017). PAW (and enzyme combined with PAW) were examined for pre-treatment and membrane biofouling mitigation. This research indicates that PAW can be integrated into periodic cleaning-in-place (CIP) regimens or as pretreatments step to reduce biofilm formation on membranes (Shah et al., 2024). PAW was investigated for seed treatment, fungal/bacterial suppression on crops, and postharvest wash water (Guo et al., 2022). Pilot results are promising but further exposure protocols and research on the impacts of residue and minimal quality are required.

1.3.4 Research gaps of antibiofilm activity of PAW

The reporting antibiofilm activity of PAW varies from the generation method, RONS concentrations, input gases, pH, and different biofilm models. Therefore, a reproducible comparison study is required to help with developing a standard protocol for PAW generation. Moreover, the quantification of mechanism of antibiofilm activity remained further studied. For example, using scavenger assays, isotopic labelling, and high-resolution transcriptomics/proteomics to quantify the roles of RONS in biofilm matrix degradation and direct bactericidal action that on extracellular protein, eDNA, exopolysaccharides, and bacterial membrane specifically. Removal from single-species, thin biofilms to aged, multispecies, and soiled biofilm models representative of realistic biofilm models materials that applied in food production, water treatment, and clinical devices.

1.4 Research aims and thesis outline

To fill the research gaps mentioned above, this thesis will define the interaction of cold atmospheric plasmas with biofilms, with the aim of biofilm eradication and ultimately offering an environmentally friendly alternative to current detergents and antibiotics.

Bacteria strains selection

In this study, *E. coli* and *S. aureus* were selected as representative bacterial strains commonly used in wastewater treatment research due to their distinct physiological characteristics and taxonomic classification (Anastasi et al., 2012; Waller et al., 2023). *E. coli* is a Gram-negative, rod-shaped facultative anaerobe typically found in the lower intestines of warm-blooded organisms and it serves as a key indicator organism for fecal contamination in environmental water samples. In contrast, *S. aureus* is a Gram-positive and spherical bacterium known for its thick peptidoglycan-rich cell wall and its capacity to form resilient biofilms, which contribute to its resistance against various environmental stressors and antimicrobial treatment. By evaluating the efficacy of PAW treatment against both *E. coli* and *S. aureus,* this study provides a comparative and comprehensive assessment of PAW's antimicrobial potential across Gram-negative and Gram-positive bacteria biofilm in the context of wastewater treatment.

Table 1. Biological sample and PAW condition applied in each chapter.

	Biological sample	**PAW condition**
Chapter 2	24 h-grown *E. coli* ATCC25922	0-10min air gaseous PAW
Chapter 3	48 h-grown *E. coli* ATCC 25922	0-10 min air/N_2/O_2/Argon PAW
Chapter 4	48 h-grown *E. coli* UTI89 and *S. aureus* NCTC8325	0-20 min air PAW
Chapter 5	48 h-grown *E. coli* UTI89 and *S. aureus* NCTC8325	0-20 min air PAW

The research will elucidate the fundamental mechanisms of action for plasma intervention technologies that are sufficiently active to cope with the resistant nature of biofilms, yet are of low

energy, do not adversely affect surface properties and critically leave no residual chemistry. This will be achieved through the following objectives

- Optimize the condition of plasma activated water generation
- Map the structural and biomolecular changes induced by atmospheric plasma within the biofilm architecture.
- Determine the plasma-induced effect on different bacteria biofilm communities
- Determine the cellular responses of plasma-stressed bacteria to the chemically and structurally biofilm

1.5 Reference

Abdelaziz, A. A., Kamer, A. M. A., Al-Monofy, K. B., & Al-Madboly, L. A. (2023). Pseudomonas aeruginosa's greenish-blue pigment pyocyanin: its production and biological activities. *Microbial Cell Factories, 22*(1), 110. https://doi.org/10.1186/s12934-023-02122-1

Abdo, A. I., Nguyen, H. T., Kaul, L. D., Schmitt-John, T., Kopecki, Z., Ogunniyi, A. D., & Richter, K. (2025). Plasma-activated water accelerates wound healing and reduces Staphylococcus aureus infection in vivo. *Biofilm*, 100308. https://doi.org/10.1016/j.bioflm.2025.100308

Agus, R., Avino, F., Ibba, L., Myers, B., Zampieri, L., Martines, E., Howling, A., & Furno, I. (2024). Implementing water recirculation in a novel portable plasma-activated water reactor enhances antimicrobial effect against Escherichia coli. *Chemical Engineering Journal, 486*, 149915. https://doi.org/10.1016/j.cej.2024.149915

Anastasi, E. M., Matthews, B., Stratton, H., & Katouli, M. (2012). Pathogenic Escherichia coli found in sewage treatment plants and environmental waters. *Applied and Environmental Microbiology, 78*(16), 5536-5541. https://doi.org/10.1128/AEM.00657-12

Balan, G. G., Rosca, I., Ursu, E. L., Doroftei, F., Bostanaru, A. C., Hnatiuc, E., Nastasa, V., Sandru, V., Stefanescu, G., Trifan, A., & Mares, M. (2018). Plasma-activated water: a new and effective alternative for duodenoscope reprocessing. *Infect Drug Resist, 11*, 727-733. https://doi.org/10.2147/IDR.S159243

Basiri, N., Zarei, M., Kargar, M., & Kafilzadeh, F. (2023). Effect of plasma-activated water on the biofilm-forming ability of Salmonella enterica serovar Enteritidis and expression of the related genes. *International Journal of Food Microbiology, 406*, 110419. https://doi.org/10.1016/j.ijfoodmicro.2023.110419

Brun, P., Bernabè, G., Marchiori, C., Scarpa, M., Zuin, M., Cavazzana, R., Zaniol, B., & Martines, E. (2018). Antibacterial efficacy and mechanisms of action of low power atmospheric pressure cold plasma: membrane permeability, biofilm penetration and antimicrobial sensitization. *Journal of Applied Microbiology, 125*(2), 398-408. https://doi.org/10.1111/jam.13780

Cámara, M., Green, W., MacPhee, C. E., Rakowska, P. D., Raval, R., Richardson, M. C., Slater-Jefferies, J., Steventon, K., & Webb, J. S. (2022). Economic significance of biofilms: a multidisciplinary and cross-sectoral challenge. *npj Biofilms and Microbiomes, 8*(1), 42. https://doi.org/10.1038/s41522-022-00306-y

Campoccia, D., Montanaro, L., & Arciola, C. R. (2021). Extracellular DNA (eDNA). A Major Ubiquitous Element of the Bacterial Biofilm Architecture. *International journal of molecular sciences, 22*(16), 9100. https://doi.org/10.3390/ijms22169100

Chakraborty, P., Bajeli, S., Kaushal, D., Radotra, B. D., & Kumar, A. (2021). Biofilm formation in the lung contributes to virulence and drug tolerance of Mycobacterium tuberculosis. *Nature communications, 12*(1), 1606. https://doi.org/10.1038/s41467-021-21748-6

Chen, T.-P., Liang, J., & Su, T.-L. (2018). Plasma-activated water: antibacterial activity and artifacts? *Environmental Science and Pollution Research, 25*(27), 26699-26706. https://doi.org/10.1007/s11356-017-9169-0

Chen, T.-P., Su, T.-L., & Liang, J. (2017). Plasma-Activated Solutions for Bacteria and Biofilm Inactivation. *Current Bioactive Compounds, 13*(1), 59-65. https://doi.org/10.2174/1573407212666160609082945

Ciemniecki, J. A., & Newman, D. K. (2020). The potential for redox-active metabolites to enhance or unlock anaerobic survival metabolisms in aerobes. *Journal of bacteriology, 202*(11), 00797-00719. https://doi.org/10.1128/JB.00797-19

Costa, K. C., Glasser, N. R., Conway, S. J., & Newman, D. K. (2017). Pyocyanin degradation by a tautomerizing demethylase inhibits Pseudomonas aeruginosa biofilms. *Science, 355*(6321), 170-173. https://doi.org/10.1126/science.aag3180

Cullen, P. J., Lalor, J., Scally, L., Boehm, D., Milosavljević, V., Bourke, P., & Keener, K. (2018). Translation of plasma technology from the lab to the food industry. *Plasma Processes and Polymers, 15*(2), 1700085. https://doi.org/10.1002/ppap.201700085

Delben, J. A., Zago, C. E., Tyhovych, N., Duarte, S., & Vergani, C. E. (2016). Effect of Atmospheric-Pressure Cold Plasma on Pathogenic Oral Biofilms and In Vitro Reconstituted Oral Epithelium. *PLOS ONE, 11*(5), e0155427-e0155427. https://doi.org/10.1371/JOURNAL.PONE.0155427

Dula, S., Ajayeoba, T. A., & Ijabadeniyi, O. A. (2021). Bacterial biofilm formation on stainless steel in the food processing environment and its health implications. *Folia Microbiologica, 66*(3), 293-302. https://doi.org/10.1007/s12223-021-00864-2

Flemming, H.-C., & Wingender, J. (2010). The biofilm matrix. *Nature reviews microbiology, 8*(9), 623-633. https://doi.org/10.1038/nrmicro2415

Gao, Y., Li, M., Sun, C., & Zhang, X. (2022). Microbubble-enhanced water activation by cold plasma. *Chemical Engineering Journal, 446*, 137318. https://doi.org/10.1016/j.cej.2022.137318

Gilmore, B. F., Flynn, P. B., O'Brien, S., Hickok, N., Freeman, T., & Bourke, P. (2018). Cold Plasmas for Biofilm Control: Opportunities and Challenges. *Trends in Biotechnology, 36*(6), 627-638. https://doi.org/10.1016/j.tibtech.2018.03.007

Guo, D., Liu, H., Zhou, L., Xie, J., & He, C. (2021). Plasma-activated water production and its application in agriculture. *Journal of the Science of Food and Agriculture, 101*(12), 4891-4899. https://doi.org/10.1002/jsfa.11258

Guo, J., Wang, J., Xie, H., Jiang, J., Li, C., Li, W., Li, L., Liu, X., & Lin, F. (2022). Inactivation effects of plasma-activated water on Fusarium graminearum. *Food Control, 134*, 108683. https://doi.org/10.1016/j.foodcont.2021.108683

Jo, J., Price-Whelan, A., & Dietrich, L. E. (2022). Gradients and consequences of heterogeneity in biofilms. *Nature reviews microbiology, 20*(10), 593-607. https://doi.org/10.1038/s41579-022-00692-2

Karygianni, L., Ren, Z., Koo, H., & Thurnheer, T. (2020). Biofilm Matrixome: Extracellular Components in Structured Microbial Communities. *Trends in microbiology, 28*(8), 668-681. https://doi.org/10.1016/j.tim.2020.03.016

Kaushik, N. K., Ghimire, B., Li, Y., Adhikari, M., Veerana, M., Kaushik, N., Jha, N., Adhikari, B., Lee, S.-J., & Masur, K. (2018). Biological and medical applications of plasma-activated media, water and solutions. *Biological Chemistry, 400*(1), 39-62. https://doi.org/10.1515/hsz-2018-0226

Kolbe, B. H., Coad, B., & Richter, K. (2024). Plasma-activated water's potential contribution to 'One Health'. *Microbiology Australia*. https://doi.org/10.1071/MA24024

Lewis, A. M., Willard, D. J., Manesh, M. J. H., Sivabalasarma, S., Albers, S.-V., & Kelly, R. M. (2023). Stay or Go: Sulfolobales Biofilm Dispersal Is Dependent on a Bifunctional VapB Antitoxin. *mBio, 14*(2), e00053-00023. https://doi.org/10.1128/mbio.00053-23

Li, W., Zhou, R., Zhou, R., Weerasinghe, J., Zhang, T., Gissibl, A., Cullen, P. J., Speight, R., & Ostrikov, K. (2022). Insights into amoxicillin degradation in water by non-thermal plasmas. *Chemosphere, 291*, 132757. https://doi.org/10.1016/j.chemosphere.2021.132757

Limoli, D. H., Jones, C. J., & Wozniak, D. J. (2015). Bacterial Extracellular Polysaccharides in Biofilm Formation and Function. *Microbiology Spectrum, 3*(3), 3.3.29. https://doi.org/doi:10.1128/microbiolspec.MB-0011-2014

Liu, Y., Wang, J., Liu, C., Chen, G., Cai, Z., Sang, X., & Zhang, J. (2022). TMT-based proteomic analysis of the inactivation effect of high voltage atmospheric cold plasma treatment on Pseudomonas aeruginosa. *LWT, 169*, 113981. https://doi.org/10.1016/j.lwt.2022.113981

López, M., Calvo, T., Prieto, M., Múgica-Vidal, R., Muro-Fraguas, I., Alba-Elías, F., & Alvarez-Ordóñez, A. (2019). A Review on Non-thermal Atmospheric Plasma for Food Preservation: Mode of Action, Determinants of Effectiveness, and Applications. *Frontiers in Microbiology, 10*. https://doi.org/10.3389/fmicb.2019.00622

Lu, P., Chen, C., Wang, Q., Wang, Z., Zhang, X., & Xie, S. (2013). Phylogenetic diversity of microbial communities in real drinking water distribution systems [Article]. *Biotechnology and Bioprocess Engineering, 18*(1), 119-124. https://doi.org/10.1007/s12257-012-0230-z

Luo, A., Wang, F., Sun, D., Liu, X., & Xin, B. (2022). Formation, Development, and Cross-Species Interactions in Biofilms [Mini Review]. *Frontiers in Microbiology, Volume 12 - 2021*. https://doi.org/10.3389/fmicb.2021.757327

Ma, Y., Deng, Y., Hua, H., Khoo, B. L., & Chua, S. L. (2023). Distinct bacterial population dynamics and disease dissemination after biofilm dispersal and disassembly. *The ISME Journal, 17*(8), 1290-1302. https://doi.org/10.1038/s41396-023-01446-5

Mai-Prochnow, A., Zhou, R., Zhang, T., Ostrikov, K. K., Mugunthan, S., Rice, S. A., & Cullen, P. J. (2021). Interactions of plasma-activated water with biofilms: inactivation, dispersal effects and mechanisms of action. *npj Biofilms and Microbiomes, 7*(1), 1-12. https://doi.org/10.1038/s41522-020-00180-6

Man, C., Zhang, C., Fang, H., Zhou, R., Huang, B., Xu, Y., Zhang, X., & Shao, T. (2022). Nanosecond-pulsed microbubble plasma reactor for plasma-activated water generation and bacterial inactivation. *Plasma Processes and Polymers, 19*(6), 2200004. https://doi.org/10.1002/ppap.202200004

McClenaghan, L. A., Thompson, T. P., Shambharkar, A., Duncan, R. M., Bourke, P., Skvortsov, T., & Gilmore, B. F. (2025). Potassium iodide enhances the antimicrobial activity of plasma-activated water. *Biofilm*, 100313. https://doi.org/10.1016/j.bioflm.2025.100313

McConnell, G., Trägårdh, J., Amor, R., Dempster, J., Reid, E., & Amos, W. B. (2016). A novel optical microscope for imaging large embryos and tissue volumes with sub-cellular resolution throughout. *eLife, 5*, e18659. https://doi.org/10.7554/eLife.18659

Moreno-Couranjou, M., Mauchauffé, R., Bonot, S., Detrembleur, C., & Choquet, P. (2018). Anti-biofouling and antibacterial surfaces via a multicomponent coating deposited from an up-scalable atmospheric-pressure plasma-assisted CVD process. *Journal of Materials Chemistry B, 6*(4), 614-623. https://doi.org/10.1039/C7TB02473H

Muhammad, A. I., Liao, X., Cullen, P. J., Liu, D., Xiang, Q., Wang, J., Chen, S., Ye, X., & Ding, T. (2018). Effects of nonthermal plasma technology on functional food components. *Comprehensive Reviews in Food Science and Food Safety, 17*(5), 1379-1394. https://doi.org/10.1111/1541-4337.12379

Nguyen, H. T., Nguyen, T. H., & Otto, M. (2020). The staphylococcal exopolysaccharide PIA–Biosynthesis and role in biofilm formation, colonization, and infection. *Computational and Structural Biotechnology Journal, 18*, 3324-3334. https://doi.org/10.1016/j.csbj.2020.10.027

Panlilio, H., & Rice, C. V. (2021). The role of extracellular DNA in the formation, architecture, stability, and treatment of bacterial biofilms. *Biotechnology and bioengineering, 118*(6), 2129-2141. https://doi.org/10.1002/bit.27760

Philipp, L.-A., Bühler, K., Ulber, R., & Gescher, J. (2024). Beneficial applications of biofilms. *Nature reviews microbiology, 22*(5), 276-290. https://doi.org/10.1038/s41579-023-00985-0

Qureshi, N. (2009). Beneficial biofilms: wastewater and other industrial applications. In *Biofilms in the Food and Beverage Industries* (pp. 474-498). https://doi.org/10.1533/9781845697167.4.474

Rathore, V., Patel, D., Butani, S., & Nema, S. K. (2021). Investigation of Physicochemical Properties of Plasma Activated Water and its Bactericidal Efficacy. *Plasma Chemistry and Plasma Processing, 41*(3), 871-902. https://doi.org/10.1007/s11090-021-10161-y

Rathore, V., Patil, C., Sanghariyat, A., & Nema, S. K. (2022). Design and development of dielectric barrier discharge setup to form plasma-activated water and optimization of process parameters. *The European Physical Journal D, 76*(5), 77. https://doi.org/10.1140/epjd/s10053-022-00397-4

Rothwell, J. G., Alam, D., Carter, D. A., Soltani, B., McConchie, R., Zhou, R., Cullen, P. J., & Mai-Prochnow, A. (2022). The antimicrobial efficacy of plasma-activated water against Listeria and E. coli is modulated by reactor design and water composition. *Journal of Applied Microbiology, 132*(4), 2490-2500. https://doi.org/10.1111/jam.15429

Rothwell, J. G., Hong, J., Morrison, S. J., Vyas, H. K. N., Xia, B., Mai-Prochnow, A., McConchie, R., Phan-Thien, K.-Y., Cullen, P. J., & Carter, D. A. (2023). An Effective Sanitizer for Fresh Produce Production: In Situ Plasma-Activated Water Treatment Inactivates Pathogenic Bacteria and Maintains the Quality of Cucurbit Fruit. *Microbiology Spectrum, 11*(4), e00034-00023. https://doi.org/10.1128/spectrum.00034-23

Ruhal, R., Sahu, A., Koujalagi, T., Das, A., Prasanth, H., & Kataria, R. (2024). Biofilm-specific determinants of enterococci pathogen. *Archives of Microbiology, 206*(10), 397. https://doi.org/10.1007/s00203-024-04119-9

Saharan, B. S., Beniwal, N., & Duhan, J. S. (2024). From formulation to function: A detailed review of microbial biofilms and their polymer-based extracellular substances. *The Microbe, 5*, 100194. https://doi.org/10.1016/j.microb.2024.100194

Sauer, K., Stoodley, P., Goeres, D. M., Hall-Stoodley, L., Burmølle, M., Stewart, P. S., & Bjarnsholt, T. (2022). The biofilm life cycle: expanding the conceptual model of biofilm formation. *Nature reviews microbiology, 20*(10), 608-620. https://doi.org/10.1038/s41579-022-00767-0

Shah, U., Rivero, W., Wang, Q., Zheng, H., & Salvi, D. (2024). Exploration of plasma-activated water (PAW) as a cleaning-in-place (CIP) solution for fouling removal and microbial reduction. *Journal of Food Process Engineering, 47*(7), e14669. https://doi.org/10.1111/jfpe.14669

Sharma, D. K., & Rajpurohit, Y. S. (2024). Multitasking functions of bacterial extracellular DNA in biofilms. *Journal of bacteriology, 206*(4), e00006-00024. https://doi.org/10.1128/jb.00006-24

Sharma, G., Sharma, S., Sharma, P., Chandola, D., Dang, S., Gupta, S., & Gabrani, R. (2016). Escherichia coli biofilm: development and therapeutic strategies. *Journal of Applied Microbiology, 121*(2), 309-319. https://doi.org/10.1111/jam.13078

Shineh, G., Mobaraki, M., Perves Bappy, M. J., & Mills, D. K. (2023). Biofilm Formation, and Related Impacts on Healthcare, Food Processing and Packaging, Industrial Manufacturing, Marine Industries, and Sanitation–A Review. *Applied Microbiology, 3*(3), 629-665. https://doi.org/10.3390/applmicrobiol3030044

Sies, H., Mailloux, R. J., & Jakob, U. (2024). Fundamentals of redox regulation in biology. *Nature Reviews Molecular Cell Biology, 25*(9), 701-719. https://doi.org/10.1038/s41580-024-00730-2

Soni, A., Choi, J., & Brightwell, G. (2021). Plasma-Activated Water (PAW) as a Disinfection Technology for Bacterial Inactivation with a Focus on Fruit and Vegetables. *Foods, 10*(1), 166. https://doi.org/10.3390/foods10010166

Stapelmann, K., Kylián, O., Denis, B., & Rossi, F. (2008). On the application of inductively coupled plasma discharges sustained in Ar/O2/N2 ternary mixture for sterilization and decontamination of medical instruments. *Journal of Physics D: Applied Physics, 41*(19), 192005. https://doi.org/10.1088/0022-3727/41/19/192005

Thalhammer, K. O., & Newman, D. K. (2023). A phenazine-inspired framework for identifying biological functions of microbial redox-active metabolites. *Current opinion in chemical biology, 75*, 102320. https://doi.org/10.1016/j.cbpa.2023.102320

Thirumdas, R., Kothakota, A., Annapure, U., Siliveru, K., Blundell, R., Gatt, R., & Valdramidis, V. P. (2018). Plasma activated water (PAW): Chemistry, physico-chemical properties, applications in food and agriculture. *Trends in food science & technology, 77*, 21-31. https://doi.org/10.3390/pr11072213

Tiwari, B., Dinesh, S., Prithiviraj, V., Yang, X., & Roopesh, M. (2025). Bacterial biofilm inactivation by plasma activated nanobubble water. *Journal of Water Process Engineering, 69*, 106676. https://doi.org/10.1016/j.jwpe.2024.106676

Tonks, L., & Langmuir, I. (1929). Oscillations in Ionized Gases. *Physical Review, 33*(2), 195-210. https://doi.org/10.1103/PhysRev.33.195

Toyofuku, M., Inaba, T., Kiyokawa, T., Obana, N., Yawata, Y., & Nomura, N. (2016). Environmental factors that shape biofilm formation. *Biosci Biotechnol Biochem, 80*(1), 7-12. https://doi.org/10.1080/09168451.2015.1058701

Tresp, H., Hammer, M. U., Winter, J., Weltmann, K. D., & Reuter, S. (2013). Quantitative detection of plasma-generated radicals in liquids by electron paramagnetic resonance spectroscopy. *Journal of Physics D: Applied Physics, 46*(43), 435401. https://doi.org/10.1088/0022-3727/46/43/435401

Ünal Turhan, E., Erginkaya, Z., Korukluoğlu, M., & Konuray, G. (2019). Beneficial biofilm applications in food and agricultural industry. In *Health and safety aspects of food processing technologies* (pp. 445-469). Springer. https://doi.org/10.1007/978-3-030-24903-8_15

Vyas, H. K. N., Hoque, M. M., Xia, B., Alam, D., Cullen, P. J., Rice, S. A., & Mai-Prochnow, A. (2025). Transcriptional signatures associated with the survival of Escherichia coli biofilm during treatment with plasma-activated water. *Biofilm, 9*, 100266. https://doi.org/10.1016/j.bioflm.2025.100266

Vyas, H. K. N., Xia, B., Alam, D., Gracie, N. P., Rothwell, J. G., Rice, S. A., Carter, D., Cullen, P. J., & Mai-Prochnow, A. (2023). Plasma activated water as a pre-treatment strategy in the context of biofilm-infected chronic wounds. *Biofilm, 6*, 100154. https://doi.org/10.1016/j.bioflm.2023.100154

Waller, C., Marzinek, J. K., McBurnie, E., Bond, P. J., Williamson, P. T., & Khalid, S. (2023). Impact on S. aureus and E. coli membranes of treatment with chlorhexidine and alcohol solutions: insights from molecular simulations and nuclear magnetic resonance. *Journal of Molecular Biology, 435*(11), 167953. https://doi.org/10.1016/j.jmb.2023.167953

Wan, K., Guo, L., Ye, C., Zhu, J., Zhang, M., & Yu, X. (2021). Accumulation of antibiotic resistance genes in full-scale drinking water biological activated carbon (BAC) filters during backwash cycles. *Water Research, 190*, 116744. https://doi.org/10.1016/j.watres.2020.116744

Wang, H., Han, R., Yuan, M., Li, Y., Yu, Z., Cullen, P. J., Du, Q., Yang, Y., & Wang, J. (2023). Evaluation of plasma-activated water: Efficacy, stability, physicochemical properties, and mechanism of inactivation against Escherichia coli. *LWT, 184*, 114969. https://doi.org/10.1016/j.lwt.2023.114969

Wang, Q., & Salvi, D. (2021). Evaluation of plasma-activated water (PAW) as a novel disinfectant: Effectiveness on Escherichia coli and Listeria innocua, physicochemical properties, and storage stability. *LWT, 149*, 111847. https://doi.org/10.1016/j.lwt.2021.111847

Wang, S., Liu, Y., Zhou, R., Liu, F., Fang, Z., Ostrikov, K. K., & Cullen, P. J. (2021). Microsecond pulse gas–liquid discharges in atmospheric nitrogen and oxygen: Discharge mode, stability, and plasma characteristics. *Plasma Processes and Polymers, 18*(2), 2000135. https://doi.org/10.1002/ppap.202000135

Wang, S., Yang, D., Liu, F., Wang, W., & Fang, Z. (2018). Spectroscopic study of bipolar nanosecond pulse gas-liquid discharge in atmospheric argon. *Plasma Science and Technology, 20*(7), 075404. https://doi.org/10.1088/2058-6272/aabac8

Wang, X., Preston, J. F., & Romeo, T. (2004). The pgaABCD Locus of Escherichia coli Promotes the Synthesis of a Polysaccharide Adhesin Required for Biofilm Formation. *Journal of bacteriology, 186*(9), 2724-2734. https://doi.org/10.1128/jb.186.9.2724-2734.2004

Wong, K. S., Chew, N. S. L., Low, M., & Tan, M. K. (2023). Plasma-Activated Water: Physicochemical Properties, Generation Techniques, and Applications. *Processes, 11*(7), 2213. https://doi.org/10.3390/pr11072213

Xia, B., Vyas, H. K. N., Zhou, R., Zhang, T., Hong, J., Rothwell, J. G., Rice, S. A., Carter, D., Ostrikov, K., Cullen, P. J., & Mai-Prochnow, A. (2023). The importance of superoxide anion for Escherichia coli biofilm removal using plasma-activated water. *Journal of Environmental Chemical Engineering, 11*(3), 109977. https://doi.org/10.1016/j.jece.2023.109977

Xiao, D., Cheng, C., Shen, J., Lan, Y., Xie, H., Shu, X., Meng, Y., Li, J., & Chu, P. K. (2014). Characteristics of atmospheric-pressure non-thermal N2 and N2/O2 gas mixture plasma jet. *Journal of applied physics, 115*(3), 033303. https://doi.org/10.1063/1.4862304

Yahaya, A. G., Okuyama, T., Kristof, J., Blajan, M. G., & Shimizu, K. (2021). Direct and Indirect Bactericidal Effects of Cold Atmospheric-Pressure Microplasma and Plasma Jet. *Molecules, 26*(9), 2523. https://doi.org/10.3390/molecules26092523

Yates, M. D., Barr Engel, S., Eddie, B. J., Lebedev, N., Malanoski, A. P., & Tender, L. M. (2018). Redox-gradient driven electron transport in a mixed community anodic biofilm. *FEMS Microbiology Ecology, 94*(6), 081. https://doi.org/10.1093/femsec/fiy081

Zhao, Y.-M., Ojha, S., Burgess, C. M., Sun, D.-W., & Tiwari, B. K. (2021). Inactivation efficacy of plasma-activated water: influence of plasma treatment time, exposure time and bacterial species. *International Journal of Food Science and Technology, 56*(2), 721-732. https://doi.org/10.1111/ijfs.14708

Zhao, Y.-M., Zhang, L., Bao, Y., Guo, Y., Ma, H., He, R., Bourke, P., & Sun, D.-W. (2025). The inhibitory mechanisms of plasma-activated water on biofilm formation of Pseudomonas fluorescens by disrupting quorum sensing. *Food Research International*, 117436. https://doi.org/10.1016/j.foodres.2025.117436

Zhao, Y., Shao, L., Jia, L., Meng, Z., Liu, Y., Wang, Y., Zou, B., Dai, R., Li, X., & Jia, F. (2022). Subcellular inactivation mechanisms of Pseudomonas aeruginosa treated by cold atmospheric plasma and application on chicken breasts. *Food Research International, 160*, 111720. https://doi.org/10.1016/j.foodres.2022.111720

Zhou, C., Wu, Y., Thappeta, K. R. V., Subramanian, J. T. L., Pranantyo, D., Kang, E.-T., Duan, H., Kline, K., & Chan-Park, M. B. (2017). In vivo anti-biofilm and anti-bacterial non-leachable coating thermally polymerized on cylindrical catheter. *ACS Applied Materials & Interfaces, 9*(41), 36269-36280. https://doi.org/10.1021/acsami.7b07053

Zhou, R., Zhou, R., Wang, P., Xian, Y., Mai-Prochnow, A., Lu, X., Cullen, P. J., Ostrikov, K., & Bazaka, K. (2020). Plasma-activated water: generation, origin of reactive species and biological applications. *Journal of Physics D: Applied Physics, 53*(30), 303001. https://doi.org/10.1088/1361-6463/ab81cf

2 Chapter 2 Comparison study of the antibiofilm activity of direct- and indirect- PAW treatment

2.1 Abstract

Cold plasma, a partially ionized gas, and plasma-activated water (PAW) have demonstrated potent antimicrobial activity. The bubble spark discharge (BSD) plasma reactor is an effective method for generating PAW. However, the optimal conditions for using the BSD reactor to treat biofilms remain unclear. In this study, both direct and indirect PAW treatments were applied to *Escherichia coli* (ATCC 25922) biofilms. We evaluated cell viability after different PAW treatment methods and exposure times. Additionally, the stability of PAW activity during storage was assessed, including the measurement of reactive oxygen and nitrogen species (RONS)—such as H_2O_2, NO_3^-, and NO_2^-—in PAW, as well as cell enumeration. Our results show that a 10-minute direct PAW treatment generated using air was the most effective for *E. coli* biofilm removal on stainless steel surfaces. We also demonstrated that RONS levels in PAW remained stable for up to 24 hours when stored at 4°C. Even after storage, PAW retained its ability to inactivate *E. coli* biofilms. This study highlights the importance of optimizing PAW application for biofilm removal, maximizing RONS production under real-world and industry-relevant conditions.

2.2 Introduction

Biofilms, composed of microbial communities embedded in an extracellular matrix, pose significant challenges in both clinical and industrial settings due to their enhanced resistance to conventional disinfectants and antibiotics (Toyofuku et al., 2016). Traditional methods for biofilm removal, such as chemical treatments and physical disruption, often fail to achieve complete eradication, leading to persistent contamination and increased risk of infections (Cámara et al., 2022; Carrascosa et al., 2021). In recent years, non-thermal plasma technologies, including cold plasma and plasma-activated water (PAW), have gained attention as promising alternatives for biofilm control due to their unique mechanisms of action (Mai-Prochnow et al., 2021).

Cold plasma, a partially ionized gas consisting of reactive species such as electrons, ions, and photons, has been widely investigated for its antimicrobial properties(Handorf et al., 2021; Park et al., 2017; Xu et al., 2020). Plasma-activated water (PAW), generated by exposing water to cold plasma, exhibits enhanced disinfectant capabilities through the generation of reactive oxygen and nitrogen species (RONS), such as hydrogen peroxide (H_2O_2), nitrate (NO_3^-), and nitrite (NO_2^-). These reactive species have been shown to effectively disrupt microbial cells and biofilms by oxidizing cellular components and impairing vital processes (Djemaoune et al., 2019). Moreover, PAW has been found to retain its antimicrobial activity even after storage, making it a potentially practical solution for biofilm treatment in real-world applications (Wang & Salvi, 2021).

One promising approach for generating PAW is the bubble spark discharge (BSD) plasma reactor, which utilizes an electrical discharge in the presence of gas bubbles in liquid to produce reactive species (Zhou et al., 2020a). The BSD reactor has been demonstrated to generate PAW with high levels of RONS, contributing to its effectiveness in biofilm removal, particularly in challenging environments such as stainless steel surfaces commonly used in food processing and medical devices (Zhou et al., 2020a). Recent studies have shown that both direct and indirect PAW treatments can

significantly reduce biofilm biomass and bacterial viability, highlighting the potential of BSD-generated PAW as a novel and effective biofilm control method (Vyas et al., 2023; Xia et al., 2023).

The importance of reactive species in PAW's antimicrobial activity cannot be overstated. RONS play a crucial role in the inactivation of biofilms by disrupting the structural integrity of the extracellular matrix and penetrating bacterial cells to cause oxidative damage (Mai-Prochnow et al., 2021; Nicol et al., 2020). The concentration and stability of these species are key factors influencing the efficacy of PAW in biofilm removal (Ghimire et al., 2021). Understanding the optimal conditions for generating and applying PAW, including factors such as treatment time, storage stability, and the nature of the biofilm matrix, is essential for maximizing its biofilm eradication potential in both laboratory and industrial settings.

2.3 Materials and Methods

2.3.1 Strain and biofilm formation

Escherichia coli ATCC 25922 was routinely maintained on tryptic soy agar (TSA) (tryptone (pancreatic digest of casein) 17.0 g/L, soytone (peptic digest of soybean) 3.0 g/L, glucose 2.5 g/L, sodium chloride 5.0 g/L, dipotassium phosphate 2.5 g/L, agar 15 g/L). One colony from a fresh agar plate was inoculated into 10 mL tryptic soy broth TSB) and incubated for 14 h at 37 °C, shaking at 160 rpm. For biofilm formation, the overnight cultures were diluted 1/100 to obtain an approximate cell density of 10E5 CFU/mL. 1 mL of the diluted culture was inoculated into wells of a 24-well plate containing sterile stainless-steel coupons (diameter: 12.7 mm and thickness: 3.8 mm from BioSurface Technologies, Bozeman, Montana, USA). Plates were incubated for 24 h at 37 °C with 110 rpm shaking to allow for cell attachment and subsequent biofilm formation.

2.3.2 PAW generation

The plasma bubble reactor (PlasmaLeap Technologies, Sydney) consists of a metal rod high voltage electrode inside a quartz tube (Figure 2.1) with four holes (2 µm diameter) evenly spaced at the immersed end to allow for the plasma discharge to contact the water. The gas flow was controlled by a digital M series mass flow meter (Alicat Scientific, United States).

The plasma-activated water (PAW) was generated as previously described (Rothwell et al., 2022). Briefly, a Leap100 (PlasmaLeap Technologies, Sydney) power source was used with an input voltage of 150 V, a discharge frequency of 1500 Hz, a resonance frequency of 60 kHz and a duty cycle of 100 µs. The treatment time was 10min with 1 standard liter per minute (slm) of compressed air gas flow.

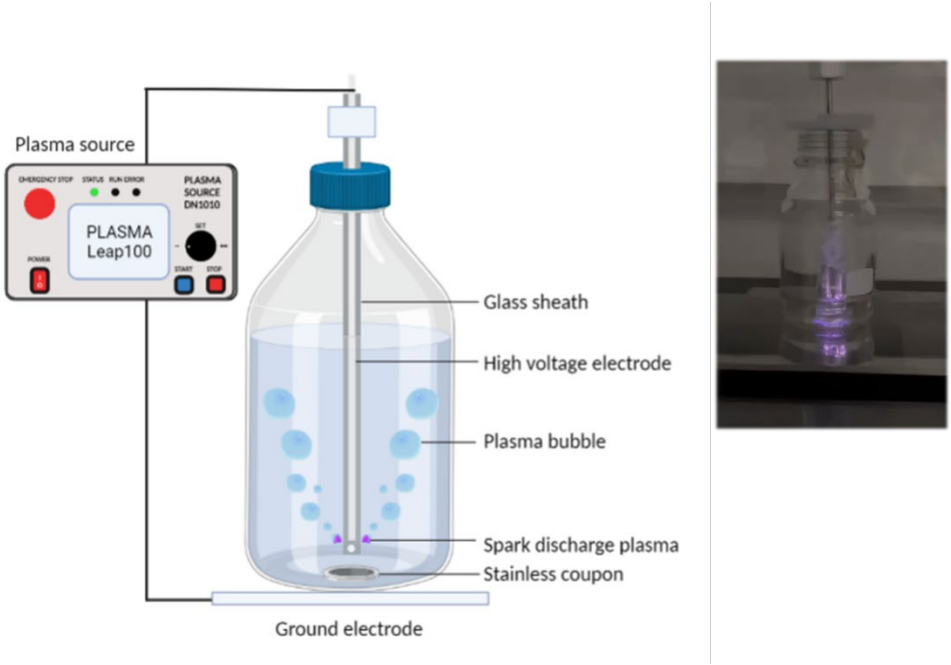

Figure 2.1. A schematic illustration of the plasma-activated water (PAW) generated by a bubble spark discharge (BSD) plasma reactor. The BSD generator includes glass sheath, high voltage electrode, ground electrode and Leap100 plasma power source. There are 4 holes (2 µm diameter) on the glass sheath to allow water bubbling.

2.3.3 Direct and indirect PAW treatment on *E. coli* biofilm

Coupons with the attached biofilm were aseptically removed from the well plate and placed into 250 mL Schott bottles containing 100 mL sterile MilliQ (Figure 2.2) The plasma bubble reactor was submerged in the water containing the coupons for 10 min direct plasma chemical experiment. As comparison, the PAW was generated as shown in Figure 2.1. Then 1 ml of 10-min generated PAW

was added into the 24-well plates containing coupons with the attached biofilm for 1, 30, and 60 minutes, respectively (Figure 2.2).

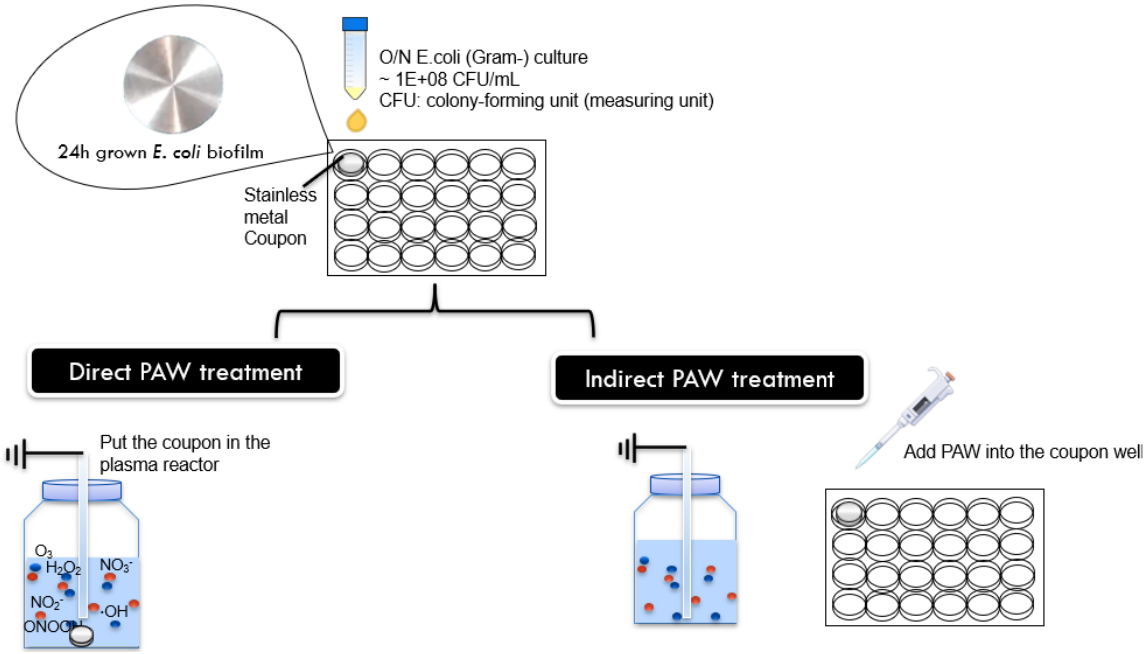

Figure 2.2. A schematic illustration of direct and indirect PAW treatment on *E. coli* biofilm.

2.3.4 Cell enumeration

Immediately following the PAW treatment, coupons were extracted from the treatment bottle and placed into a Falcon tube containing 2 mL 1x phosphate buffered saline (PBS). The biofilm was removed from the coupon surface by scraping it with a sterile flat-end spatula and placed into falcon tubes. The Falcon tubes were then submerged in a sonicating water bath for 3 min at 45 kHz followed by 10 s vortexing to ensure complete dislodgement of biofilms. This did not affect cell viability (data not shown). Serial dilutions were then drop-plated (10 µL) onto TSA in triplicates. Plates were incubated overnight at 37 °C before determining the colony-forming units (CFU).

2.3.5 Cell viability of biofilms cells on coupon surfaces and in the surrounding solution

To further evaluate the antibiofilm activity of PAW against *E. coli*, the viability of biofilm cells was quantified both on the coupons surfaces and in the surrounding water. Briefly, the 24h grown E. coli biofilms were exposed to direct PAW treatment (as described in Method 2.3.2) for 10 min. Following

treatment, the surviving biofilm cells remaining on the coupon surfaces and those released into the PAW solution were enumerated separately by CFU counting,

2.3.6 PAW reactive species measurements

Concentrations of hydrogen peroxide (H_2O_2), nitrate (NO_3^-), and nitrite (NO_2^-) were assessed in the PAW generated using air gas 10 min. The concentration of H_2O_2 was measured by a titanium sulphate method (Zhou et al., 2021) where H_2O_2 reacts with titanium oxysulphate ($TiOSO_4$) resulting in a yellow-coloured complex (pertitanic acid) that is quantified with UV-Vis spectroscopy at 408 nm (the standard curve of H_2O_2 is shown in supportive information Fig. S1). NO_3^- and NO_2^- species were measured using a Hanna Instrument multiparameter photometer (HI83399) with colorimetric nitrate kit (HI93766-50) and colorimetric nitrite reagent (HI93708-0), respectively. All standards were prepared in MilliQ water.

2.3.7 PAW stability measurement

To assess the stability of PAW, the cell enumeration and reactive species were measured under 10 min-generated PAW which stored at 4°C for 0, 1, 5, and 24 h, respectively. Briefly, the 24h grown E. coli biofilms were exposed to 1, 5, and 24 h-stored PAW treatment for 60 min. Following treatment, the surviving biofilm cells remaining on the coupon surfaces and those released into the PAW solution were enumerated separately by CFU counting. The concentrations of H_2O_2, NO_3^-, and NO_2^- were measured by the method described in 2.3.6. MQ water and bubbling water (without Plasma) were also stored at 4°C, as the control.

2.3.8 Statistical analysis

Experiments were performed 3 times and values are expressed as mean ± standard deviation ($\mu \pm \sigma$). A parametric, unpaired t-Test (2 tail, $p<0.05$) or a One-way ANOVA (with Tukeys multiple comparisons test, $p<0.05$) was performed where appropriate to identify significant differences in log reduction of each sample compared to the control.

2.4 Results

2.4.1 Biofilm removal under direct PAW treatment

Biofilms grown on stainless steel coupons were placed into Schott bottles during the 10-minute PAW generation period. Following treatment, the remaining viable cells were enumerated by colony-forming unit (CFU) counting. A significant reduction in CFU was observed for the PAW-treated samples compared to the control (Figure 2.3), with a 5-log reduction (mean value) achieved for the direct PAW treatment.

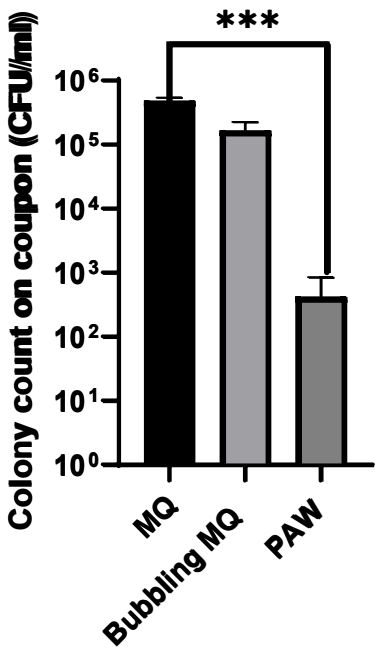

Figure 2.3. Reduction of *E. coli* biofilms under direct PAW treatment. (P < 0.05, unpaired t-Test, n=3).

2.4.2 Biofilm removal under indirect PAW treatment

For the indirect PAW treatment, biofilms grown on stainless steel coupons were placed into 24-well plates, and 1 mL of 10-mingenerated PAW was applied for 1, 30, and 60 minutes. The viable cells were then enumerated by CFU counting. A significant reduction in CFU was observed after 30 and 60

minutes of treatment compared to the control (Figure 2.4), with a 1-log reduction (mean value) for the indirect PAW treatment.

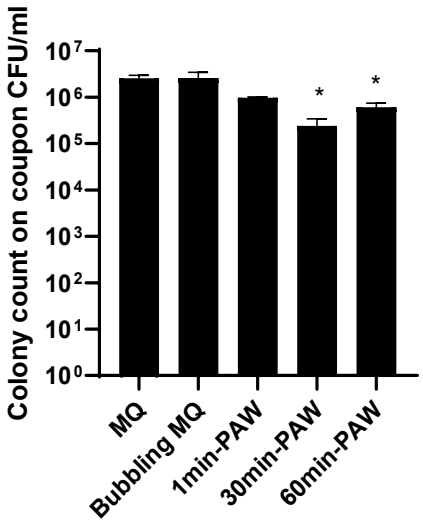

Figure 2.4. Reduction of *E. coli* biofilms under indirect PAW treatment. (P < 0.05, unpaired t-Test, n=3).

Viability of biofilm cells on coupon surfaces and in the surrounding solution

E. coli biofilms grown on stainless steel coupons were subjected to direct PAW treatment for 10 min. Viable cell counts were subsequently determined for both the coupon surfaces and the surrounding solution, A substantial reduction in CFU was observed in both compartments, with an average decrease of approximately 5 log units. These findings indicate that PAW is highly effective not only in reducing biofilms attached to stainless steel surfaces but also in inactivating biofilm-associated cells dispersed into the surrounding environment.

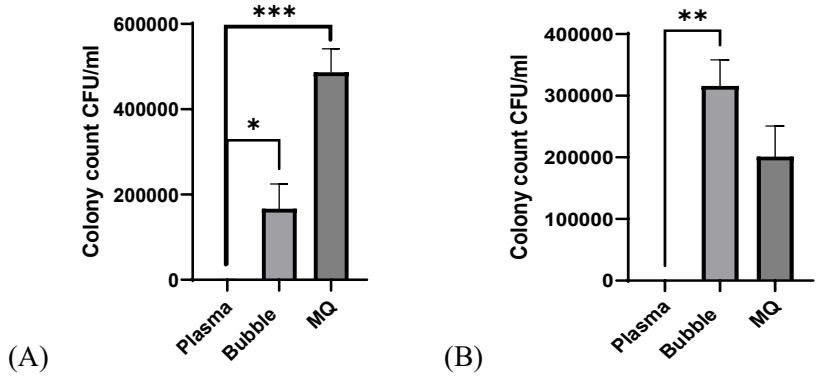

Figure 2.5. Reduction of *E. coli* biofilms under direct 10 min PAW treatment on (A) stainless steel coupon surfaces and (B) surrounding PAW solution (P < 0.05, unpaired t-Test, n=3).

2.4.3 Characterisation of PAW stability: ability to remove biofilm cells

Biofilms grown on stainless steel coupons were placed into 24-well plates and treated with 1 mL of PAW stored for 0, 1, 5, and 24 hours for 30 minutes. The remaining viable cells were enumerated by colony-forming unit (CFU) counting. A significant reduction in CFU was observed for all stored PAWs compared to the control (Figure 2.5), with an approximate 1-log reduction (mean value) across all conditions. Notably, PAW was also able to inactivate the dispersed biofilm cells in the surrounding solution. This finding suggests that indirect PAW treatment shows a mild inactivation rate compared to the direct PAW treatment. Further modification of PAW generation or combining with other antimicrobial agents that improving PAW activity against biofilm cells are required.

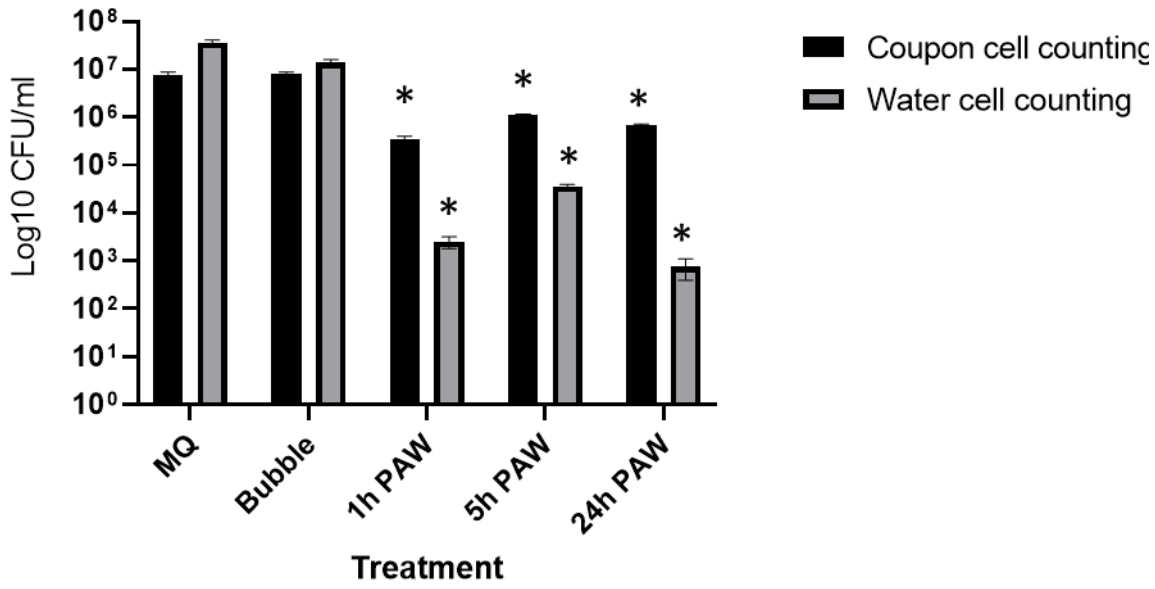

Figure 2.6. CFU counting of *E. coli* biofilm cells on both of coupon surfaces and in the surrounding solution under PAW stored at 4°C for 0, 1, 5, and 24 hours. (P < 0.05, unpaired t-Test, n=3).

2.4.4 Characterisation of PAW stability: activity of reactive species

As shown in Figure 2.6, reactive oxygen and nitrogen species (RONS) were detected under all stored PAW conditions. Notably, high levels of nitrate (NO_3^-) were present in the PAW, with 82.36 ppm

detected in the 5-hour stored PAW. A low concentration of nitrite (NO_2^-) was detected in freshly generated PAW (0.55 ppm), but it was undetectable after storage (Table 2.1). Hydrogen peroxide (H_2O_2), a known antimicrobial RONS generated in PAW, was also present in the stored PAWs. Specifically, after 24 hours of storage, H_2O_2 concentrations fluctuated between 23.47 and 25.57 ppm (Table 2.1).

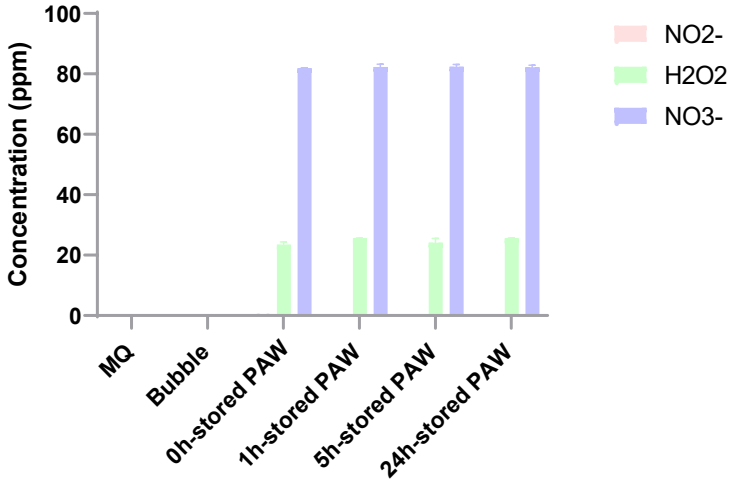

Figure 2.7. The reactive species H_2O_2, NO_2^-, and NO_3^- activity of PAW after 0, 1, 5, and 24 h storage at 4°C.

Table 2.1. Reactive species concentration (ppm) measurement of stored PAW

Sample	NO_2^- (ppm)	NO_3^- (ppm)	H_2O_2 (ppm)
24h PAW	**0**	**82.24**	**25.57**
5h PAW	**0**	**82.36**	**24.16**
1h PAW	**0**	**82.32**	**25.57**
0h PAW	**0.55**	**81.90**	**23.47**
Bubbling MQ	**0**	**0.00**	**0.00**
MQ	**0**	**0.00**	**0.00**

2.5 Discussion

In this study, the direct PAW treatment showed the greatest antibacterial activity against 24h *E. coli* biofilms, compared to the biofilm treated with indirect PAW treatment. The indirect PAW treatment exhibited time-dependent antibacterial activity, demonstrating a significant 1-log reduction after 60 min treatment. While for direct treatment, a 5-log reduction was observed on the viability of biofilm cells and even to a non-detectable level compared to the control. Notably, this antibacterial activity of direct PAW treatment not only observed on biofilm cells that grown on coupon surfaces, but also on dispersed cells in the surrounding solution. There is one research also compared the direct and indirect PAW efficacy against bacterial planktonic cells (*E. coli*, *L, monocytogenes,* and *Salmonella enterica*), which reported a similar result as ours that the direct PAW was more effective to inactivate bacteria cells (Rothwell et al., 2022).

While several studies have found PAW to be strongly antibacterial for planktonic cells (Rathore et al., 2021a; Shen et al., 2016a), the reduction of biofilm cells to a low level is a rare finding. Here, after only a 10-min direct treatment, we have demonstrated the efficacy of our PAW is around 5-log reduction, which is a very promising result given that biofilms are highly resistant to most antimicrobials and removal strategies. Sen and Mutlu (2013) investigated a DBD plasma treatment that can effectively inactivate *E. coli* grown on stainless steel surfaces with 5-log reduction under 22.9±3.3 minutes treatment when powered by 100 Watt plasma. Another study by Fernández-Gómez et al., (2023) achieve a comparable reduction (5.6-log) for *L. monocytogenes* biofilms in a stainless steel exposed to PAW generated by surface DBD (SDBD) cold plasma reactor for 30 minutes.

It is widely accepted that RONS produced in the PAW are responsible for their antibacterial effect (Girard et al., 2018; Mai-Prochnow et al., 2015; Sergeichev et al., 2021). The formation of RONS in PAW is complex as there are many physical and chemical properties in play. In our plasma-generating experimental design, using a BSD electrode, a constant gas flow results in the plasma being bubbled through four small holes at the bottom of the glass cover for the electrode. The gaseous plasma surrounding the electrode contains several reactive species. The contact of the plasma bubble with the water then leads to the generation of a large amount of short- and long-lived ROS and RNS,

mainly including reactive oxygen atoms, anion and ions, including (O, O(^{1}D), $^1O_2$, O_2^+, and O_2^-), $^{\bullet}OH$, $ONOO^-$, NO, H_2O_2, NO_2^-, NO_3^-, O_3 (Mai-Prochnow et al., 2021).

High amounts of NO_3^- were detected in the freshly generated PAW and all of the other stored PAWs. NO_2^- were non-detectable in the stored PAWs. According to a previous study (Rathore et al., 2021a), NO_2^- in the PAW reacts with dissolved ozone and H_2O_2 to give NO_3^-, which makes NO_2^- less stable than NO_3^- in the PAW. At first, it seems unusual for the PAW-air to have a higher NO_3^- /NO_2^- content than the H_2O_2. However, other authors reported a similar result where a 20% ratio of $O_2/(O_2+N_2)$ (-equivalent to air) gas composition generated more NO_3^- and NO_2^-. One possible mechanism is that with the addition of O_2 in the gas, the atomic oxygen O emission can react with excited nitrogen species to form •NO, resulting in generation of more abundant NO_3^- and NO_2^- species (Girard et al., 2018).

This work also expands the PAW activity against bacterial biofilm over storage condition. We found that the 24h stored PAW still exhibited a 1-log reduction on the 24h *E. coli* biofilm cells grown on both of coupon surfaces and in the surrounding solution, which is similar to the antibacterial activity of the freshly generated PAW. The presence of H_2O_2, NO_3^-, and NO_2^- generated in the PAW were widely studied as the mechanisms behind the antibacterial activities of the PAW (Thirumdas et al., 2018). While H_2O_2, NO_2^-, and NO_3^- were detected by quantitative tests and they are strong oxidants, their impacts were limited in our system. More studies are needed to understand the antibiofilm activity of PAW treatment.

2.6 Conclusions

In summary, the direct treatment of plasma-activated water (PAW) can effectively remove 5-log of 24h *E. coli* biofilms grown on stainless-steel surfaces. The indirect PAW treatment achieved 1-log reduction after 30 minutes. The 10 min-generated PAW remain antibiofilm activity after 24h storage at 4°C. The long-live reactive species, especially H_2O_2 and NO^{3-}, remain active under the storage.

This research presents new knowledge on the use of BSD reactor to generate PAW and its efficacy on bacterial biofilms removal of direct and indirect application. It also presents the stability of stored

PAW and long-lived reactive species in the observed antibacterial efficacy. This has implications for drinking and wastewater water treatment, as well as possible treatment of food products or medical devices where conventional disinfection or sanitation is neither suitable, nor effective.

Utilising compressed atmospheric air as a gas input source is an economically viable option when generating PAW. This further underscores its attractiveness for use. Lastly, the plasma source used in this work also has the advantage of being small and portable making it suitable for diverse applications in the water treatment industry, food industry, clinical equipment sterilization, medicine, and environment.

2.7 References

Cámara, M., Green, W., MacPhee, C. E., Rakowska, P. D., Raval, R., Richardson, M. C., Slater-Jefferies, J., Steventon, K., & Webb, J. S. (2022). Economic significance of biofilms: a multidisciplinary and cross-sectoral challenge. *npj Biofilms and Microbiomes, 8*(1), 42. https://doi.org/10.1038/s41522-022-00306-y

Carrascosa, C., Raheem, D., Ramos, F., Saraiva, A., & Raposo, A. (2021). Microbial Biofilms in the Food Industry—A Comprehensive Review. *International Journal of Environmental Research and Public Health, 18*(4), 2014. https://doi.org/10.3390/ijerph18042014

Djemaoune, Y., Cases, E., & Saurel, R. (2019). The effect of high‐pressure microfluidization treatment on the foaming properties of pea albumin aggregates. *Journal of Food Science, 84*(8), 2242-2249. https://doi.org/10.1111/1750-3841.14734

Fernández-Gómez, P., Cobo-Díaz, J. F., Oliveira, M., González-Raurich, M., Alvarez-Ordóñez, A., Prieto, M., Walsh, J. L., Sivertsvik, M., Noriega-Fernández, E., & López, M. (2023). Susceptibility and transcriptomic response to plasma-activated water of Listeria monocytogenes planktonic and sessile cells. *Food Microbiology, 113*, 104252. https://doi.org/10.1016/j.fm.2023.104252

Ghimire, B., Szili, E. J., Patenall, B. L., Lamichhane, P., Gaur, N., Robson, A. J., Trivedi, D., Thet, N. T., Jenkins, A. T. A., Choi, E. H., & Short, R. D. (2021). Enhancement of hydrogen peroxide production from an atmospheric pressure argon plasma jet and implications to the antibacterial activity of plasma activated water. *Plasma Sources Science and Technology, 30*(3), 035009. https://doi.org/10.1088/1361-6595/abe0c9

Girard, F., Peret, M., Dumont, N., Badets, V., Blanc, S., Gazeli, K., Noël, C., Belmonte, T., Marlin, L., Cambus, J.-P., Simon, G., Sojic, N., Held, B., Arbault, S., & Clément, F. (2018). Correlations

between gaseous and liquid phase chemistries induced by cold atmospheric plasmas in a physiological buffer. *Physical Chemistry Chemical Physics, 20*(14), 9198-9210. https://doi.org/10.1039/C8CP00264A

Handorf, O., Pauker, V. I., Weihe, T., Schäfer, J., Freund, E., Schnabel, U., Bekeschus, S., Riedel, K., & Ehlbeck, J. (2021). Plasma-Treated Water Affects Listeria monocytogenes Vitality and Biofilm Structure. *Frontiers in Microbiology, 12*, 652481. https://doi.org/10.3389/fmicb.2021.652481

Mai-Prochnow, A., Bradbury, M., Ostrikov, K., & Murphy, A. B. (2015). Pseudomonas aeruginosa Biofilm Response and Resistance to Cold Atmospheric Pressure Plasma Is Linked to the Redox-Active Molecule Phenazine. *PLOS ONE, 10*(6), e0130373. https://doi.org/10.1371/journal.pone.0130373

Mai-Prochnow, A., Zhou, R., Zhang, T., Ostrikov, K. K., Mugunthan, S., Rice, S. A., & Cullen, P. J. (2021). Interactions of plasma-activated water with biofilms: inactivation, dispersal effects and mechanisms of action. *npj Biofilms and Microbiomes, 7*(1), 1-12. https://doi.org/10.1038/s41522-020-00180-6

Nicol, M. J., Brubaker, T. R., Honish, B. J., Simmons, A. N., Kazemi, A., Geissel, M. A., Whalen, C. T., Siedlecki, C. A., Bilén, S. G., Knecht, S. D., & Kirimanjeswara, G. S. (2020). Antibacterial effects of low-temperature plasma generated by atmospheric-pressure plasma jet are mediated by reactive oxygen species. *Scientific Reports, 10*(1), 3066. https://doi.org/10.1038/s41598-020-59652-6

Park, J. Y., Park, S., Choe, W., Yong, H. I., Jo, C., & Kim, K. (2017). Plasma-Functionalized Solution: A Potent Antimicrobial Agent for Biomedical Applications from Antibacterial Therapeutics to Biomaterial Surface Engineering. *ACS Applied Materials & Interfaces, 9*(50), 43470-43477. https://doi.org/10.1021/acsami.7b14276

Rathore, V., Patel, D., Butani, S., & Nema, S. K. (2021). Investigation of Physicochemical Properties of Plasma Activated Water and its Bactericidal Efficacy. *Plasma Chemistry and Plasma Processing, 41*(3), 871-902. https://doi.org/10.1007/s11090-021-10161-y

Rothwell, J. G., Alam, D., Carter, D. A., Soltani, B., McConchie, R., Zhou, R., Cullen, P. J., & Mai-Prochnow, A. (2022). The antimicrobial efficacy of plasma-activated water against Listeria and E. coli is modulated by reactor design and water composition. *Journal of Applied Microbiology, 132*(4), 2490-2500. https://doi.org/10.1111/jam.15429

Sen, Y., & Mutlu, M. (2013). Sterilization of Food Contacting Surfaces via Non-Thermal Plasma Treatment: A Model Study with Escherichia coli-Contaminated Stainless Steel and Polyethylene Surfaces. *Food and Bioprocess Technology, 6*(12), 3295-3304. https://doi.org/10.1007/s11947-012-1007-2

Sergeichev, K. F., Lukina, N. A., Sarimov, R. M., Smirnov, I. G., Simakin, A. V., Dorokhov, A. S., & Gudkov, S. V. (2021). Physicochemical properties of pure water treated by pure argon

plasma jet generated by microwave discharge in opened atmosphere. *Frontiers in Physics, 8*, 614684. https://doi.org/10.3389/fphy.2020.614684

Shen, J., Tian, Y., Li, Y., Ma, R., Zhang, Q., Zhang, J., & Fang, J. (2016). Bactericidal Effects against S. aureus and Physicochemical Properties of Plasma Activated Water stored at different temperatures. *Scientific Reports, 6*(1), 28505. https://doi.org/10.1038/srep28505

Thirumdas, R., Kothakota, A., Annapure, U., Siliveru, K., Blundell, R., Gatt, R., & Valdramidis, V. P. (2018). Plasma activated water (PAW): Chemistry, physico-chemical properties, applications in food and agriculture. *Trends in food science & technology, 77*, 21-31. https://doi.org/10.3390/pr11072213

Toyofuku, M., Inaba, T., Kiyokawa, T., Obana, N., Yawata, Y., & Nomura, N. (2016). Environmental factors that shape biofilm formation. *Biosci Biotechnol Biochem, 80*(1), 7-12. https://doi.org/10.1080/09168451.2015.1058701

Vyas, H. K. N., Xia, B., Alam, D., Gracie, N. P., Rothwell, J. G., Rice, S. A., Carter, D., Cullen, P. J., & Mai-Prochnow, A. (2023). Plasma activated water as a pre-treatment strategy in the context of biofilm-infected chronic wounds. *Biofilm, 6*, 100154. https://doi.org/10.1016/j.bioflm.2023.100154

Wang, Q., & Salvi, D. (2021). Evaluation of plasma-activated water (PAW) as a novel disinfectant: Effectiveness on Escherichia coli and Listeria innocua, physicochemical properties, and storage stability. *LWT, 149*, 111847. https://doi.org/10.1016/j.lwt.2021.111847

Xia, B., Vyas, H. K. N., Zhou, R., Zhang, T., Hong, J., Rothwell, J. G., Rice, S. A., Carter, D., Ostrikov, K., Cullen, P. J., & Mai-Prochnow, A. (2023). The importance of superoxide anion for Escherichia coli biofilm removal using plasma-activated water. *Journal of Environmental Chemical Engineering, 11*(3), 109977. https://doi.org/10.1016/j.jece.2023.109977

Xu, Z., Zhou, X., Yang, W., Zhang, Y., Ye, Z., Hu, S., Ye, C., Li, Y., Lan, Y., & Shen, J. (2020). In vitro antimicrobial effects and mechanism of air plasma‐activated water on Staphylococcus aureus biofilm. *Plasma Processes and Polymers, 17*(8), 1900270. https://doi.org/10.1002/ppap.201900270

Zhou, R., Zhang, T., Zhou, R., Wang, S., Mei, D., Mai-Prochnow, A., Weerasinghe, J., Fang, Z., Ostrikov, K. K., & Cullen, P. J. (2021). Sustainable plasma-catalytic bubbles for hydrogen peroxide synthesis. *Green Chemistry, 23*(8), 2977-2985. https://doi.org/10.1039/D1GC00198A

Zhou, R., Zhou, R., Wang, P., Xian, Y., Mai-Prochnow, A., Lu, X., Cullen, P., Ostrikov, K. K., & Bazaka, K. (2020). Plasma-activated water: Generation, origin of reactive species and biological applications. *Journal of Physics D: Applied Physics, 53*(30), 303001. https://doi.org/10.1088/1361-6463/ab81cf

Supplementary information

S2.1 Standard curves of H_2O_2, $NaNO_3$, and $NaNO_2$ for RONS measurement

A serial dilution of H_2O_2, $NaNO_3$, and $NaNO_2$ solurion were prepared. The absorbance of these solutions were determined by UV-vis spectroscopy. The standard curves were calculated for further RONS measurements for PAW.

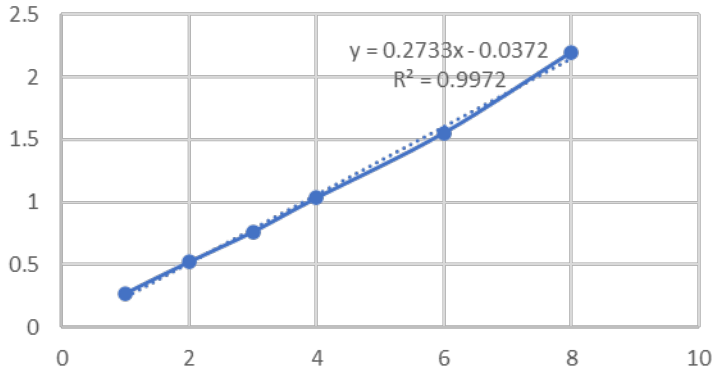

Figure S2.1 Standard curve of $NaNO_2$ solution. Concentration unit is ppm. Absorbance was determined at 526 nm.

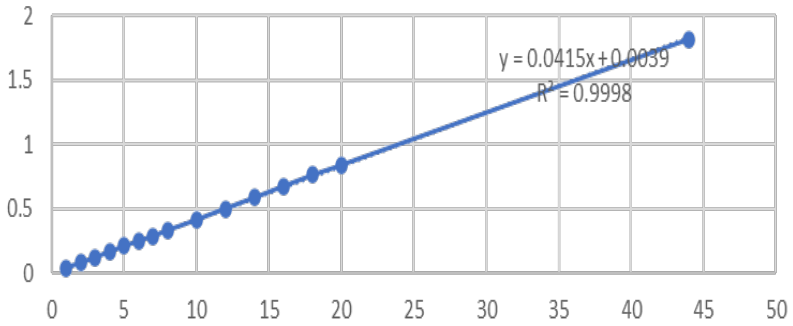

Figure S2.2 Standard curve of $NaNO_3$ solution. Concentration unit is ppm. Absorbance was determined at 220 nm.

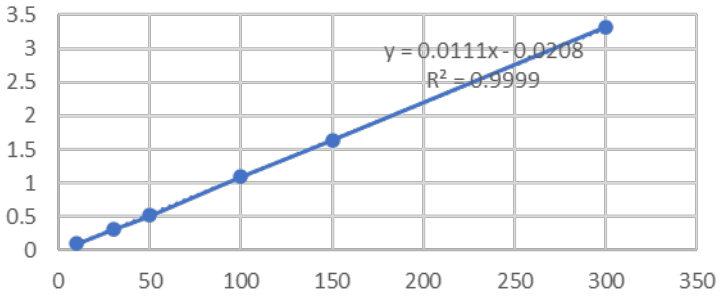

Figure S2.3 Standard curve of H_2O_2 solution. Concentration unit is ppm. Absorbance was determined at 408 nm.

S2.2 Comparison of cell viability under different treatments

The viability of biofilm cells exposed with indirect PAW treatment for 1 h was compared with bubble water, MilliQ control, and tap water. There was approximately 61% reduction rate of PAW treated biofilm cells compared to the MilliQ control. While for other treatment, there was no significant difference between bubbling water and tap water compared to the control.

(A) 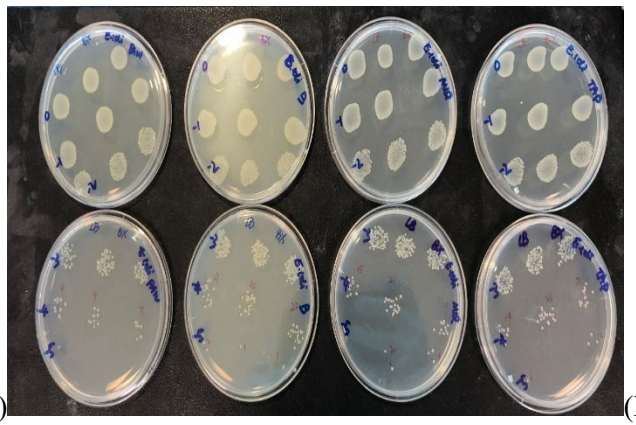 (B) 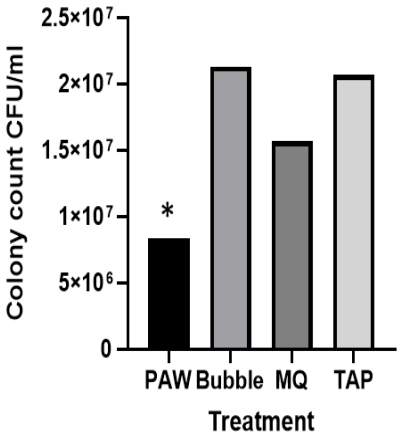

Figure S2.4 Cell viability of 24h *E. coli* ATCC25922 biofilm cells under PAW, bubbling water, MilliQ water, and Tap water treatment for 1 h. (A) Spot plating images; (B) CFU counting bar plot (P<0.05, n=3).

3 Chapter 3 The importance of superoxide anion for Escherichia coli biofilm removal using plasma-activated water

Authorship contribution statement

Binbin Xia: Conceptualization, Methodology, Investigation, Validation, Data curation, Formal analysis, Writing – original draft preparation;

Heema Kumari Nilesh Vyas: Investigation, Methodology, Writing – reviewing and editing.

Renwu Zhou*: Investigation, Formal data analysis, Writing – reviewing, editing.

Tianqi Zhang: Resources.

Jungmi Hong: Investigation, Data curation, Formal data analysis, Writing – reviewing and editing.

Joanna G. Rothwell: Writing – reviewing and editing.

Scott A. Rice: Writing – reviewing, Project administration, Funding acquisition.

Dee Carter Writing – reviewing, Project administration, Funding acquisition.

Kostya (Ken) Ostrikov: Writing – review and editing.

Patrick J. Cullen: Supervision, Sources.

Anne Mai-Prochnow*: Conceptualization, Supervision, Investigation, Formal data analysis; Writing-review and editing, Funding acquisition, Project administration.

* corresponding author

3.1 Abstract

Microbial biofilms cause contaminations in different environmental settings, including pipelines, filters, membranes, food and processing infrastructure. They ultimately pose a major risk to human health and necessitate costly cleaning and repair. Cold plasma, a partially ionised gas, and plasma-activated water (PAW) exhibit powerful disinfectant activity. However, the optimal generating conditions, such as the choice of gas used to produce PAW, remain unclear. Here, a range of different PAWs were generated from argon, nitrogen, air, and oxygen in a plasma bubble spark discharge (BSD) reactor capable of directly treating *Escherichia coli* (ATCC 25922) biofilms directly. We measured the reactive oxygen and nitrogen species (RONS) (H_2O_2, NO_3^-, NO_2^-) in PAW and the excited species via optical emission spectroscopy (OES). PAW generated using oxygen (PAW-O_2) was the most effective and completely removed *E. coli* biofilms on stainless steel surfaces. Confocal microscopy demonstrated that PAW treatment removed most biofilm cells from the surface with only a few dead cells remaining. We demonstrated that intracellular ROS level increases significantly in the PAW-O_2-treated biofilms. Using molecular scavengers, we showed that superoxide anion radical ($\bullet O_2^-$) played a critical role in the inactivation of *E. coli* biofilms. We also confirmed the generation of $\bullet O_2^-$ in the PAW-O_2 via electron paramagnetic resonance (EPR) spectrometry. The potential chemical reactions that occurred in PAW were hypothesized via optical emission spectra (OES). Our results demonstrate the importance of input gas and plasma operating conditions to maximise effective RONS production for optimal biofilm removal under real environmental and industry-relevant conditions.

3.2 Introduction

Contamination of surfaces in contact with biofilm-forming bacteria is a major problem for drinking water supplies, industrial water processing systems, membranes, filters, and food processing stainless-steel units (Dula et al., 2021; Lu et al., 2013; Wan et al., 2021). Biofilms are particularly hard to eradicate because of their higher resistance to antimicrobials and disinfectants compared to planktonic cells (Chakraborty et al., 2021; Costerton et al., 1999). Such contamination can lead to equipment failure, energy losses, product contamination, and environmental pollution, resulting in adverse human health outcomes and significant costs to industries (Cámara et al., 2022). Therefore, a new decontamination method is critically needed that can effectively decontaminate resistant biofilms, whilst also avoiding damage to the surface of the treated material or leaving toxic chemical residues.

One promising treatment method with these characteristics is cold atmospheric plasma (CAP) processing. Plasma is the fourth state of matter and is generated when a gas is exposed to an electric field voltage, leading to the ionisation of gas molecules and the generation of diverse excited and reactive species (Mai-Prochnow et al., 2021). CAP presents a broad range of antimicrobial activity, including antibacterial, antiviral, and antifungal actions (Chen et al., 2018; Gilmore et al., 2018; Jenns et al., 2022; Renn et al., 2022; Xu et al., 2023). The antimicrobial activity is mainly attributed to the formation of reactive oxygen and nitrogen species (RONS) (Chen et al., 2018; D. Guo et al., 2021; Thirumdas et al., 2018; Zhao et al., 2022). RONS encompasses both transient species, such as hydroxyl radical (OH), atomic oxygen (O), peroxynitrite anion (ONOO-), and superoxide anion (O_2^-), which have been shown to have a half-life of just a few seconds, or even less than one second, as well as more stable species like ozone (O_3), hydrogen peroxide (H_2O_2), and nitrogen oxides (NO_x), which can persist for several minutes, days, or even years (Zhou et al., 2020b).

An innovative way of using CAP as an antimicrobial technology is to generate the plasma discharge in water to produce plasma-activated water (PAW) (Mai-Prochnow et al., 2021). PAW has the potential to be used as a washing step and is suitable for large-scale applications in chemical engineering industries (Lin et al., 2021). It is appropriate for disinfecting sensitive and hard-to-access

surfaces, including food and heat-sensitive devices (Mai-Prochnow et al., 2020; Rathore & Nema, 2021).

While plasma is generally effective, the optimal generating conditions and mode of action are still unclear. Diverse PAW production methods have been explored, including plasma discharge above the water surface, plasma discharges in bubbles dissolved in the water, and direct plasma discharges in the water (Gao et al., 2022; Kaushik et al., 2018; Zhou et al., 2020b). The design and operating conditions significantly affect the plasma composition (Bălan et al., 2018; Man et al., 2022; Thirumdas et al., 2018; Wang et al., 2018; Zhou et al., 2020b). Not surprisingly, the use of different operating gases leads to the generation of different cocktails of active species, which determine the antimicrobial efficacy (Rathore et al., 2021a; Yahaya et al., 2021). While CAP can be generated using a range of gases or gas mixtures, different gases lead to the formation of unique combinations of reactive species. Air, argon, nitrogen and oxygen are frequently used as working gases (Cullen et al., 2018; Li et al., 2022b; Muhammad et al., 2018; Stapelmann et al., 2008; Wang et al., 2021), and in particular, the addition of oxygen leads to the generation of ROS with strong antibacterial effects (Yahaya et al., 2021).

An important aspect when generating PAW is the electrode design. Most PAW studies to date typically use a plasma discharge that is generated close to the water surface (Haghighat et al., 2017; Li et al., 2017; Ma et al., 2015). Such a design can limit the penetration of the plasma species that are formed in the gas phase into the water. On the other hand, our previous research demonstrated that an underwater plasma discharge-generated PAW provided a higher antimicrobial reactivity compared to conventional plasma jet reactors (Royintarat et al., 2019). The current study utilises a submerged PAW system called a bubble spark discharge (BSD) (Rothwell et al., 2022) which allows a much larger surface area for reactive species to diffuse into the water via plasma gas bubbles in a system. This BSD system has previously shown to exhibit acute antimicrobial activity against planktonic bacteria directly using air as the discharge gas (Rothwell et al., 2022). Other underwater plasma discharge electrodes have also been shown to have antimicrobial activity against planktonic bacteria cells (Mai-Prochnow et al., 2020; Rathore et al., 2021a).

While most of the research studies have investigated the antimicrobial efficacy of PAW against planktonic bacteria, the bacteria biofilm state that survives on surfaces thrives the real threat to several industries. Therefore, it is critical to test the antimicrobial efficacy of PAW against biofilms. In the present study, *E. coli* biofilms grown on stainless-steel surfaces were chosen to study the disinfectant efficacy of the PAW generated with different gas sources (argon, nitrogen, oxygen, and atmospheric air). We found that the physical and chemical properties and the resulting antimicrobial efficacy of the generated PAW vary depending on the chosen gas source. Therefore, in this study, our focus was to identify the chemical species formed in the PAW generated via the differing gas inputs and study their pH, oxidation-reduction potential (ORP), and electrical conductivity (EC). Then *E. coli* biofilms treated with the PAW were investigated for their viability (colony forming units, live/dead staining coupled with confocal microscopy), and intracellular biofilm ROS accumulation.

3.3 Materials and Methods

3.3.1 Strain and biofilm formation

Escherichia coli ATCC 25922 was routinely maintained on tryptic soy agar (TSA) (tryptone (pancreatic digest of casein) 17.0 g/L, soytone (peptic digest of soybean) 3.0 g/L, glucose 2.5 g/L, sodium chloride 5.0 g/L, dipotassium phosphate 2.5 g/L, agar 15 g/L). One colony from a fresh agar plate was inoculated into 10 mL tryptic soy broth TSB) and incubated for 14 h at 37 °C, shaking at 160 rpm. For biofilm formation, the overnight cultures were diluted 1/100 to obtain an approximate cell density of 10E5 CFU/mL. 1 mL of the diluted culture was inoculated into wells of a 24-well plate containing sterile stainless-steel coupons (diameter: 12.7 mm and thickness: 3.8 mm from BioSurface Technologies, Bozeman, Montana, USA). Plates were incubated for 48 h at 30 °C with 110 rpm shaking to allow for cell attachment and subsequent biofilm formation.

3.3.2 Plasma treatment

The plasma bubble reactor (PlasmaLeap Technologies, Sydney) consists of a metal rod high voltage electrode inside a quartz tube (Figure 3.1) with four holes (2 µm diameter) evenly spaced at the immersed end to allow for the plasma discharge to contact the water. The gas flow was controlled by

a digital M series mass flow meter (Alicat Scientific, United States). Coupons with the attached biofilm were aseptically removed from the well plate and placed into 250 mL Schott bottles containing 100 mL sterile MilliQ (Figure 3.1). The plasma bubble reactor was submerged in the water containing the coupons for direct plasma chemical experiment (Lin et al., 2021).

The plasma-activated water (PAW) was generated as previously described (Rothwell et al., 2022). Briefly, a Leap100 (PlasmaLeap Technologies, Sydney) power source was used with an input voltage of 150 V, a discharge frequency of 1500 Hz, a resonance frequency of 60 kHz and a duty cycle of 100 µs. The treatment time was 10min with 1 standard liter per minute (slm) of gas flow. Four different gases were tested, including argon (Ar), nitrogen (N_2), air, and oxygen (O_2). As a control, coupons were placed into 100 mL sterile MilliQ for 10min.

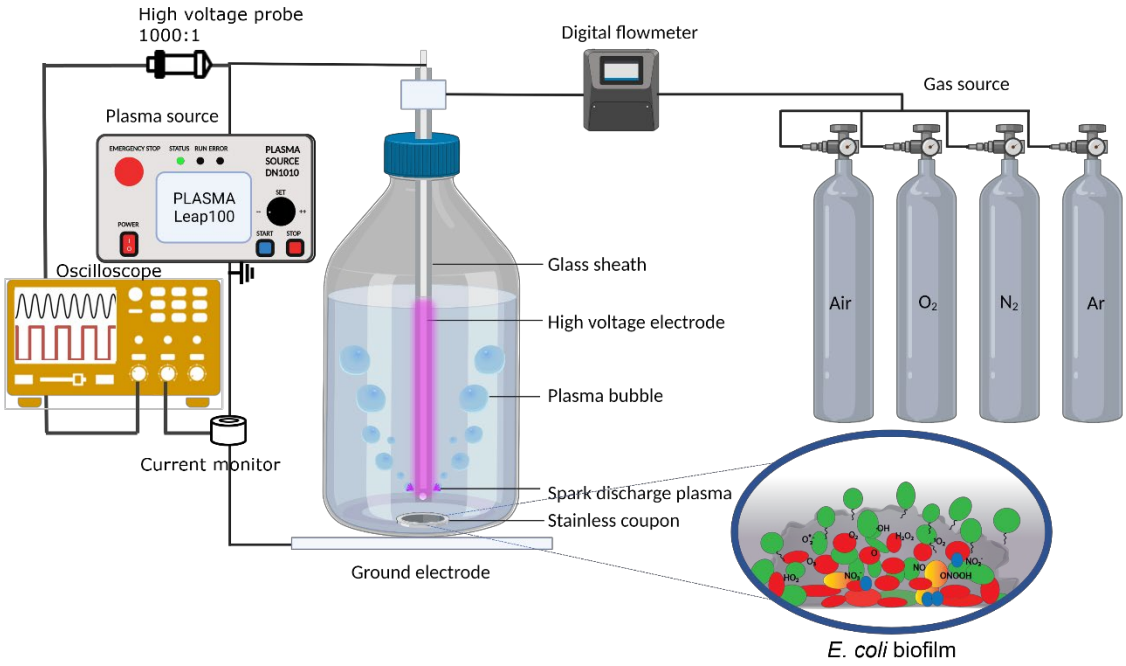

Figure 3.1. A schematic illustration of the *in-situ* biofilm treatment using plasma-activated water (PAW) generated by a bubble spark discharge (BSD) plasma reactor. An *E. coli* biofilm was grown on a stainless-steel coupon and placed at the bottom of the Schott bottle containing 100mL of MilliQ water. The plasma bubble reactor consists of a high-voltage electrode and a glass sheath. To generate spark discharge plasma, the high-voltage electrode was powered by PlasmaLeap100. The voltage and current of the power source are monitored by the oscilloscope equipped with a high-voltage probe and a current monitor.

3.3.3 Cell enumeration

Immediately following the PAW treatment, coupons were extracted from the treatment bottle and placed into a Falcon tube containing 2 mL 1x phosphate buffered saline (PBS). The biofilm was removed from the coupon surface by scraping it with a sterile flat-end spatula and placed into falcon tubes. The Falcon tubes were then submerged in a sonicating water bath for 3 min at 45 kHz followed by 10 s vortexing to ensure complete dislodgement of biofilms. This did not affect cell viability (data not shown). Serial dilutions were then drop-plated (10 µL) onto TSA in triplicates. Plates were incubated overnight at 37 °C before determining the colony-forming units (CFU).

3.3.4 PAW reactive species measurements

Concentrations of hydrogen peroxide (H_2O_2), nitrate (NO_3^-), and nitrite (NO_2^-) along with pH, temperature, and electrical conductivity were assessed in the PAW generated using argon, N_2, air, and O_2 gases for 10 min. The concentration of H_2O_2 was measured by a titanium sulphate method (Zhou et al., 2021) where H_2O_2 reacts with titanium oxysulphate ($TiOSO_4$) resulting in a yellow-coloured complex (pertitanic acid) that is quantified with UV-Vis spectroscopy at 408 nm (the standard curve of H_2O_2 is shown in supportive information Figure S3.1). NO_3^- and NO_2^- species were measured using a Hanna Instrument multiparameter photometer (HI83399) with colorimetric nitrate kit (HI93766-50) and colorimetric nitrite reagent (HI93708-0), respectively. All standards were prepared in MilliQ water. pH, temperature, electrical conductivity (EC), and oxidation-reduction potential (ORP) were measured using a Hanna Instrument pH/ISE/EC meter (HI5522) supplied with a double junction pH electrode (HI12300), temperature probe (HI7662-W), a four-ring conductivity probe (HI76312), and an OPR electrode (HI3131), respectively.

3.3.5 Optical emission spectroscopy

The optical emission spectra (OES) of the plasma discharges generated in nitrogen, air, argon, and oxygen at 150 V, 1500 Hz were obtained by a spectrometer (Andor Shamrock SR-500i optical

emission spectrometer, Oxford Instruments, UK) referred to a recent published method (Li et al., 2022a).

3.3.6 Molecular scavenger experiments

To investigate the effect of specific active species that were generated in the plasma, a range of molecular scavengers were used as previously described (Rothwell et al., 2022), including 200 mM Mannitol (scavenges hydroxyl radical), 100 µm uric acid (scavenges ozone), 20 mM Tiron (scavenges superoxide anion), 100 mM N-Acetyl-L-cysteine (general antioxidant and free radical scavenger), and 10 mM Sodium pyruvate (scavenges hydrogen peroxide). The scavengers were added directly into the treatment bottle before the plasma generation commenced.

3.3.7 EPR measurement of superoxide anion radicals

The formations of superoxide and superoxide-related hydroxyl radicals were detected with an electron paramagnetic resonance (EPR) spectrometer (Bruker Elexys E580, Bruker Inc., Billerica, MA, USA) using a spin trap DMPO (5,5-dimethylpyrroline-N-oxide). Spectra were recorded at room temperature, with microwave power at 10 dB and a modulation amplitude of 2.0 Gauss. The scanning time was 60 s and repeated 5 times in all experiments. The PAW was activated in 100 mL of MilliQ water using 4-hole bubble spark dielectric plasma reactor with an oxygen flow rate of 1slm. After 60s of activation, 125 µL of the PAW-O_2 was collected and was measured immediately by EPR after mixing with 11.5 µL of pure DMPO. The PAW-O_2 with 20 mM Tiron (PAW-O_2 + Tiron) and MilliQ water bubbled with O_2 gas (but no plasma) with the same amount of DMPO were used as the control.

3.3.8 Confocal microscopy

Live/dead staining was performed on the biofilms formed on the coupon surfaces (Syto9 for viable cells and propidium iodide for dead cells, Invitrogen) according to the manufacturers' instructions. Briefly, 10µL of the staining solution was added directly to the coupons with the attached biofilms and incubated in the dark for 10 min. The coupons were then transferred to a microscopy dish with a glass coverslip bottom and examined using a Nikon Ti-E confocal microscope equipped with a 40x

objective. The Excitation/Emission wavelengths (Ex/Em) for Syto9 and PI are 480/500nm and 490/635nm, respectively.

3.3.9 Detection of intracellular ROS

Biofilms were stained with 2',7'-dichlorofluorescin diacetate (DCFDA) to assess intracellular ROS according to the manufacturers' instructions. Briefly, a 96-well plate containing 48h *E. coli* biofilms was washed once with 150 µL MilliQ and challenged for 30 min with control (MilliQ), PAW-O_2, and PAW-O_2 + Tiron scavenger. Biofilms were then stained with 150 µL of 20 µM DCFDA solution (or 150 µL MilliQ for background controls) and incubated in the dark for 30 min. Once stained, the excess stain was removed, and biofilms were washed once with 150 µL MilliQ. Fluorescence was detected via ClarioStar plate reader at an Ex/Em of 485-15 nm/535-15 nm.

3.3.10 Statistical analysis

Experiments were performed 3 times and values are expressed as mean ± standard deviation ($\mu \pm \sigma$). A parametric, unpaired t-Test (2 tail, $p<0.05$) or a One-way ANOVA (with Tukeys multiple comparisons test, $p<0.05$) was performed where appropriate to identify significant differences in log reduction of each sample compared to the control.

3.4 Results and Discussion

3.4.1 Biofilm removal using different input gases for the generation of PAW

Biofilms grown on stainless steel coupons were placed into the Schott bottle during the 10 min PAW generation time and remaining viable cells were enumerated by CFU counting. A significant reduction in CFU was observed for the PAW generated with all of the 4 gases when compared to the control (Figure 3.2), with a 2-log reduction for the PAW-air, 1 log for the PAW-N_2 and 0.5 log for the PAW-Ar. A complete reduction in viability was only seen for biofilms treated with PAW-O_2 (6-log reduction). To further characterize the kinetic inactivation of PAW on 48h-grown *E. coli* biofilm, the D-value (Decimal value: exposure time to achieve 1-log reduction) was calculated. Our results show that PAW-O_2 exhibited the shortest D-value (1.72 minutes), followed by PAW-Air (5.29 minutes), PAW-N_2 (10.91 minutes), and PAW-Ar (15.56 minutes). Several other studies use a D-value to shed light on the inactivation kinetics of cold plasma mediated cell death (Flynn et al., 2019; Soni et al., 2021) . Interestingly, the achieved D-values ranges considerably, depending on the initial bacterial concentration, attachment surface and plasma treatment conditions. A study by Sen and Mutlu (2013) calculated the D-value of pure oxygen DBD plasma that can effectively inactivate *E. coli* grown on stainless steel surfaces. The most efficient result with the fastest kinetics had a larger D-value of 22.9±3.3 minutes when powered by 100 Watt plasma compared to our study. Recent research by Fernández-Gómez et al., (2023) achieved a D-value of 11.3 min for *L. monocytogenes* biofilms with a final comparable (5.6-log) reduction in a stainless steel exposed to PAW generated by a surface DBD cold plasma reactor for 30 minutes.

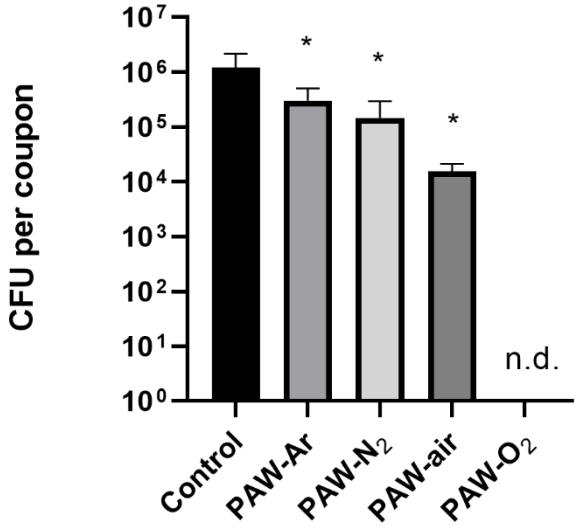

Figure 3.2. Reduction of *E. coli* biofilms using PAW generated in argon, nitrogen, air, and oxygen assessed by CFU. 48h biofilms were grown on stainless steel coupons and treated with PAW generated with different gases in a bubble reactor. All four treatment conditions were significantly different from the control, but only PAW-O_2 caused a complete loss of biofilm viability ($P < 0.05$, unpaired t-Test, n=3).

While several studies have found PAW to be strongly antibacterial for planktonic cells (Rathore et al., 2021b; Shen et al., 2016b), the reduction of biofilm cells to undetectable levels is a rare finding. Here, after only a 10-min treatment, we have demonstrated the efficacy of our PAW, which is a very promising result given that biofilms are highly resistant to most antimicrobials and removal strategies. As summarised in Table 3.1, Pan et al(Pan et al., 2017) achieved a comparable (6-log) reduction of *Enterococcus faecalis* biofilm in a dental unit waterline system treated by the PAW generated by 260L/h of air plasma jet, however, this consumed around four times more gas than this study. The PAW generated by BSD reactor supplied with Argon exhibited biofilm removal activity on both gram-positive and gram-negative bacteria-formed biofilm, ranging from 2-3.6 log reduction (Mai-Prochnow et al., 2016). Other studies report considerably more modest reductions in biofilms by PAW (Tan & Karwe, 2021).

The inactivation kinetics of *E. coli* biofilms when exposed to plasma are suggested to have a three phases mechanism, including the destruction of DNA by UV irradiation, erosion of the microorganism through intrinsic photo-desorption, and etching (Sen & Mutlu, 2013). However, as the

treatment has complex effects on cells, for example, gene regulation that affect the metabolism of starch and sucrose and thus carbohydrate transport and metabolism functions (Fernández-Gómez et al., 2023), determining the survival curve of bacterial biofilms that are exposed to plasma remains a challenging task.

Table 3.1 Comparisons between the results of this study and other relevant research

Reactor	PAW-supplied gas (input volume)	Biofilm bacteria strains	Reduction (log_{10})	Reference
BSD	Argon (3.1 L/min)	*Pseudomonas aeruginosa (PAO1)* *Pseudomonas libanensis* *Enterobacter cloacae*	3.3-3.6 log	(Mai-Prochnow et al., 2016)
BSD	Argon (3.1 L/min)	*Kocuria carniphila*	2 log	(Mai-Prochnow et al., 2016)
Plasma jet	Air (260L/h)	*Enterococcus faecalis*	6 log	(Pan et al., 2017)
Plasma jet	Air (42.5L/h)	*Enterobacter aerogenes*	3.0-3.8 log	(Tan & Karwe, 2021)
BSD	O_2 (1L/min)	*E. coli (ATCC25922)*	6.1 log	This study

3.4.2 Characterisation of PAW generated with different gases

We have demonstrated that the PAW-O_2 leads to the highest CFU reduction of *E. coli* biofilms, but the PAW generated with three other gases (Ar, N_2, and air) also showed antimicrobial activity. It is widely accepted that RONS produced in the PAW are responsible for their antibacterial effect (Girard et al., 2018; Mai-Prochnow et al., 2015; Sergeichev et al., 2021). The amount and type of RONS in the different PAW types will significantly affect antimicrobial activity. The formation of RONS in PAW is complex as there are many physical and chemical properties in play. In our plasma-generating experimental design, using a bubble spark discharge (BSD) electrode, a constant gas flow results in the plasma being bubbled through four small holes at the bottom of the glass cover for the electrode. The gaseous plasma surrounding the electrode contains several reactive species. The contact of the plasma bubble with the water then leads to the generation of a large amount of short- and long-lived ROS and RNS, mainly including reactive oxygen atoms, anion and ions, including (O, O(^{1}D), $^1O_2$, O_2^+, and O_2^-), $^{\bullet}OH$, $ONOO^-$, NO, H_2O_2, NO_2^-, NO_3^-, O_3 (Mai-Prochnow et al., 2021). Because the highest CFU reduction was observed when biofilms were treated with the PAW-O_2, we

hypothesised a higher concentration of certain antimicrobial species were generated in the PAW-O_2 compared to the other PAWs. To characterise the physical and chemical properties of the four different PAW, types of ROS (H_2O_2), and RNS (NO_2^-, NO_3^-) as well as the pH, temperature, electronic conductivity, and ORP were determined.

H_2O_2 (a known antimicrobial RONS generated in PAW) was predominant in the PAW-Ar and the PAW-O_2 (Figure 3.3A). Specifically, after 10 min plasma treatment, PAW-Ar showed the highest amount of H_2O_2 (54.94 ± 1.39 mg/L) while the PAW-air showed the lowest amount of H_2O_2 (4.10 ± 0.19 mg/L. The PAW-O_2 (15.09 ± 0.38 mg/L) showed a similar amount of H_2O_2 compared to the PAW-N_2 (13.95 ± 0.24 mg/L). A high ROS concentration such as H_2O_2 is often linked to bactericidal efficacy of the PAW (Ghimire et al., 2021). However, our CFU results indicate the highest antimicrobial activity for the PAW-O_2 and not the PAW-Ar that had the highest H_2O_2 levels, indicating that H_2O_2 is not the main reactive species responsible for biofilm removal in our study. Nevertheless, H_2O_2 may still contribute to bacterial inactivation. In the acidic environment of the PAW, H_2O_2 concentration along with the O_2^- radical contributes mostly to the oxidation properties of the PAW (Thirumdas et al., 2018). However, in contrast to our results, it was found that the PAW (air) generated a higher amount of H_2O_2 compared to the PAW (nitrogen) (Rathore et al., 2021a). The authors contributed this to the formation of more NOx species in air spark plasma leading to the consumption of H_2O_2 in the PAW (air) compared to the PAW (nitrogen).

High amounts of NO_3^- and NO_2^- were detected in the PAW-air (NO_3^-: 101.40 ± 1.56 mg/L; NO_2^-: 2.00 ± 1.00 mg/L) and lower amounts in the PAW-N_2 (NO_3^-: 23.53 ± 3.49 mg/L; NO_2^-:1.67 ± 0.58 mg/L), (Figure 3.3A), NO_3^- and NO_2^- were non-detectable in the PAW-Ar and the PAW-O_2. According to a previous study (Rathore et al., 2021a), NO_2^- in the PAW reacts with dissolved ozone and H_2O_2 to give NO_3^-, which makes NO_2^- less stable than NO_3^- in the PAW. At first, it seems unusual for the PAW-air to have a higher NO_3^- /NO_2^- content than the PAW-N_2. However, other authors reported a similar result where a 20% ratio of O_2/(O_2+N_2) (-equivalent to air) gas composition generated more NO_3^- and NO_2^- than 100% N_2. One possible mechanism is that with the addition of O_2

in the gas, the atomic oxygen O emission can react with excited nitrogen species to form •NO, resulting in generation of more abundant NO_3^- and NO_2^- species (Girard et al., 2018).

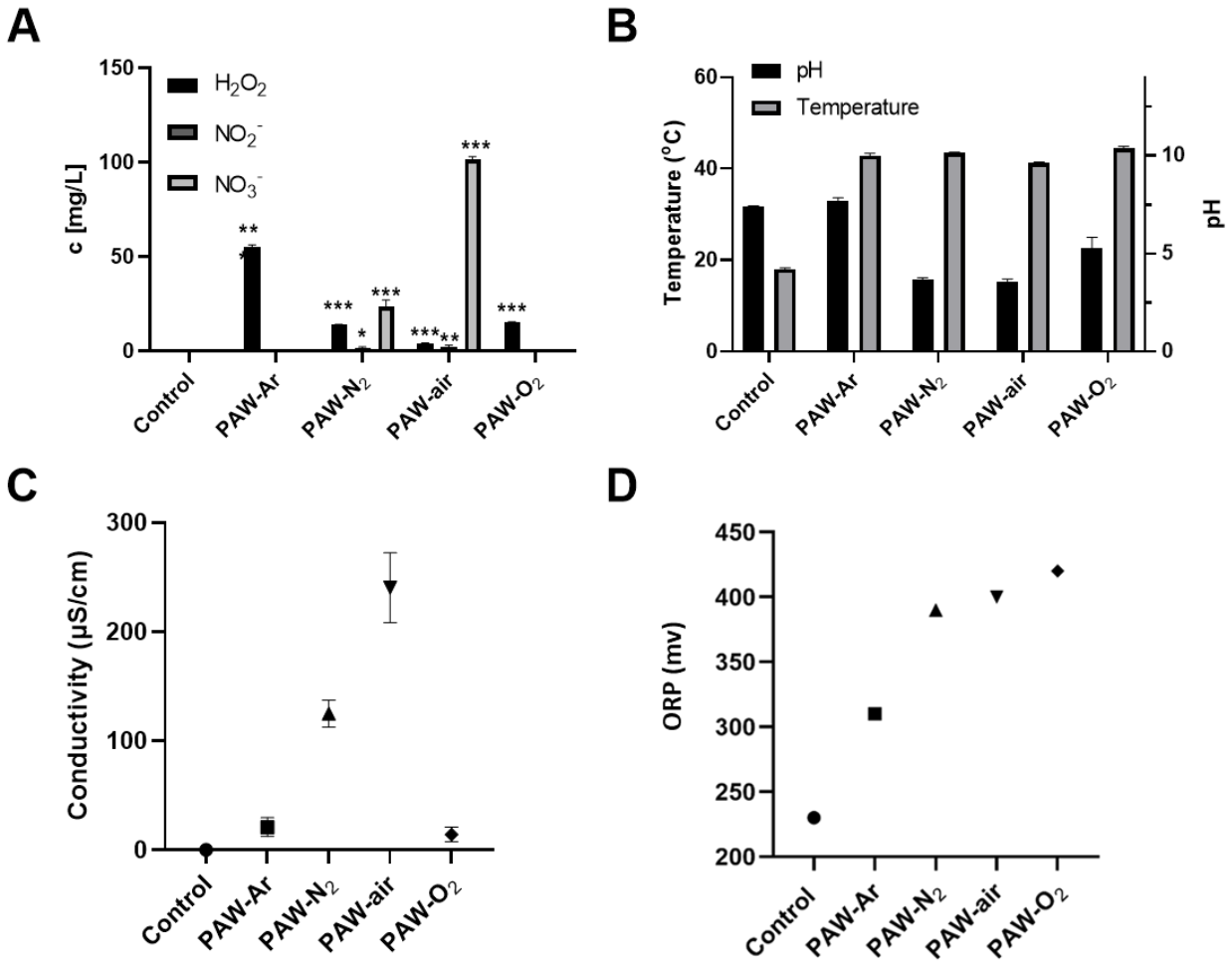

Figure 3.3. Physical and chemical characterisation of PAW-Ar, PAW-N_2, PAW-air and PAW-O_2. A) reactive oxygen and nitrogen species of hydrogen peroxide (H_2O_2), (NO_3^-), and nitrite (NO_2^-), B) pH and temperature, C) electric conductivity, and D) oxidation-reduction potential (ORP) values of PAW using four different gas sources (argon, N_2, air, and O_2) at 10 minutes treatment time. Error bars represent standard deviation of three experiment repetitions.

PAW has been shown to have a low pH and this may further contribute to its antimicrobial activity (Ma et al., 2015; Xu et al., 2020). The negative charge of some RNS (NO_3^- and NO_2^-) can lead to the acidification of the solution (Royintarat et al., 2019), which might catalyze the antibacterial activity of PAWs (Chen et al., 2018; D. Guo et al., 2021; Zhao et al., 2022). As shown in Figure 3.3B, the lowest

pH value was obtained when the PAW is generated using air (3.55 ± 0.16) with similarly low pH values ($p>0.05$) for the PAW-N_2 (3.67 ± 0.09) and the PAW-O_2 (5.29 ± 0.54) In contrast the pH of the PAW-Ar (7.67 ± 0.02) remained similar to the control (7.41 ± 0.02) which is due to the lack of NO_x species (Bolouki et al., 2021). A recent study of plasma water with Ar gas using a DBD plasma jet reactor obtained a similar pH compared to our result (pH ranging from 6 to 8) (Bolouki et al., 2021). The PAW-O_2 obtained a higher pH value than the PAW-N_2 and the PAW-air. This is similarly due to the lack of nitrogen which results in lower concentrations of NO_3^- and NO_2^- ions in the PAW (Rathore et al., 2021a). Notably, there is no significant difference in the temperature among four types of PAWs used in this study, ranging from 41.27 ± 0.15 ℃ to 44.50 ± 0.36 ℃ (Fig. 3B). Other studies also found that the effect of temperature can be insignificant on the antimicrobial activity against bacteria biofilms (Handorf et al., 2020).

To further characterise the PAW activity, the electrical conductivity (EC) of the PAW generated using different gases was determined. EC is a measure of how easily an electrical charge can pass through a material or liquid (*e.g.*, water). A higher EC may be related to enhanced antimicrobial activity (Rehan et al., 2020). We have observed a significantly ($p<0.05$) higher EC of the PAW when air (240.30 ± 31.98 μS•cm^{-1}) and N_2 (125.10 ± 12.34 μS•cm^{-1}) were used as the plasma-forming gas. This can be attributed to a larger amount of NO_x (resulting in a lower pH) present in the plasma phase in comparison to the PAW-Ar (20.96 ± 8.65 μS•cm^{-1}) and the PAW-O_2 (14.20 ± 6.69 μS•cm^{-1}). A similar result where the conductivity of MilliQ water increases after the plasma treatment was reported elsewhere (Rathore et al., 2021a). The EC follows a similar trend to NO_x (Figure 3.3A) which supports the reliability of the results since the EC and NO_x are strongly interdependent with each other.

Another indicator for antibacterial activity is ORP as it provides a measure of how oxidizing the PAW is and thus shows its potential to inactivate microorganisms. Our data show an increase in ORP for all four PAW types compared to the MilliQ control (Figure 3.3D). The highest ORP was measured for the PAW-O_2. This correlates with the highest CFU reduction of the PAW-O_2 compared to the other gases. Several studies have demonstrated an ORP increase with increasing the PAW generation time

and that was correlated with a higher antimicrobial activity (Guo et al., 2017; J. Guo et al., 2021; Pan et al., 2017).

3.4.3 Optical emission spectra of PAW discharge

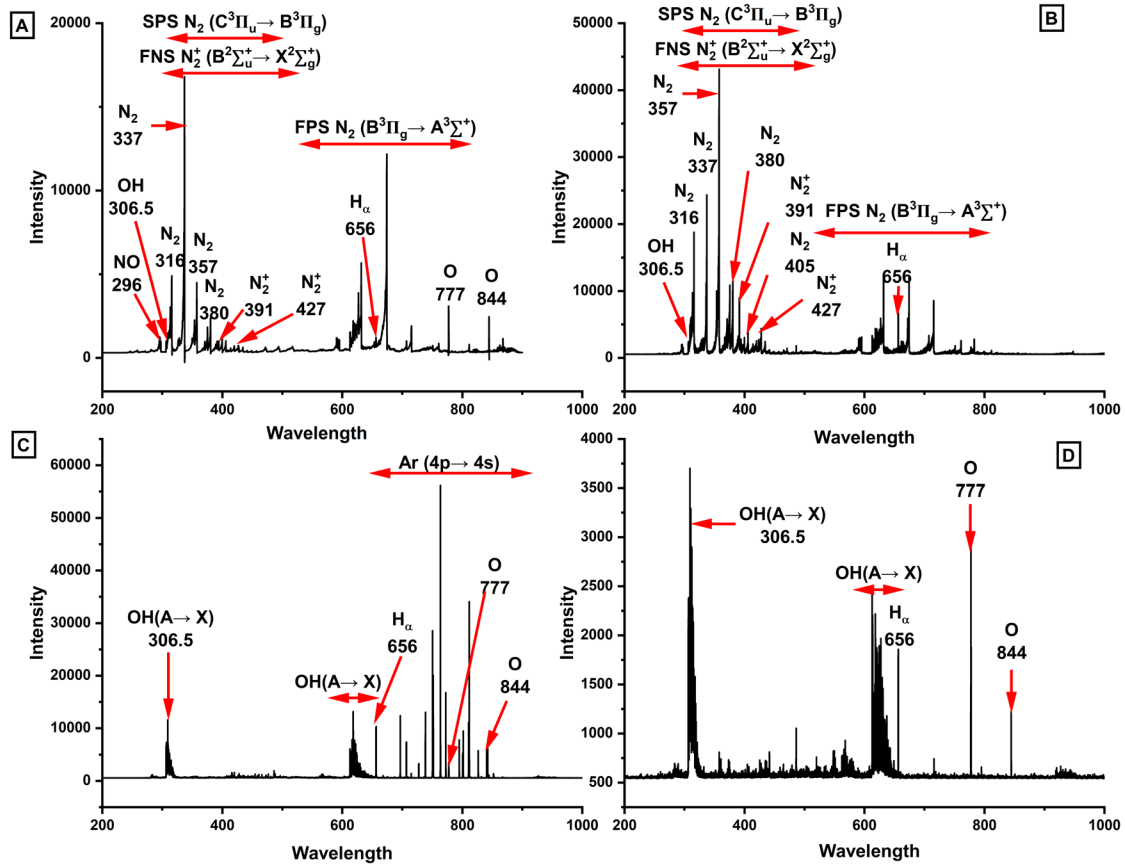

Figure 3.4. Optical emission spectroscopy for A) air, B) nitrogen, C) argon, and D) oxygen bubble spark discharge plasma in interaction with MilliQ water.

The representative emission spectrum and the identified emission bands of the bubble discharge plasma ranging from 200 to 900 nm of wavelength was shown in Figure 3.4. The OES spectra of air and nitrogen BSDs (Figure 3.4. A and B) exhibited predominantly excited nitrogen species, including the second positive system (SPS) of molecule nitrogen N_2 ($C^3\Pi_u \rightarrow B^3\Pi_g$) at 300-470nm, the first negative system (FNS) of molecular nitrogen ion N_2^+ ($B^2\Sigma_u^+ \rightarrow X^2\Sigma_g^+$) at 391 and 427nm, and the first positive system (FPS) of molecular nitrogen N_2 ($B^3\Pi_g \rightarrow A^3\Sigma^+$) ranging between 500nm and 800nm. The emission spectra of Ar discharge in Figure 3.4. C shows higher emission intensity from hydroxyl

radicals (306.5 nm and 600-650nm) and excited oxygen (777 nm and 844 nm) and hydrogen atoms (656 nm) as overall emission intensity significantly higher compared to the rest. A recent study (Bolouki et al., 2021) of dielectric discharge barrier plasma with argon, oxygen, nitrogen, and air gases interaction with distilled water presented similar optical emission spectra to air and nitrogen discharge (Figure 3.4. A and B) from this work, while their OH emission results do not agree with the emission of the energy state OH(A) to ground state OH(X) in Ar and O_2 BSDs observed in this work (Figure 3.4. C and D). The emission spectra of O_2 discharge (Figure 3.4D) exhibited a lower radical density compared to that of Ar BSD, which might be due to low ionization, vibrational and electronic excitation as well as H_2O dissociation reaction of O_2 plasma compared to Ar plasma (see in supportive information Fig. S3.5). Moreover, from our V-I measurement (Fig. S3.4) and energy loss fraction calculation (see in supportive information Table. S1, and Fig. S5), Ar BSD generated the highest average power in comparison with air, N_2, and O_2 BSDs, which enables high-density excited OH(A) resulting in enhanced emission intensity of OH(A→X).

Based on the OES measurement results, we summarised the possible important gas phase reactions in PAW-N_2, PAW-air, PAW-Ar, and PAW-O_2 BSD plasmas interacting with water molecules within gas bubbles.

$$e + H_2O \rightarrow \cdot OH + H + e \quad (1)$$

$$e + H_2O \rightarrow H_2O^* + e \quad (2)$$

$$e + H_2O^* \rightarrow H_2O^+ + 2e \quad (3)$$

$$H_2O + H_2O^+ \rightarrow \cdot OH + H_3O^+ \quad (4)$$

$$H_2O + hv \rightarrow \cdot OH + H \quad (5)$$

$$H_2O + M^* \rightarrow \cdot OH + H + M \quad (6)$$

The M^* represents the excited neutral species, such as excited nitrogen, oxygen and argon species, in reaction 6.

In nitrogen BSD plasma, excited nitrogen atoms and molecules take important roles to sustain reactive plasma conditions as well as electron interactions such as dissociation and excitation.

$$N_2 + e \rightarrow N + N + e \quad (7)$$

$$N_2 + e \rightarrow {N_2}^* + e \quad (8)$$

$$N^* + H_2O \rightarrow N + \cdot OH + H \quad (9)$$

$$N^* + H_2O \rightarrow NH + \cdot OH \quad (10)$$

$$N_2^* + H_2O \rightarrow H + \cdot OH + N_2 \quad (11)$$

Regarding oxygen BSD plasma, various forms of reactive oxygen species can be generated including excited oxygen molecular and atomic species, ions and ozone, superoxide anion radicals and also hydrogen radicals through the interaction with water or its derivatives such as OH^- or HO_2 (Bolouki et al., 2021):

$$O_2 + e \rightarrow O^+ + O + 2e \quad (12)$$

$$O_2 + e \rightarrow O^- + O \quad (13)$$

$$O + O_2 \rightarrow O_3 \quad (14)$$

$$O + H_2O \rightarrow 2OH \cdot \quad (15)$$

$$O_3 + OH^- \rightarrow HO_2^- + O_2 \quad (16)$$

$$O_3 + HO_2^- \rightarrow OH \cdot + {O_2}^- + O_2 \quad (17)$$

In the case of air BSD plasma, on top of the above-mentioned important reactions in N_2 and O_2 plasma, additional chemical reactions between nitrogen and oxygen species need to be addressed to explain NO_x generation (Bolouki et al., 2021; Xiao et al., 2014).

$$N + O + M \rightarrow \cdot NO + \mathrm{M} \quad (18)$$

$$N + O_2 \rightarrow \cdot NO + O \quad (19)$$

$$O + N_2 \rightarrow \cdot NO + N \quad (20)$$

In Reaction (18), M indicates background molecules such as N_2 or O_2 species in air discharge as a third body to absorb released energy.

In the argon BSD plasma, the presence of high-density metastable Ar* species is demonstrated by the measured strong optical emission between 690 to 912nm (Fig. 4C) from the transition Ar(4p) to Ar(4s) states. As shown in the reaction (23), high energy Ar*(11.55 eV) metastables can induce

further ionization which is fundamentally important characteristics of Ar discharge to sustain high-density plasma even at low applied voltage conditions. This metastable Ar* species contribute to effectively generating hydroxyl radicals by the interaction with water molecules(Wang et al., 2018).

$$Ar + e \rightarrow Ar^{+} + e + e \quad (21)$$

$$Ar + e \rightarrow Ar^{*} + e \quad (22)$$

$$Ar^{*} + Ar^{*} \rightarrow Ar^{*} + Ar^{+} + 2e \quad (23)$$

$$Ar^{*} + H_2O \rightarrow Ar + \cdot OH + H \quad (24)$$

Overall, the above OES measurement combined with the suggested mechanism from the literature supports the experimental observations on the generation of reactive species such as $OH\cdot$, O_2^-, $NO\cdot$, and excited atoms in the gas phase of BSDs plasma, which then leads to the solvation and diffusion of RONS at the bubble-water interface and formation of activated water.

3.5 The use of molecular scavengers to detect reactive species in PAW

Measuring H_2O_2, NO_3^-, NO_2^- and other physical characteristics of the PAW helps shed some light on the antibacterial effects of the generated PAW. However, these measurements do not fully explain why the PAW-O_2 has the highest CFU reduction. We, therefore, used several molecular scavengers, including mannitol (scavenges $OH\cdot$), uric acid (UA, scavenges O_3), Tiron (scavenges O_2^-), N-Acetyl-L-cysteine (NAC, scavenges ROS), and sodium pyruvate (SP, H_2O_2) to selectively remove reactive species from the PAW-O_2, and observed its effect on reducing for *E. coli* biofilms viability (Figure 3.5). If removing a reactive species from the PAW-O_2 caused it to lose its antibacterial effect, it can be concluded that the scavenged specie(s) was responsible for the observed effect. The addition of the scavengers UA (O_3) and mannitol ($^{\cdot}OH$) did not affect the CFU numbers, with no viable cells detected after their addition (Fig. 5). NAC (ROS) and SP (H_2O_2) prevented the complete removal of biofilm cells exposed to the PAW-O_2 with a few viable cells detected after the addition of those scavengers, however, this was not statistically significant compared to PAW-O_2 without scavengers. Only Tiron, the scavenger for the O_2^- radicals, was able to significantly prevent biofilm killing from exposure to the PAW-O_2 (Rothwell et al., 2022; Taiwo, 2008) (Fig. 5).

According to our findings (Figure 3.5), the elimination of biofilm might be attributed to the presence of O_2^- radical and H_2O_2 within the ROS. A previous study has indicated that CAP-generated O_2^- radical and H_2O_2 can cause a considerable amount of tumour cell death, although their toxicity towards tumour cells was found to be inadequate when used alone (Xu et al., 2015). Moreover, the O_2^- radical is highly active and has been previously shown to substantially enhance the bactericidal effects of the PAW (Ma et al., 2020; Rothwell et al., 2022). The oxygen toxicity of $\bullet O_2^-$ radicals is thought to be responsible for their antibacterial activity(Winterbourn, 2020). Though whether the detrimental effect of $\bullet O_2^-$ on the bacteria biofilm could be the inactivation of the bacterial dehydratases, an iron/sulphur clusters of proteins that are responsible for synthesizing branched-chain amino acids (Imlay, 2003), its interaction with bacteria biofilm is still actively debated (Winterbourn, 2020).

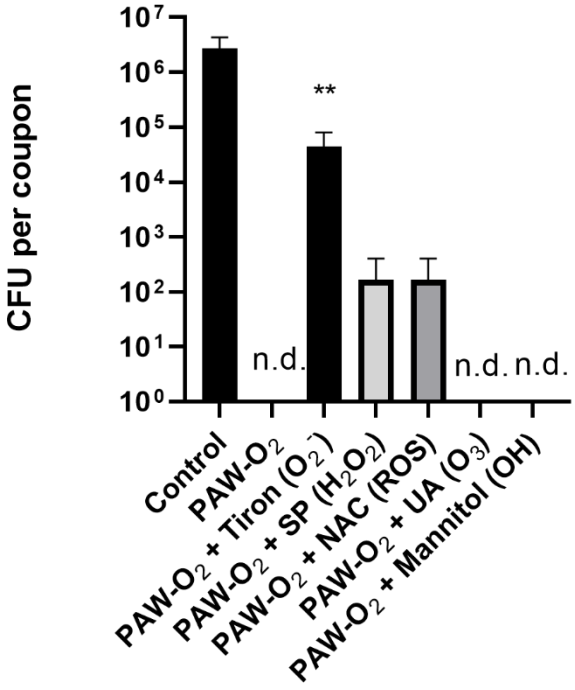

Figure 3.5. CFU reduction of *E. coli* biofilms using PAW generated in oxygen with the addition of scavengers. 48h biofilms were grown on stainless steel coupons and treated with PAW generated in oxygen in a bubble reactor. Scavengers (Tiron, NAC, SP, UA and Mannitol) were added directly to the PAW during generation. CFU reduction for PAW-O_2 with the superoxide anion scavenger Tiron is significantly different from the PAW-O_2 treatment without scavenger ($P < 0.01$, unpaired t-Test).

3.5.1 Detection of superoxide anion radicals in PAW

The fact that the addition of the superoxide scavenger Tiron to the PAW-O_2 was able to prevent biofilm removal suggests that superoxide is a major factor in the antibacterial activity of the PAW-O_2. We, therefore, aimed to detect $\bullet O_2^-$ in the PAW-O_2 using electron paramagnetic resonance (EPR) spectroscopy.

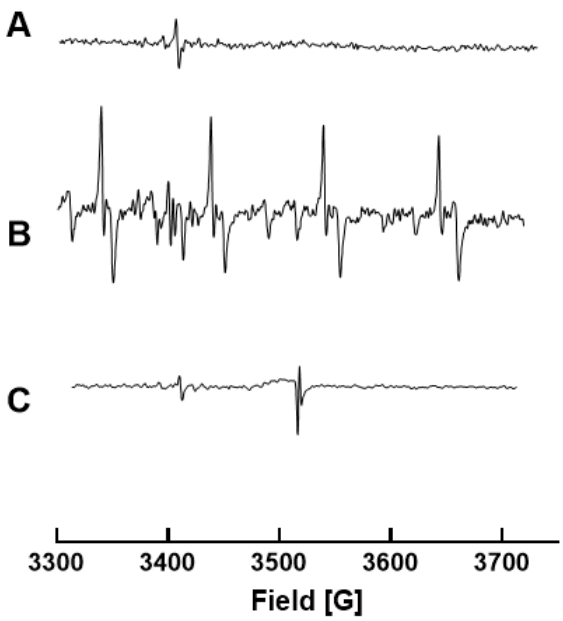

Figure 3.6. Electron paramagnetic resonance spectra of 800mM of DMPO with A)60s O_2 bubbling MQ water; B) 60s PAW-O_2 treated MQ water; C) 60s PAW-O_2 treated MQ water with 20mM Tiron.

EPR combined with spin trap reagents (e.g. DMPO) has been broadly used in the detection of short-lived $\bullet O_2^-$ radicals (Hu et al., 2021). However, the DMPO also reacts with •OH forming a relatively poor stable spin adducts DMPO-OH (Zhou et al., 2020b). Thus, the resulting signal may also be attributed to •OH radicals. To overcome this and selectively detect $\bullet O_2^-$ species, the Tiron scavenger was used as a negative control to capture the potential $\bullet O_2^-$ in the PAW. Our EPR spectra results indicate that the DMPO had no hyperfine interaction with the non-plasma control (O_2 bubbling water) with only a small one-peak signal (Figure 3.6A), while the DMPO showed four strong peaks with the ratio of 1:1:1:1 in the PAW-O_2 (Figure 3.6B). These peaks are strongly associated with $\bullet O_2^-$ because

these species were not observed when Tiron was added to the PAW-O_2 and thus no $\bullet O_2^-$ species was present (negative control) (Figure 3.6C).

3.5.2 *E. coli* biofilm imaging characterisation

To investigate the effect of direct PAW treatment on *E. coli* biofilms, cells were stained with live/dead kit after the treatment and observed under a confocal microscope (Figure 3.7A). The untreated control *E. coli* biofilms consisted of mainly live (green) cells with only a few dead cells (red) present. This was similar for the PAW- N_2 and the PAW-Ar (Figure 3.7B and C) samples. In contrast, a significant number of dead cells occurred in biofilms treated with the PAW-air (Figure 3.7D). While there were not many cells left on the PAW-O_2 treated biofilms, most of the cells were dead and approximately 91.4% of reduction in biofilm thickness compared to the control (Figure 3.7A and E). When Tiron (O_2^- scavenger) is added to the PAW-O_2 sample leading to a loss of efficacy of suspected superoxide species, more viable biofilm cells can be observed (Figure 3.7F), which confirms the results of the scavengers' assay (Figure 3.5). O_2^- radicals were apparently only able to form in the plasma generated using pure oxygen and not in other mixtures of O_2 and N_2 gases (Helena Tresp et al., 2013). These fluorescent staining results, along with the results of the cell enumeration where the PAW-O_2 had the lowest CFU numbers n (Figure 2.3), correlate with the activity of O_2^- radicals. It appears that direct PAW treatment can remove biofilms from the coupon, and cells that are still present are killed. This has been previously observed for a *Listeria monocytogenes* biofilm model (Chen et al., 2018; Handorf et al., 2021), after 15min plasma water treatments, with the inactivation occurring in the biofilm centre and expanding to the edges. That study also showed that the treated biofilm matrix appeared as a homogenous structure with a 60 % reduction in thickness compared to the control (10 μm).

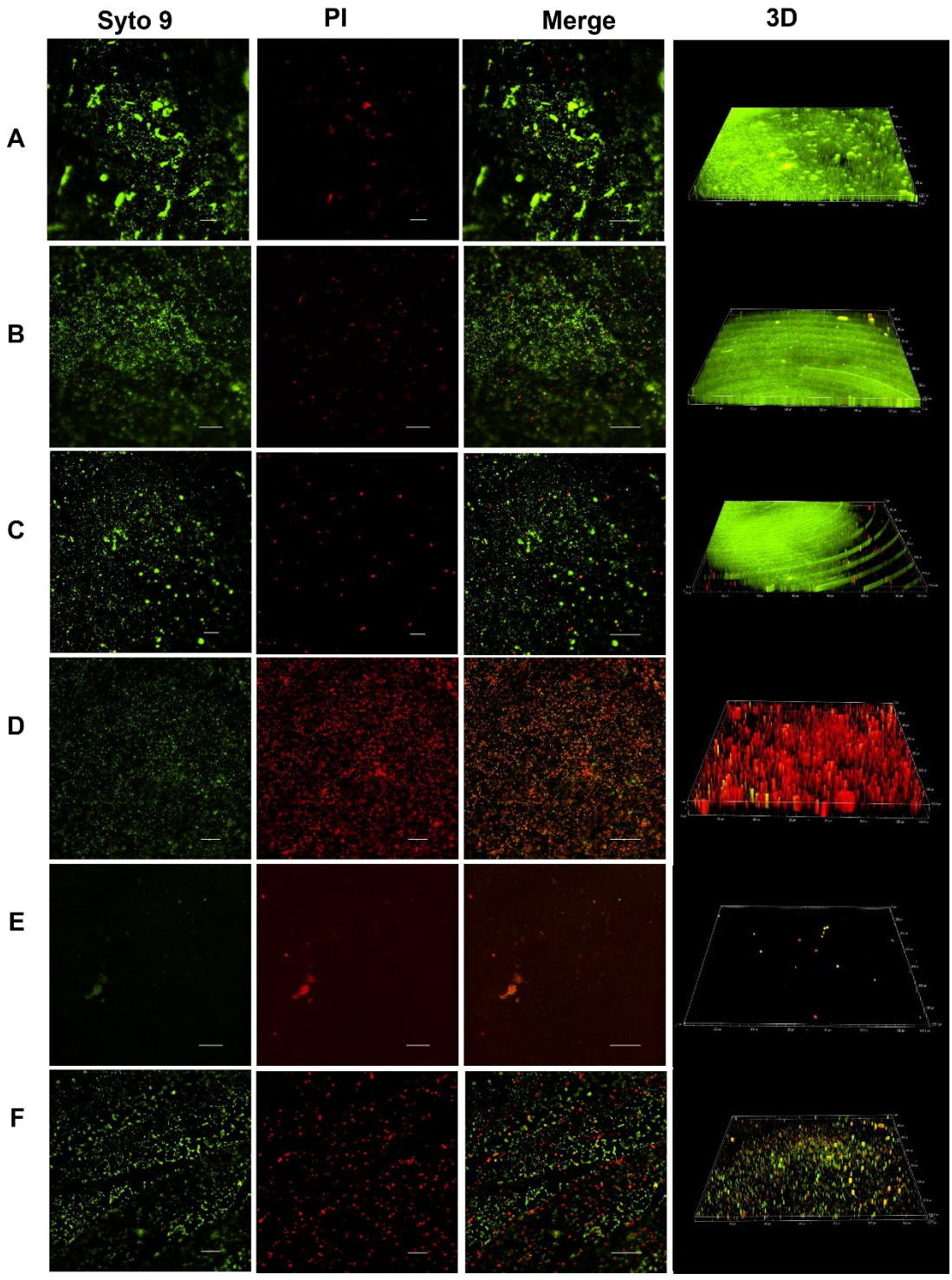

Figure 3.7. PAW-induced *E. coli* biofilm removal. Biofilms were stained using live/dead kit and observed with an inverted Nikon Ti-E confocal microscope. 3D Z-stack images (upper and lower side of coupon surfaces) are presented on the right column. All images were taken with a x40 magnification. The scale bar is 50 µm. A) control, B) PAW-N_2, C) PAW-Ar, D) PAW-air, E) PAW-O_2 and F) PAW-O_2 + Tiron scavenger. Experiments were repeated three times and a minimum of five images were taken for each observed stainless-steel coupon.

3.5.3 Intracellular detection of RONS in *E. coli* biofilms

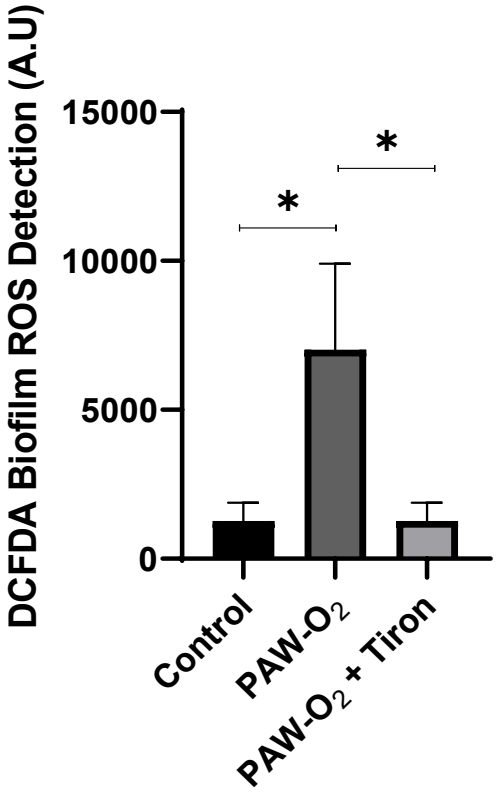

Figure 3.8. Detection of intracellular ROS in *E. coli* biofilms following treatment with PAW-O_2, PAW-O_2 + Tiron, and Control. ROS was measured using DCFDA staining of the 48 h biofilms. The presence of ROS is significantly higher in biofilms treated with the PAW-O_2 compared to biofilms treated with the PAW- O_2 + Tiron and control (MilliQ) ($P<0.05$, One-Way ANOVA with Tukey's multiple comparisons test).

To investigate the role of oxidative stress induced by the PAW-O_2, fluorescence staining with DCFDA was used to detect the accumulated ROS in *E. coli* biofilm. DCFDA is a cell-permeable and upon oxidation (e.g., via RONS created in the PAW) is converted to the fluorescent dichlorofluorescein (DCF) that can be measured in a plate reader. After treatment with the PAW-O_2 (Figure 3.8), ROS levels were increased significantly by approximately 4.5-fold compared to the control. While the addition of 20 mM of Tiron (O_2^- scavenger) to the PAW-O_2 treated biofilms resulted in significantly less accumulation of ROS (Figure 3.8). These data suggest that O_2^- radicals play an important role in intracellular ROS accumulation and may be responsible for the significant biofilms removal caused by PAW-O_2. However, the mechanism of O_2^- radicals penetrating the biofilm matrix is still unclear. One study found that the O_2^- radicals could penetrate and attack the targeted

bacteria membrane under an acidic environment (Korshunov & Imlay, 2002). This might lead to the accumulation of ROS within the biofilm cells.

In this study, the PAW generated with O_2 showed the greatest antibacterial activity against 48h *E. coli* biofilms, demonstrating a 6-log reduction, compared to biofilms treated with PAW generated with inputs of air, N_2, and Argon. The confocal microscopy images also revealed the removal of biofilms from the coupon surface with only dead cells remaining after the PAW-O_2 treatment. An acidic pH, a higher ORP, and the presence of H_2O_2, NO_3^-, and NO_2^- generated in the PAW were widely studied as the mechanisms behind the antibacterial activities of the PAW (Thirumdas et al., 2018). However, the presence of superoxide anion radical appears to play a major role in PAW-mediated biofilm removal. While H_2O_2, NO_2^-, and NO_3^- were detected by quantitative tests and they are strong oxidants, their impacts were limited in our system because their concentrations are less than the effective biofilm killing concentration of 1000mg/L of HNO_3 and H_2O_2 in this study (see supportive information Fig. S3.2). We also confirm that the elevated levels of intracellular ROS in *E. coli* biofilms after PAW-O_2 treatment suggesting that superoxide anion radical plays a crucial role in inducing a high intracellular oxidative stress within *E. coli* biofilms cells in response to the PAW-O_2 treatment.

3.6 Conclusions

In summary, a bubble spark discharge (BSD) with an input gas of oxygen generated plasma-activated water (PAW) can completely remove 48h *E. coli* biofilms grown on stainless-steel surfaces. The short-lived superoxide anion radical was found to be a decisive factor in the antimicrobial effect caused by direct exposure to PAW-O_2. Input gas sources of atmospheric air, argon, and nitrogen were used to generate PAW, and were found to generate a mixture of reactive species with variable biofilm removal efficacy.

This research presents new knowledge on the use of PAW to remove bacterial biofilms and points to the importance of short-lived reactive species in the observed antibacterial efficacy. This has implications for drinking and wastewater water treatment, as well as possible treatment of food

products or medical devices where conventional disinfection or sanitation is neither suitable, nor effective. Utilising compressed atmospheric air (or oxygen) as a gas input source is an economically viable option when generating PAW. This further underscores its attractiveness for use. Lastly, the plasma source used in this work also has the advantage of being small and portable making it suitable for diverse applications in the water treatment industry, food industry, clinical equipment sterilization, medicine, and environment.

3.7 Supporting Information

S3.1. Measurement of H_2O_2 concentrations in PAW

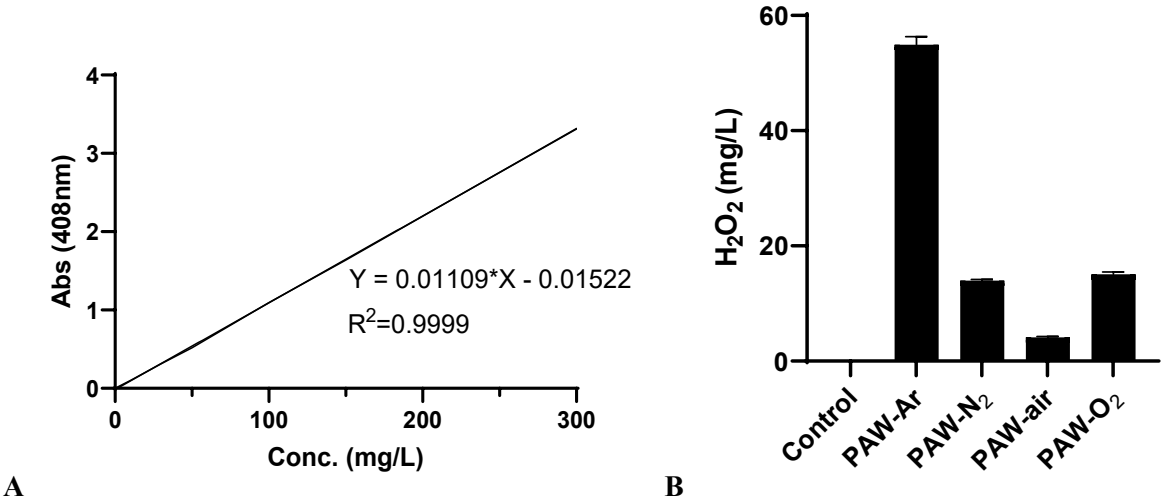

A B

Figure S3.1. H_2O_2 measurement via UV-vis measurement method. A. standard curve of various concentrations of H_2O_2 solutions. B. The concentrations of H_2O_2 generated in MilliQ water activated by argon, nitrogen, air, and oxygen gases.

To quantify the H_2O_2 levels in different PAWs, a serials concentration of H_2O_2 (0-300 mg/L) solution was prepared and measured by a titanium sulphate method (Zhou et al., 2021) where H_2O_2 reacts with titanium oxysulphate ($TiOSO_4$) resulting in a yellow-coloured complex (pertitanic acid) that is quantified with UV-Vis spectroscopy at 408 nm. The standard curve was calculated as shown in Figure S3.1A.

$$\text{Absorbance} = 0.01109 * \text{H}_2\text{O}_2\text{concentration}\ [\frac{\text{mg}}{\text{L}}] - 0.01522 \qquad R^2 = 0.9999 \qquad \text{(Eq. S1)}$$

According to Equation (S1), the absorbance of PAW-Ar, PAW-N_2, PAW-air, and PAW-O_2 was transferred to relevant H_2O_2 concentration as shown in Figure S3.1B.

S3.2. The biofilm viability of HNO_3/H_2O_2 mixture treatment

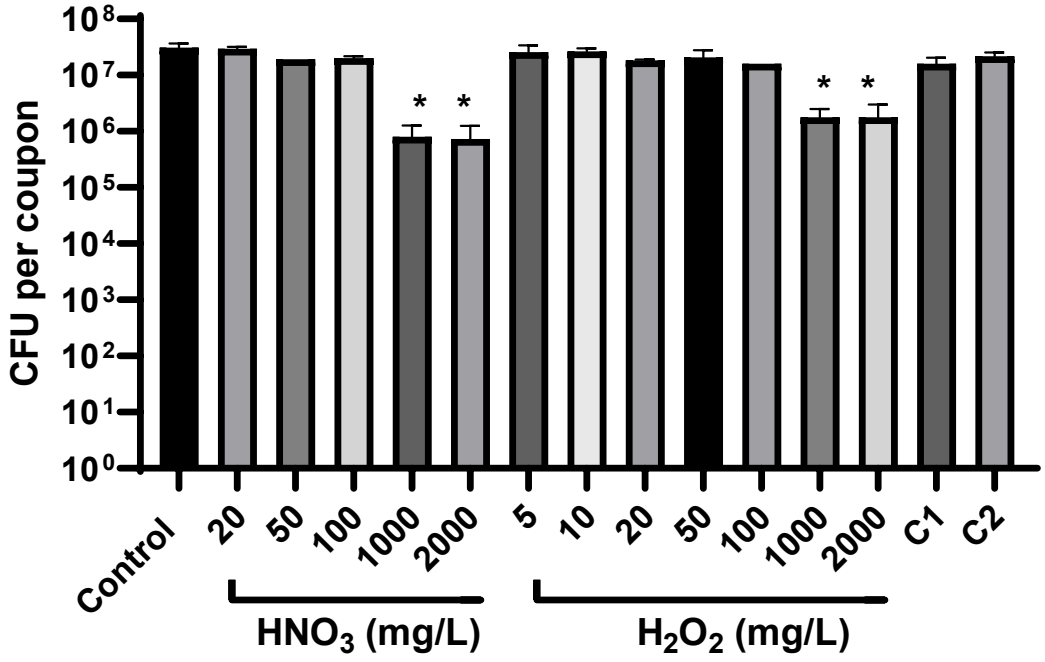

Figure S3.2. The viability of 48h *E.coli* biofilm grown on the coupon after treatment of HNO_3 (20mg/L, 50mg/L, and 100mg/L), and H_2O_2 (10mg/L, 20mg/L, 50mg/L, and 100mg/L). C1: 20mg/L H_2O_2+25mg/L HNO_3; C2: 10mg/L H_2O_2+100mg/L HNO_3. *P<0.05.

To investigate antibiofilm activity of the main long-lived reactive species generated in different PAWs, differing concentration of HNO_3, H_2O_2 and HNO_3/H_2O_2 mixture corresponding to different PAWs were investigated (Figure 3.3A). The combination of HNO_3/H_2O_2 of C1 and C2 represents that of PAW-N_2 and PAW-air, respectively. While 50mg/L of H_2O_2 represents PAW-Ar and 20mg/L of H_2O_2 represents PAW-O_2. As shown in Fig. S2, only 1000 and 2000 mg/L of HNO_3 and H_2O_2 observed a significant reduction of biofilm viability (~1.5-2 log). However, no concentration assessed in this study was able to completely eradicate the 48h *E. coli* biofilm. Therefore, the H_2O_2 and HNO_3 play a non-significant role in deactivation of biofilm in the BSDs reactor.

S3.3 Voltage and current measurement of BSD reactor

The time-series voltage and current across BSD reactor supplied with Ar, N2, air, and O2 gases were measured using a North StarPVM-6 high voltage probe and a HET10AB15U10 current probe, respectively, sampled by a RIGOL DS6104 oscilloscope as shown in the experimental setup of Fig. S3.

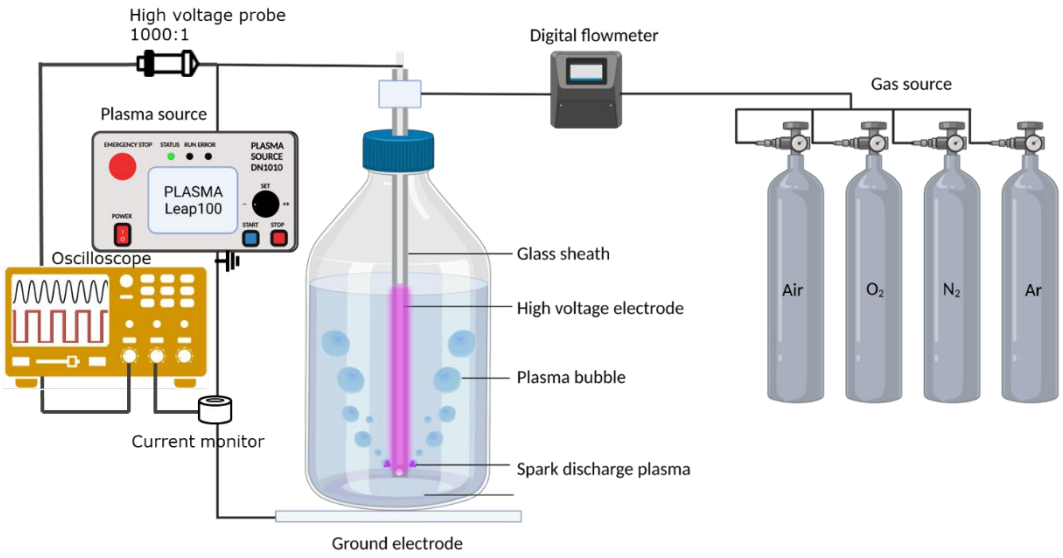

Figure S3.3. A schematic illustration of plasma-activated water (PAW) generated by a bubble spark discharge (BSD) plasma reactor. The plasma bubble reactor consists of a high-voltage electrode and a glass sheath. To generate spark discharge plasma, the high-voltage electrode was powered by PlasmaLeap100. The voltage and current of the power source are monitored by the oscilloscope equipped with a high-voltage probe and a current monitor.

The complex formation of RONS in the PAW depends on many physical and chemical parameters and processes. The measured voltage and current include important information on the electron energy distribution and the density which governs the formation of RONS. Although exactly the same input power conditions were applied, the actual high voltage and current response appeared different for all four gases. This is because different electron energy distributions and plasma chemistry in different gas compositions affect the final composition of reactive species in that given plasma system. To characterise and compare the different plasma conditions with different gas input voltage and current measurements (V-I) were performed. As shown in Figure S3.4, the different gas sources

presented unique V-I characteristics. The N_2 and O_2 plasmas show similar V-I characteristics whereas a plasma discharge in air shows a faster decrease of current and is therefore expected to have a fast-decreasing electron density profile. The plasma argon discharge shows a significant difference from the other three gases with a lower peak voltage and current response, but high power by sustaining the effective discharge for a longer time of period. These characteristics for argon plasma are likely due to the influence of high energy metastable Ar* species that enable it to sustain a high energy electron distribution and density even at low electric field conditions by Penning ionization (Lieberman & Lichtenberg, 2005) and result in an overall enhanced density of reactive plasma species.

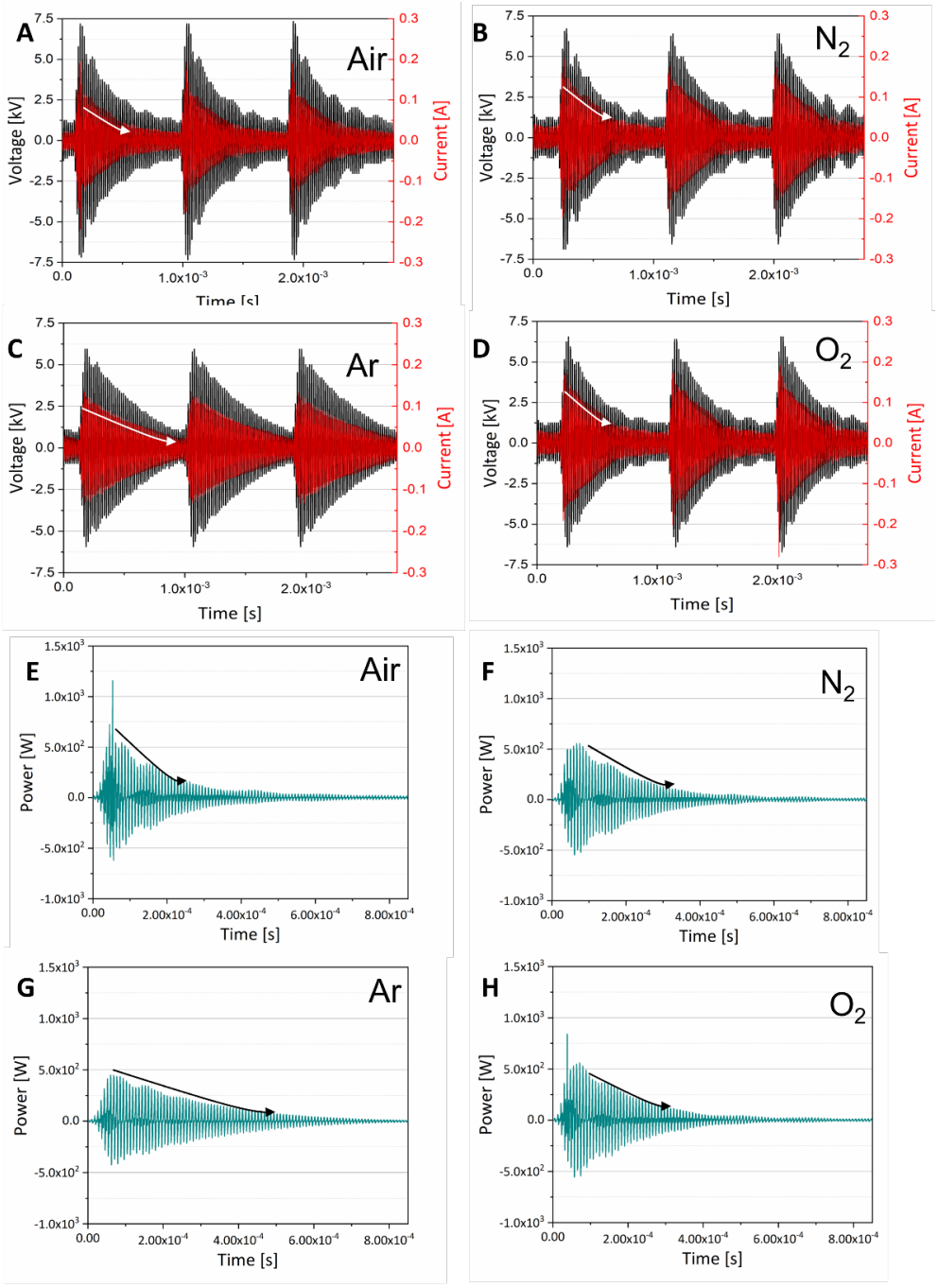

I

	V_p	I_p	P_{avg}
Air	7.19 kV	0.19 A	8.3 W
N_2	6.23 kV	0.17 A	9.4 W
Ar	5.73 kV	0.13 A	10.4 W
O_2	6.30 kV	0.17 A	9.4 W

Figure S3.9. Electrical waveforms of the voltage (left axis) and the current (right axis) of bubble spark discharge plasma reactor supplied with different input gases. A) Air gas; B) Argon gas; C) Nitrogen gas; and D) Oxygen gas; The actual output power (W) of the plasma reactor supplied using different gases E) Air gas; F) Argon gas; G) Nitrogen gas; and H) Oxygen gas; I) The summary table of maximum voltage, current, and power, as well as average power output of different gas supplied plasma reactors.

The differences in V-I characteristics can help explain the difference in our measured H_2O_2, NO_2^- and NO_3^- concentrations as each of these RONS production will be governed by electron density and energy distribution, which is determined by the reduced electric field E/N (Fig. S4 and S5), where E is electric field strength and N is the number density of molecules. For example, Yuan et al. (2017) found that •OH radicals were favoured to form at higher discharge voltages during 100 min of dielectric barrier discharge (DBD) plasma treatment. As mentioned above, we observed a high H_2O_2 concentration in the PAW-Ar and this is likely linked to the formation of high density •OH radicals in the Ar discharge (Figure S3.4I) due to the high electron energy distribution as estimated from the results of our measurement of V-I characteristics.

S3.4. Comparison of electron energy loss fraction in different gas discharges

In order to understand the different plasma characteristics of discharges from different gas element, electron energy loss fraction was calculated using Boltzmann equation solver BOLSIG+ (Hagelaar & Pitchford, 2005). A set of reactions are included from Biagi database for N_2, O_2 and Ar (Biagi, 2010) and Itikawa database for H_2O (Itikawa, 2012; Itikawa & Mason, 2005).

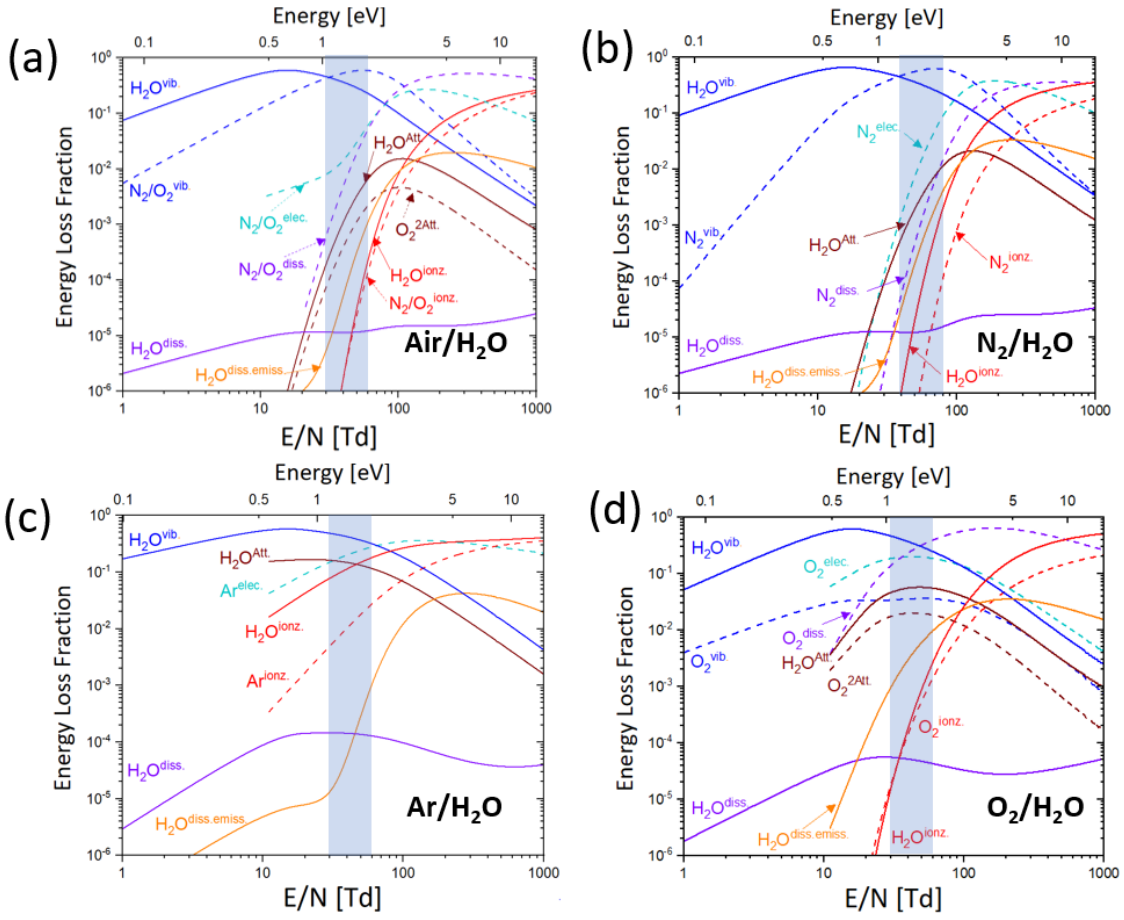

Figure S3.5. Calculated electron energy loss fraction in different gas discharge (a) Air/H_2O = 0.99: 0.01 (b) N_2/H_2O = 0.99:0.01, (c) Ar/H_2O = 0.99:0.01, and (d) O_2/H_2O = 0.99:0.01 where the gas temperature was assumed 300 K, the subscript 'vib.' 'elec.' 'ionz.' 'Att.', 'diss.' and 'diss.emiss' indicates vibrational and electronic excitation, ionization, electron attachment, molecule dissociation without optical emission, dissociation associated with optical emission respectively. H_2OAtt. includes 3 different electron interaction to generate H^-, O^- and OH^- ion from H_2O and O_2Att. presents O^{2-} ion formation by 2 body interaction different from 3 body interaction. Elastic collision and rotational excitation also are included in the calculation but not shown in the plot. The reduced electric field ranges from 30Td to 60Td is presented in shade to show a comparison clearly between different gas plasma system as a possible spatial and temporal average values.

Figure S3.5. shows how much electron energy was used for each different electron interaction in the given plasma discharge. It is presented as a function of reduced electric field E/N which indicates the

effective electric field strength E in the discharge gap divided by the number density of gas molecules N and it is an important governing factor to determine the electron energy distribution of the plasma system.

Considering the possible interaction of spark discharge with H_2O vapour inside the bubble volume, 1%vol. of H_2O concentration was assumed as possible average.

Firstly, it is noticeable the contrast of Ar/H_2O discharge in comparison to the rest with significantly high ionization, vibrational and electronic excitation as well as H_2O dissociation reaction. Therefore, it is expected to have higher density of electrons and OH radicals in Ar discharge which explains the measurement results on high density H_2O_2 production. However, for the dissociation reaction associated with optical emission, O_2 plasma shows higher values of electron energy loss fraction. This includes several different optical emission processes related to excited hydrogen and oxygen atoms, and OH radicals as provided Table S3.1. As shown in Figure S3.4, the dissociation reaction of H_2O with optical emission from excited H and O atoms still shows higher reaction coefficient in Ar discharge in comparison to O_2 discharge which supports the measurement results as shown in Fig. 4. On the contrary, the calculation result predicts higher transition reaction coefficient of energy state OH(A) to ground state OH(X) in O_2 discharge which seemingly does not agree with the OH emission intensity observed at 306.5 nm. However, considering the fact that the energy loss fraction can only be a direct indicator to describe the different characteristics of plasma when the same electron density is assumed. From the calculated higher degree of ionization at the same reduced electric field E/N as an input value and the measured highest current density and average power in Ar discharge, it is considered that it may sustain higher electron density in comparison to N_2, O_2 and Air discharge. It is again worthwhile to stress the important role of high energy metastable Ar* species which can generate more electrons by Penning ionization and also enables high density excited species including OH(A) states as it results in enhanced emission intensity. In this electron energy loss fraction calculation, only electron related interactions are included. More accurate prediction of gas product composition and important mechanism, full plasma chemistry model may be required including different chemical reaction between neutral gas species.

Table S3.1. Optical emission reaction included in the calculation for the electron energy loss fraction.

	Process	Related light emission	Reference
Dissociation of H_2O with optical emission from excited atomic hydrogen			
R1	$e + H_2O \rightarrow e + H + OH + \gamma$	Hydrogen Balmer alpha line at 656.3 nm	(Itikawa & Mason, 2005)
R2	$e + H_2O \rightarrow e + H + OH + \gamma$	Hydrogen Lyman alpha line at 121.6 nm	(Itikawa & Mason, 2005)
R3	$e + H_2O \rightarrow e + H + OH + \gamma$	Hydrogen Balmer beta line at 486.1 nm	(Itikawa & Mason, 2005)
R4	$e + H_2O \rightarrow e + O + H + H + \gamma$	Oxygen emission at 130.4 nm	(Itikawa & Mason, 2005)
R5	$e + H_2O \rightarrow e + O + H + H + \gamma$	Oxygen emission at 777.4 nm	(Itikawa & Mason, 2005)
R6	$e + H_2O \rightarrow e + O + H + H + \gamma$	Oxygen emission at 844.7 nm	(Itikawa & Mason, 2005)
R7	$e + H_2O \rightarrow e + OH + H + \gamma$	OH emission at 306.4 nm	(Itikawa & Mason, 2005)

where the product indicated in bold font are the source elements to generate optical emission through transition from electronically excited states to ground states and γ indicates photon emission.

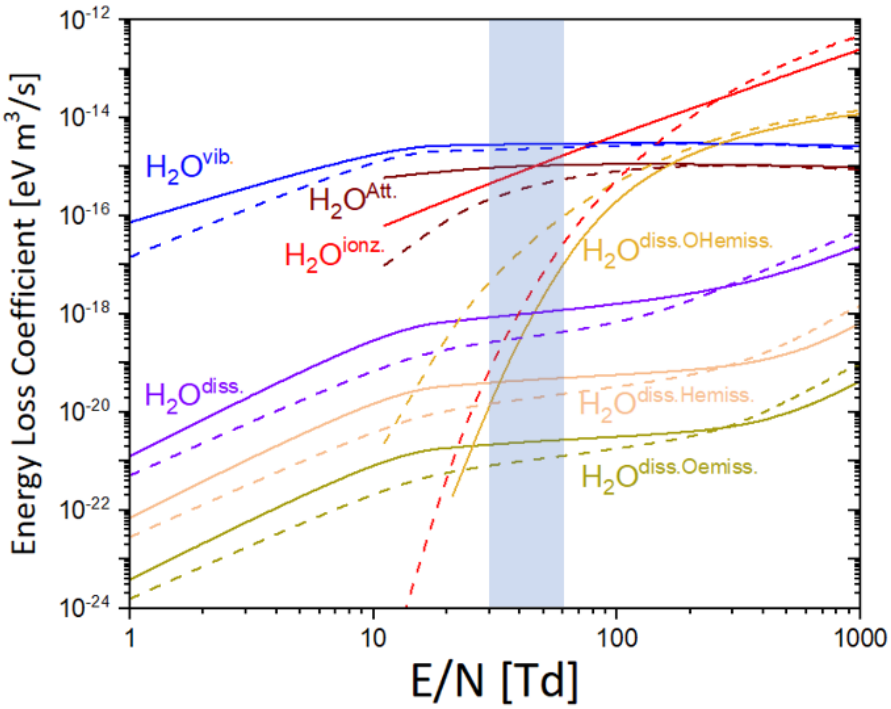

Figure S3.6. Comparison of energy loss coefficient of different electron interaction with H_2O between Ar-H_2O and O_2-H_2O plasma system where the solid curve indicates Ar-H_2O and the dotted curve presents O_2-H_2O plasma

Apart from the significance of dissociation, vibrational and electronic excitation, ionization of H_2O by electron interaction, the interaction with H_2O^+ ion, high energy photons and excited neutrals are considered to be important in order to enhance reactive species such as ·OH radicals and hydrogen and oxygen atoms (Bolouki et al., 2021; Wang et al., 2021).

3.8 References

Balan, G. G., Rosca, I., Ursu, E. L., Doroftei, F., Bostanaru, A. C., Hnatiuc, E., Nastasa, V., Sandru, V., Stefanescu, G., Trifan, A., & Mares, M. (2018). Plasma-activated water: a new and effective alternative for duodenoscope reprocessing. *Infect Drug Resist, 11*, 727-733. https://doi.org/10.2147/IDR.S159243

Biagi, S. F. (2010). *Fortran program* Version MAGBOLTZ versions 8.9 (O2), v8.97 (N2) and v7.1 (Ar)). www.lxcat.net/Biagi

Bolouki, N., Kuan, W.-H., Huang, Y.-Y., & Hsieh, J.-H. (2021). Characterizations of a Plasma-Water System Generated by Repetitive Microsecond Pulsed Discharge with Air, Nitrogen, Oxygen, and Argon Gases Species. *Applied Sciences, 11*(13), 6158. https://doi.org/10.3390/app11136158

Cámara, M., Green, W., MacPhee, C. E., Rakowska, P. D., Raval, R., Richardson, M. C., Slater-Jefferies, J., Steventon, K., & Webb, J. S. (2022). Economic significance of biofilms: a multidisciplinary and cross-sectoral challenge. *npj Biofilms and Microbiomes, 8*(1), 42. https://doi.org/10.1038/s41522-022-00306-y

Chakraborty, P., Bajeli, S., Kaushal, D., Radotra, B. D., & Kumar, A. (2021). Biofilm formation in the lung contributes to virulence and drug tolerance of Mycobacterium tuberculosis. *Nature communications, 12*(1), 1606. https://doi.org/10.1038/s41467-021-21748-6

Chen, T.-P., Liang, J., & Su, T.-L. (2018). Plasma-activated water: antibacterial activity and artifacts? *Environmental Science and Pollution Research, 25*(27), 26699-26706. https://doi.org/10.1007/s11356-017-9169-0

Cullen, P. J., Lalor, J., Scally, L., Boehm, D., Milosavljević, V., Bourke, P., & Keener, K. (2018). Translation of plasma technology from the lab to the food industry. *Plasma Processes and Polymers, 15*(2), 1700085. https://doi.org/10.1002/ppap.201700085

Dula, S., Ajayeoba, T. A., & Ijabadeniyi, O. A. (2021). Bacterial biofilm formation on stainless steel in the food processing environment and its health implications. *Folia Microbiologica, 66*(3), 293-302. https://doi.org/10.1007/s12223-021-00864-2

Fernández-Gómez, P., Cobo-Díaz, J. F., Oliveira, M., González-Raurich, M., Alvarez-Ordóñez, A., Prieto, M., Walsh, J. L., Sivertsvik, M., Noriega-Fernández, E., & López, M. (2023). Susceptibility and transcriptomic response to plasma-activated water of Listeria monocytogenes planktonic and sessile cells. *Food Microbiology, 113*, 104252. https://doi.org/10.1016/j.fm.2023.104252

Flynn, P. B., Graham, W. G., & Gilmore, B. F. (2019). Acinetobacter baumannii biofilm biomass mediates tolerance to cold plasma. *Letters in Applied Microbiology, 68*(4), 344-349. https://doi.org/10.1111/lam.13122

Gao, Y., Li, M., Sun, C., & Zhang, X. (2022). Microbubble-enhanced water activation by cold plasma. *Chemical Engineering Journal, 446*, 137318. https://doi.org/10.1016/j.cej.2022.137318

Ghimire, B., Szili, E. J., Patenall, B. L., Lamichhane, P., Gaur, N., Robson, A. J., Trivedi, D., Thet, N. T., Jenkins, A. T. A., Choi, E. H., & Short, R. D. (2021). Enhancement of hydrogen peroxide production from an atmospheric pressure argon plasma jet and implications to the antibacterial activity of plasma activated water. *Plasma Sources Science and Technology, 30*(3), 035009. https://doi.org/10.1088/1361-6595/abe0c9

Gilmore, B. F., Flynn, P. B., O'Brien, S., Hickok, N., Freeman, T., & Bourke, P. (2018). Cold Plasmas for Biofilm Control: Opportunities and Challenges. *Trends in Biotechnology, 36*(6), 627-638. https://doi.org/10.1016/j.tibtech.2018.03.007

Girard, F., Peret, M., Dumont, N., Badets, V., Blanc, S., Gazeli, K., Noël, C., Belmonte, T., Marlin, L., Cambus, J.-P., Simon, G., Sojic, N., Held, B., Arbault, S., & Clément, F. (2018). Correlations between gaseous and liquid phase chemistries induced by cold atmospheric plasmas in a physiological buffer. *Physical Chemistry Chemical Physics, 20*(14), 9198-9210. https://doi.org/10.1039/C8CP00264A

Guo, D., Liu, H., Zhou, L., Xie, J., & He, C. (2021). Plasma‐activated water production and its application in agriculture. *Journal of the Science of Food and Agriculture, 101*(12), 4891-4899. https://doi.org/10.1002/jsfa.11258

Guo, J., Huang, K., Wang, X., Lyu, C., Yang, N., Li, Y., & Wang, J. (2017). Inactivation of Yeast on Grapes by Plasma-Activated Water and Its Effects on Quality Attributes. *Journal of Food Protection, 80*(2), 225-230. https://doi.org/10.4315/0362-028x.Jfp-16-116

Guo, J., Qin, D., Li, W., Wu, F., Li, L., & Liu, X. (2021). Inactivation of *Penicillium italicum* on kumquat via plasma-activated water and its effects on quality attributes [Article]. *International Journal of Food Microbiology, 343*, Article 109090. https://doi.org/10.1016/j.ijfoodmicro.2021.109090

Hagelaar, G., & Pitchford, L. C. (2005). Solving the Boltzmann equation to obtain electron transport coefficients and rate coefficients for fluid models. *Plasma Sources Science and Technology, 14*(4), 722. https://doi.org/10.1088/0963-0252/14/4/011

Haghighat, G., Sohrabi, A., Shaibani, P. M., Van Neste, C. W., Naicker, S., & Thundat, T. (2017). The role of chloride ions in plasma-activated water treatment processes. *Environmental Science: Water Research & Technology, 3*(1), 156-168. https://doi.org/10.1039/C6EW00308G

Handorf, O., Below, H., Schnabel, U., Riedel, K., & Ehlbeck, J. (2020). Investigation of the chemical composition of plasma-treated water by MidiPLexc and its antimicrobial effect on L. monocytogenes and Pseudomonas fluorescens monospecies suspension cultures. *Journal of Physics D: Applied Physics, 53*(30), 305204. https://doi.org/10.1088/1361-6463/ab866b

Handorf, O., Pauker, V. I., Weihe, T., Schäfer, J., Freund, E., Schnabel, U., Bekeschus, S., Riedel, K., & Ehlbeck, J. (2021). Plasma-Treated Water Affects Listeria monocytogenes Vitality and Biofilm Structure. *Frontiers in Microbiology, 12*, 652481. https://doi.org/10.3389/fmicb.2021.652481

Hu, X., Zhang, Y., Wu, R. A., Liao, X., Liu, D., Cullen, P. J., Zhou, R.-W., & Ding, T. (2021). Diagnostic analysis of reactive species in plasma-activated water (PAW): current advances and outlooks. *Journal of Physics D: Applied Physics, 55*(2), 023002. https://doi.org/10.1088/1361-6463/ac286a

Imlay, J. A. (2003). Pathways of Oxidative Damage. *Annual Review of Microbiology, 57*(1), 395-418. https://doi.org/10.1146/annurev.micro.57.030502.090938

Itikawa, Y. (2012). *Itikawa database*. www.lxcat.net/Itikawa

Itikawa, Y., & Mason, N. (2005). Cross sections for electron collisions with water molecules. *Journal of Physical and Chemical reference data, 34*(1), 1-22. https://doi.org/10.1063/1.1799251

Jenns, K., Sassi, H. P., Zhou, R., Cullen, P. J., Carter, D., & Mai-Prochnow, A. (2022). Inactivation of foodborne viruses: Opportunities for cold atmospheric plasma. *Trends in food science & technology*. https://doi.org/10.1016/j.tifs.2022.04.006

Kaushik, N. K., Ghimire, B., Li, Y., Adhikari, M., Veerana, M., Kaushik, N., Jha, N., Adhikari, B., Lee, S.-J., & Masur, K. (2018). Biological and medical applications of plasma-activated media, water and solutions. *Biological Chemistry, 400*(1), 39-62. https://doi.org/10.1515/hsz-2018-0226

Korshunov, S. S., & Imlay, J. A. (2002). A potential role for periplasmic superoxide dismutase in blocking the penetration of external superoxide into the cytosol of Gram-negative bacteria. *Molecular Microbiology, 43*(1), 95-106. https://doi.org/10.1046/j.1365-2958.2002.02719.x

Li, W., Zhou, R., Zhou, R., Weerasinghe, J., Zhang, T., Gissibl, A., Cullen, P. J., Speight, R., & Ostrikov, K. (2022). Insights into amoxicillin degradation in water by non-thermal plasmas. *Chemosphere, 291*, 132757. https://doi.org/10.1016/j.chemosphere.2021.132757

Li, Y., Pan, J., Ye, G., Zhang, Q., Wang, J., Zhang, J., & Fang, J. (2017). In vitro studies of the antimicrobial effect of non-thermal plasma-activated water as a novel mouthwash. *European Journal of Oral Sciences, 125*(6), 463-470. https://doi.org/10.1111/eos.12374

Lieberman, M. A., & Lichtenberg, A. J. (2005). Particle and Energy Balance in Discharges. In *Principles of Plasma Discharges and Materials Processing* (pp. 327-386). https://doi.org/10.1002/0471724254.ch10

Lin, L., Quoc Pho, H., Zong, L., Li, S., Pourali, N., Rebrov, E., Nghiep Tran, N., Ostrikov, K., & Hessel, V. (2021). Microfluidic plasmas: Novel technique for chemistry and chemical engineering. *Chemical Engineering Journal, 417*, 129355. https://doi.org/10.1016/j.cej.2021.129355

Lu, P., Chen, C., Wang, Q., Wang, Z., Zhang, X., & Xie, S. (2013). Phylogenetic diversity of microbial communities in real drinking water distribution systems. *Biotechnology and Bioprocess Engineering, 18*(1), 119-124. https://doi.org/10.1007/s12257-012-0230-z

Ma, M., Zhang, Y., Lv, Y., & Sun, F. (2020). The key reactive species in the bactericidal process of plasma activated water. *Journal of Physics D: Applied Physics, 53*(18), 185207. https://doi.org/0.1088/1361-6463/ab703a

Ma, R., Wang, G., Tian, Y., Wang, K., Zhang, J., & Fang, J. (2015). Non-thermal plasma-activated water inactivation of food-borne pathogen on fresh produce. *Journal of Hazardous Materials, 300*, 643-651. https://doi.org/10.1016/j.jhazmat.2015.07.061

Mai-Prochnow, A., Alam, D., Zhou, R., Zhang, T., Ostrikov, K., & Cullen, P. J. (2021). Microbial decontamination of chicken using atmospheric plasma bubbles. *Plasma Processes and Polymers, 18*(1), 2000052. https://doi.org/10.1002/ppap.202000052

Mai-Prochnow, A., Bradbury, M., Ostrikov, K., & Murphy, A. B. (2015). Pseudomonas aeruginosa Biofilm Response and Resistance to Cold Atmospheric Pressure Plasma Is Linked to the Redox-Active Molecule Phenazine. *PLOS ONE, 10*(6), e0130373. https://doi.org/10.1371/journal.pone.0130373

Mai-Prochnow, A., Clauson, M., Hong, J., & Murphy, A. B. (2016). Gram positive and Gram negative bacteria differ in their sensitivity to cold plasma. *Scientific Reports, 6*(1), 38610. https://doi.org/10.1038/srep38610

Mai-Prochnow, A., Zhou, R., Zhang, T., Ostrikov, K. K., Mugunthan, S., Rice, S. A., & Cullen, P. J. (2021). Interactions of plasma-activated water with biofilms: inactivation, dispersal effects and mechanisms of action. *npj Biofilms and Microbiomes, 7*(1), 1-12. https://doi.org/10.1038/s41522-020-00180-6

Man, C., Zhang, C., Fang, H., Zhou, R., Huang, B., Xu, Y., Zhang, X., & Shao, T. (2022). Nanosecond-pulsed microbubble plasma reactor for plasma-activated water generation and bacterial inactivation. *Plasma Processes and Polymers, 19*(6), 2200004. https://doi.org/10.1002/ppap.202200004

Muhammad, A. I., Liao, X., Cullen, P. J., Liu, D., Xiang, Q., Wang, J., Chen, S., Ye, X., & Ding, T. (2018). Effects of nonthermal plasma technology on functional food components. *Comprehensive Reviews in Food Science and Food Safety, 17*(5), 1379-1394. https://doi.org/10.1111/1541-4337.12379

Pan, J., Li, Y. L., Liu, C. M., Tian, Y., Yu, S., Wang, K. L., Zhang, J., & Fang, J. (2017). Investigation of Cold Atmospheric Plasma-Activated Water for the Dental Unit Waterline System Contamination and Safety Evaluation in Vitro. *Plasma Chemistry and Plasma Processing, 37*(4), 1091-1103. https://doi.org/10.1007/s11090-017-9811-0

Rathore, V., & Nema, S. K. (2021). Optimization of process parameters to generate plasma activated water and study of physicochemical properties of plasma activated solutions at optimum condition. *Journal of applied physics, 129*(8). https://doi.org/10.1063/5.0033848

Rathore, V., Patel, D., Butani, S., & Nema, S. K. (2021). Investigation of Physicochemical Properties of Plasma Activated Water and its Bactericidal Efficacy. *Plasma Chemistry and Plasma Processing, 41*(3), 871-902. https://doi.org/10.1007/s11090-021-10161-y

Rehan, M., Nada, A. A., Khattab, T. A., Abdelwahed, N. A. M., & El-Kheir, A. A. A. (2020). Development of multifunctional polyacrylonitrile/silver nanocomposite films: Antimicrobial activity, catalytic activity, electrical conductivity, UV protection and SERS-active sensor. *Journal of Materials Research and Technology, 9*(4), 9380-9394. https://doi.org/10.1016/j.jmrt.2020.05.079

Renn, T.-Y., Yang, C.-P., Wu, U.-I., Chen, L.-Y., Mai, F.-D., Tikhonova, M. A., Amstislavskaya, T. G., Liao, W.-C., Lin, C.-T., Liu, Y.-C., & Chang, H.-M. (2022). Water composed of reduced hydrogen bonds activated by localized surface plasmon resonance effectively enhances anti-viral and anti-oxidative activities of melatonin. *Chemical Engineering Journal, 427*, 131626. https://doi.org/10.1016/j.cej.2021.131626

Rothwell, J. G., Alam, D., Carter, D. A., Soltani, B., McConchie, R., Zhou, R., Cullen, P. J., & Mai‐Prochnow, A. (2022). The antimicrobial efficacy of plasma‐activated water against Listeria and E. coli is modulated by reactor design and water composition. *Journal of Applied Microbiology, 132*(4), 2490-2500. https://doi.org/10.1111/jam.15429

Royintarat, T., Seesuriyachan, P., Boonyawan, D., Choi, E. H., & Wattanutchariya, W. (2019). Mechanism and optimization of non-thermal plasma-activated water for bacterial inactivation by underwater plasma jet and delivery of reactive species underwater by cylindrical DBD plasma. *Current Applied Physics, 19*(9), 1006-1014. https://doi.org/10.1016/j.cap.2019.05.020

Sen, Y., & Mutlu, M. (2013). Sterilization of Food Contacting Surfaces via Non-Thermal Plasma Treatment: A Model Study with Escherichia coli-Contaminated Stainless Steel and Polyethylene Surfaces. *Food and Bioprocess Technology, 6*(12), 3295-3304. https://doi.org/10.1007/s11947-012-1007-2

Sergeichev, K. F., Lukina, N. A., Sarimov, R. M., Smirnov, I. G., Simakin, A. V., Dorokhov, A. S., & Gudkov, S. V. (2021). Physicochemical properties of pure water treated by pure argon plasma jet generated by microwave discharge in opened atmosphere. *Frontiers in Physics, 8*, 614684. https://doi.org/10.3389/fphy.2020.614684

Shen, J., Tian, Y., Li, Y., Ma, R., Zhang, Q., Zhang, J., & Fang, J. (2016). Bactericidal Effects against S. aureus and Physicochemical Properties of Plasma Activated Water stored at different temperatures. *Scientific Reports, 6*(1), 28505. https://doi.org/10.1038/srep28505

Soni, A., Choi, J., & Brightwell, G. (2021). Plasma-Activated Water (PAW) as a Disinfection Technology for Bacterial Inactivation with a Focus on Fruit and Vegetables. *Foods, 10*(1), 166. https://doi.org/10.3390/foods10010166

Stapelmann, K., Kylián, O., Denis, B., & Rossi, F. (2008). On the application of inductively coupled plasma discharges sustained in Ar/O2/N2 ternary mixture for sterilization and decontamination of medical instruments. *Journal of Physics D: Applied Physics, 41*(19), 192005. https://doi.org/10.1088/0022-3727/41/19/192005

Taiwo, F. A. (2008). Mechanism of tiron as scavenger of superoxide ions and free electrons. *Spectroscopy, 22*, 953692. https://doi.org/10.3233/SPE-2008-0362

Tan, J., & Karwe, M. V. (2021). Inactivation and removal of Enterobacter aerogenes biofilm in a model piping system using plasma-activated water (PAW). *Innovative Food Science & Emerging Technologies, 69*, 102664. https://doi.org/10.1016/j.ifset.2021.102664

Thirumdas, R., Kothakota, A., Annapure, U., Siliveru, K., Blundell, R., Gatt, R., & Valdramidis, V. P. (2018). Plasma activated water (PAW): Chemistry, physico-chemical properties, applications in food and agriculture. *Trends in food science & technology, 77*, 21-31. https://doi.org/10.3390/pr11072213

Tresp, H., Hammer, M. U., Winter, J., Weltmann, K., & Reuter, S. (2013). Quantitative detection of plasma-generated radicals in liquids by electron paramagnetic resonance spectroscopy. *Journal of Physics D: Applied Physics, 46*(43), 435401. https://doi.org/10.1088/0022-3727/46/43/435401

Wan, K., Guo, L., Ye, C., Zhu, J., Zhang, M., & Yu, X. (2021). Accumulation of antibiotic resistance genes in full-scale drinking water biological activated carbon (BAC) filters during backwash cycles. *Water Research, 190*, 116744. https://doi.org/10.1016/j.watres.2020.116744

Wang, S., Liu, Y., Zhou, R., Liu, F., Fang, Z., Ostrikov, K. K., & Cullen, P. J. (2021). Microsecond pulse gas–liquid discharges in atmospheric nitrogen and oxygen: Discharge mode, stability, and plasma characteristics. *Plasma Processes and Polymers, 18*(2), 2000135. https://doi.org/10.1002/ppap.202000135

Wang, S., Yang, D., Liu, F., Wang, W., & Fang, Z. (2018). Spectroscopic study of bipolar nanosecond pulse gas-liquid discharge in atmospheric argon. *Plasma Science and Technology, 20*(7), 075404. https://doi.org/10.1088/2058-6272/aabac8

Winterbourn, C. C. (2020, 2020/01/28). Biological chemistry of superoxide radicals. *ChemTexts, 6*(1), 7. https://doi.org/10.1007/s40828-019-0101-8

Xiao, D., Cheng, C., Shen, J., Lan, Y., Xie, H., Shu, X., Meng, Y., Li, J., & Chu, P. K. (2014). Characteristics of atmospheric-pressure non-thermal N2 and N2/O2 gas mixture plasma jet. *Journal of applied physics, 115*(3), 033303. https://doi.org/10.1063/1.4862304

Xu, D., Liu, D., Wang, B., Chen, C., Chen, Z., Li, D., Yang, Y., Chen, H., & Kong, M. G. (2015). In Situ OH Generation from O2− and H2O2 Plays a Critical Role in Plasma-Induced Cell Death. *PLOS ONE, 10*(6), e0128205. https://doi.org/10.1371/journal.pone.0128205

Xu, H., Liu, C., & Huang, Q. (2023). Enhance the inactivation of fungi by the sequential use of cold atmospheric plasma and plasma-activated water: Synergistic effect and mechanism study. *Chemical Engineering Journal, 452*, 139596. https://doi.org/10.1016/j.cej.2022.139596

Xu, Z., Zhou, X., Yang, W., Zhang, Y., Ye, Z., Hu, S., Ye, C., Li, Y., Lan, Y., & Shen, J. (2020). In vitro antimicrobial effects and mechanism of air plasma-activated water on Staphylococcus aureus biofilm. *Plasma Processes and Polymers, 17*(8), 1900270. https://doi.org/10.1002/ppap.201900270

Yahaya, A. G., Okuyama, T., Kristof, J., Blajan, M. G., & Shimizu, K. (2021). Direct and Indirect Bactericidal Effects of Cold Atmospheric-Pressure Microplasma and Plasma Jet. *Molecules, 26*(9), 2523. https://doi.org/10.3390/molecules26092523

Yuan, D., Tang, S., Qi, J., Li, N., Gu, J., & Huang, H. (2017). Comparison of hydroxyl radicals generation during granular activated carbon regeneration in DBD reactor driven by bipolar pulse power and alternating current power. *Vacuum, 143*, 87-94. https://doi.org/10.1016/j.vacuum.2017.06.003

Zhao, Y., Shao, L., Jia, L., Meng, Z., Liu, Y., Wang, Y., Zou, B., Dai, R., Li, X., & Jia, F. (2022). Subcellular inactivation mechanisms of Pseudomonas aeruginosa treated by cold atmospheric plasma and application on chicken breasts. *Food Research International, 160*, 111720. https://doi.org/10.1016/j.foodres.2022.111720

Zhou, R., Zhang, T., Zhou, R., Wang, S., Mei, D., Mai-Prochnow, A., Weerasinghe, J., Fang, Z., Ostrikov, K. K., & Cullen, P. J. (2021). Sustainable plasma-catalytic bubbles for hydrogen peroxide synthesis. *Green Chemistry, 23*(8), 2977-2985. https://doi.org/10.1039/D1GC00198A

Zhou, R., Zhou, R., Wang, P., Xian, Y., Mai-Prochnow, A., Lu, X., Cullen, P. J., Ostrikov, K., & Bazaka, K. (2020). Plasma-activated water: generation, origin of reactive species and biological applications. *Journal of Physics D: Applied Physics, 53*(30), 303001. https://doi.org/10.1088/1361-6463/ab81cf

4 Chapter 4 Antimicrobial mechanism of *in-situ* plasma activated water treatment of pathogenic *Escherichia coli* and *Staphylococcus aureus* biofilms

Author contribution

Binbin Xia*: Conceptualization, Methodology, Investigation, Validation, Data curation, Formal analysis, Writing – original draft.

Heema Kumari Nilesh Vyas: Investigation, Methodology, Writing – original draft, review & editing.

Scott A. Rice: Writing – review & editing, Project administration, Funding acquisition.

Timothy P. Newsome: Writing – review & editing.

Patrick J. Cullen: Supervision.

Anne Mai-Prochnow: Conceptualization, Supervision, Investigation, Formal data analysis, Writing – review & editing, Funding acquisition, Project administration.

*Corresponding author

4.1 Abstract

This study investigated the efficacy and mechanisms of inactivation of against *Escherichia coli* UTI89 and *Staphylococcus aureus* NCTC8325 through an *in-situ* plasma-activated water (PAW) treatment. PAW was prepared by discharging atmospheric pressure cold plasma beneath the surface of sterile distilled water. The study investigated the inactivation of biofilm cells and biofilm matrix. A complete killing of biofilm cells was achieved on both of *E. coli* (6.76 ± 0.01 log CFU/mL) and *S. aureus* (6.82 ± 0.02 log CFU/mL). This process happened earlier in *S. aureus.* Simultaneously, PAW treatment disrupted the biofilm structure, inducing a significant reduction in general biofilm biomass and extracellular polymer substances (EPS) matrix. With the disruption of EPS, PAW was enabled to further interact with the bacterial membrane, causing a significant increase in membrane permeability and disrupted membrane structure. Finally, PAW treatment led to a significant accumulation of intracellular reactive oxygen and nitrogen species within the biofilm cells. Collectively, these findings indicate that PAW effectively inactivates biofilms by targeting the biofilm EPS matrix and biofilm cells in both gram-negative and gram-positive bacteria. Given that PAW damages various components of bacterial biofilms, it emerges as an effective strategy for controlling biofilms in water treatment.

4.2 Introduction

Pathogenic biofilms pose a significant challenge in healthcare settings and various industries. They are the main cause of the rise in microbial contamination forming in water distribution systems, including pipes, tanks, and filters (Dula et al., 2021). Drinking contaminated water or engaging in water activities like swimming, sailing, and other water sports in contaminated waters can result in waterborne diseases caused by bacteria and other pathogenic microorganisms (Carrascosa et al., 2021; Dula et al., 2021; Shineh et al., 2023). Unlike planktonic cells, bacterial biofilms, form structured communities with a protective matrix, rendering them 1000-fold more resistant to conventional cleaning and disinfection methods (Billings et al., 2015; Cámara et al., 2022). The protective matrix of the biofilm limits the penetration of disinfectants, and bacterial cells within the biofilm may enter a dormant state, making them less susceptible to chemical treatments.

At the core of biofilm architecture lies the extracellular polymeric substance (EPS). This matrix, secreted by microorganisms themselves or captured from host components, plays a crucial role in shaping the behaviour, resilience, and functionality of biofilms. The EPS matrix can be comprised of polysaccharides, DNA, RNA, proteins, and lipids, which affect the permeability and mechanical properties of the biofilm (Billings et al., 2015; Karygianni et al., 2020; Limoli et al., 2015). All of these polymers act as the adhesive that binds microbial cells together, providing structural integrity to the biofilm community (Danese et al., 2000; Horvat et al., 2019). Most antimicrobial agents kill cells, but the matrix may be left behind and that may help with biofilm regrowth and recruitment of new cells (Campoccia et al., 2021). Therefore, it is important to find a treatment that will get rid of the matrix as well as kill cells.

Innovative approaches are continuously sought to combat biofilm-related issues. One promising solution that has garnered attention is plasma-activated water (PAW) (Chen et al., 2018; D. Guo et al., 2021). Plasma, often referred to as the fourth state of matter, is a highly energetic state of ionized gases, including excited and neutral atoms, electrons, free radicals, ions, and high-energy photons

(Jenns et al., 2022; Muhammad et al., 2018). When applied to water, plasma generates a reactive mixture rich in oxidizing species and free radicals. These physiochemical reactions occur between gaseous substances and liquid molecules and during the transfer of gaseous substances to liquids, resulting in a higher density of reactive oxygen and nitrogen species (RONS) of PAW (Mai-Prochnow et al., 2021; Zhou et al., 2020b). This unique composition enables PAW to exhibit potent antimicrobial properties, providing a potential avenue for disrupting and eradicating biofilms.

Despite the well documented bactericidal effect of PAW against biofilms of several species, including *Escherichia coli, Pseudomonas aeruginosa, Listeria monocytogenes,* and *Staphylococcus aureus* (L. Guo et al., 2021; Handorf et al., 2021; Vyas et al., 2023; Ziuzina et al., 2015), there remains a notable gap in understanding the mechanism of PAW's antibacterial effect on biofilms. Current research suggests that PAW mechanically induces an etching effect to prompt the detachment of biofilms from surfaces. Subsequently, RONS present in PAW, (e.g., peroxide, nitrate, OH radicals) are free to further penetrate the EPS matrix and disrupt the cell membrane integrity (Mai-Prochnow et al., 2021). The activity of PAW varies depending on factors such as the type of plasma generated, bacterial strains, and the biofilm EPS matrix components. At this stage, it remains unclear why the effects of PAW differ for these factors.

Our objective was to investigate the efficacy and mechanisms of direct PAW activity against *E. coli* UTI89 and *S. aureus* NCTC8325 biofilm. Even though PAW generated with O_2 showed the highest reduction of biofilms in Chapter 3, considering the balance of antibiofilm efficacy and the cost of real-life application, PAW generated with air was applied in this chapter. We demonstrate that PAW initially eliminates a significant portion of *E. coli* and *S. aureus* biofilm cells, resulting in disruption of biofilm structure, specifically EPS matrix. By proving its efficacy against both Gram-positive and Gram-negative bacterial biofilms and exploring its mechanisms of action, our results highlight the potential of PAW in biofilm control strategies and alleviate the associated challenges in healthcare, food safety, and water treatment.

4.3 Materials and Methods

4.3.1 Bacterial strains and cultivation

Uropathogenic *E. coli* UTI89 and pathogenic *S. aureus* NCTC8325 were chosen as the Gram-negative and Gram-positive strains, respectively. *E. coli* and *S. aureus* were routinely cultured on Luria-Bertani (LB) agar, consisting of 10.0 g/L pancreatic digest of casein tryptone, 10.0 g/L sodium chloride, 5.0 g/L yeast extract, and 7.5 g/L agar powder. A single colony from a freshly streaked agar plate was inoculated into 5 mL of LB broth and incubated overnight at 37°C with agitation at 160 rpm.

4.3.2 Biofilm formation

E. coli and *S. aureus* biofilms were formed on sterile stainless-steel coupons (Thickness = 3.8 mm, Diameter = 12.7mm; BioSurface Technologies, USA) placed in a 24-well plate. 1 mL of the diluted culture (~ $5x10^6$ CFU/mL) was inoculated into each well of the plate and then incubated for 48 hours at 37 °C without shaking to facilitate cell attachment and subsequent biofilm formation.

4.3.3 PAW generation and treatment

PAW was produced using a bubble spark discharge (BSD) reactor, following the procedure outlined in our prior research (Xia et al., 2023). Briefly, the BSD reactor was immersed in 100 mL of sterile MilliQ water contained within a 250 mL Schott bottle, with coupons bearing attached biofilms (Figure 4.1). A high-voltage power source (Leap100, PlasmaLeap Technologies, Sydney) was utilized to discharge plasma into the water, employing an input voltage of 150 V, a discharge frequency of 1500 Hz, a resonance frequency of 60 kHz, and a duty cycle of 100 µs. Treatment durations ranged from 1 to 20 min with a compressed air gas flow of 1 standard liter per minute (slm). Coupons with biofilms were immersed in 100 mL of sterile MilliQ water and subjected to plasma treatment. As a control, coupons were submerged in 100 mL of sterile MilliQ water without plasma discharge.

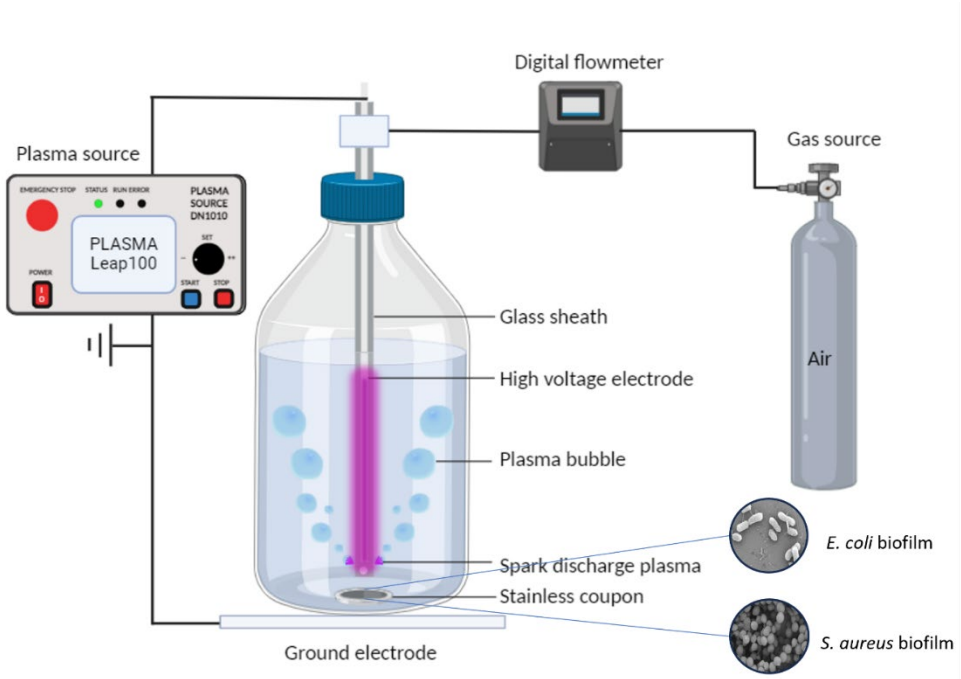

Figure 4.1. A schematic illustration of the direct biofilm treatment using plasma-activated water (PAW) generated by a bubble spark discharge (BSD) plasma reactor. *E. coli* UTI89 biofilm and *S. aureus* NCTC8325 biofilm were formed on stainless-steel coupons and positioned at the bottom of a Schott bottle containing 100 mL of MilliQ water. The BSD reactor comprises a high-voltage electrode and a glass sheath. To induce spark discharge plasma, a flow rate of 1 standard liter per minute (slm) of compressed air was utilized to bubble the water, while the high-voltage electrode was energized by the PlasmaLeap100 power source.

4.3.4 Biofilm cell viability

Immediately following the PAW treatment, coupons were retrieved from the treatment bottle and transferred into a Falcon tube containing 1 mL of 1x phosphate-buffered saline (PBS). The biofilm was detached from the coupon surface by gently scraping it with a sterile flat-end spatula. Subsequently, a 3 min water bath sonication at 45 kHz, followed by 10 s of vortexing, was employed to ensure complete dislodgment of biofilms. It is noteworthy that this procedure did not affect cell viability (data not shown). Serial dilutions were then drop-plated (10 µL) onto LB agar in triplicates. The plates were subsequently incubated overnight at 37 °C before determining the colony-forming units (CFU). The CFU log10 reduction (Equation 1) and percentage of reduction (Equation 2) were calculated as follows:

Equation 1

$$CFU\ log_{10}\ reduction = log_{10}(initial\ CFU) - log_{10}(final\ CFU)$$

Equation 2

$$Percentage\ of\ reduction = \left(1 - \frac{final\ CFU}{initial\ CFU}\right) \times 100\%$$

4.3.5 Biofilm biomass crystal violet assay

Following PAW treatment, coupons were retrieved from the treatment bottle and transferred into a Falcon tube containing 1 mL of 1× PBS. The biofilms were then air-dried thoroughly at room temperature for 30-40 min or until completely dried. Subsequently, the air-dried biofilms were stained with 900 µL of 0.2% crystal violet (v/v, Sigma-Aldrich, USA) dissolved in distilled water supplemented with 1.9% ethanol (v/v, Sigma-Aldrich) for 10 min at room temperature under static conditions. After staining, excess crystal violet was removed, and the biofilms were gently washed three times with 900 µL of PBS. The crystal violet stain incorporated into the biofilm was re-solubilized by adding 900 µL of 1% sodium dodecyl sulfate (SDS) (w/v, Sigma-Aldrich, USA), followed by a 10 min incubation at room temperature in the dark. Biofilm biomass was quantified by spectrophotometrically measuring the re-solubilized crystal violet stain, which had previously incorporated into the sample, at OD540 nm/570 nm using a CLARIOStar microplate reader. The biomass measurement encompasses both bacterial cells and the EPS matrix.

4.3.6 Biofilm EPS matrix

EPS matrix

To qualitatively visualize the distribution of biofilm extracellular polymeric substance (EPS) components, including extracellular DNA (eDNA), protein, and polysaccharides, additional fluorescent probes were utilized: Sytox Blue (S11348, Invitrogen, USA), Sypro Ruby (F10318, Invitrogen, USA), and Concanavalin A (Con A) Alexa Fluor 647, respectively (Costa Oliveira et al., 2017; Vyas et al., 2020).

Confocal laser scanning microscopy

Briefly, prior to staining, the PAW-treated biofilms were washed three times with 0.5 mL of PBS. EPS matrix of eDNA and protein were stained with 1 mL of 5 µM Sytox Blue and 1x concentration of Sypro Ruby stain, respectively, for 30 minutes in the dark. Meanwhile, the polysaccharide component

of the matrix was stained with 5 μg/mL Con A Alexa Fluor 647 for 15 minutes in the dark. Coupons without biofilm served as controls for background staining. Upon completion of the staining process, the stained biofilms were visualized using an inverted Nikon Ti-E confocal microscope equipped with a 20 x objective. Specifically, Sytox Blue was imaged at Ex/Em 440nm/482nm, SYPRO Ruby at Ex/Em 450nm/610nm, and Con A Alexa Fluor 647 at Ex/Em 625nm/680nm. Fluorescent imaging was done in triplicate (n=3). Random positions of each sample were imaged. The EPS matrix response to PAW was quantified via ImageJ analysis as expressed in relative fluorescence intensity and intensity changes.

4.3.7 Scanning electron microscopy

Scanning electron microscopy (SEM) imaging was performed to evaluate the morphological and architectural alterations induced in *E. coli* and *S. aureus* biofilms following 1 and 5 min direct PAW treatment, with comparisons made to a MilliQ control treatment. Briefly, as modified from (Vyas et al., 2023), 48 h biofilms air dried and pre-fixed for 30 min at 4 °C, and then fixed for 1 h at 4 °C. Post-fixation, washed biofilms were dehydrated via graded ethanol series (25%, 50%, 75%, and 3 × 100%). Critical point dried biofilm samples were then sputter coated with 10 nm of gold using a CCU-010 HV high compact vacuum coating system (Safematic, Switzerland). Samples were imaged using the Zeiss Sigma VP HD scanning electron microscope (ZEISS, Germany) at 500 x and 15000 x magnification. Images were captured at random positions to minimize bias.

4.3.8 Membrane permeability study

The outer membrane permeability of *E. coli* and *S. aureus* was assessed using the N-phenyl-1-naphthylamine (NPN) uptake assay following the method described by Halder (2015). Both *E. coli* and *S. aureus* were cultured to logarithmic phase, reaching approximately 10^8 cells/mL. Subsequently, 100 μL of the bacterial suspension (≈5×10^6 CFU/mL) was dispensed into each well of a 96-well plate. The plate was then centrifuged at 3900 g for 15 min, and the supernatant from each well was carefully removed and replaced with 50 μL of 10 μM NPN solution (dissolved in PBS). The stained cells were subsequently exposed to 200 μL of PAW and control Bubble water, with fluorescence

measurements taken at various time points (0, 30, 60, 120, and 180 min). As a positive control, 20 µg/mL of cetyltrimethylammonium bromide (CTAB) was used (Halder et al., 2015). The change in NPN fluorescence was quantified at excitation/emission wavelengths of 350-15 nm/420-15 nm. All experiments were performed in triplicate for statistical analysis. Membrane permeability was determined by calculating the difference between the fluorescence intensity of NPN-stained cells and the background fluorescence intensity of the cell suspension without NPN.

Membrane depolarization in *E. coli* and *S. aureus* was evaluated using 3,3'-diethylthiadicarbocyanine iodides (2 µmol/L; Sigma), a fluorogenic dye capable of measuring changes in transmembrane potential as previously described (Vyas et al., 2023). The dye was allowed to incorporate into bacteria cells for 20 minutes at 37°C. Subsequently, the bacteria were washed and exposed to PAW, as well as control treatments (MilliQ and Bubble). Fluorescence intensity was measured at excitation/emission wavelengths of 600-15/660-15 nm using a ClarioStar microplate reader, and membrane depolarization was quantified in arbitrary units. As a positive control, 200 µg/mL of cetyltrimethylammonium bromide (CTAB) was utilized (Halder et al., 2015). Membrane depolarization was determined by subtracting the fluorescence intensity of stained cells from the background fluorescence intensity of the stainless cell suspension.

4.3.9 Intracellular ROS and RNS detection

The accumulation of intracellular ROS and RNS PAW-treated *E. coli* and *S. aureus* biofilm cells were investigated using 2′,7′–dichlorofluorescin diacetate (DCFDA; Sigma Aldrich, Australia) and 4,5-diaminofluorescein diacetate (DAF-FM; Sigma-Aldrich, Australia) staining assays, as previously described (Vyas et al., 2023). In brief, 48 h *E. coli* and *S. aureus* biofilms were exposed to 200 µL of PAW or MilliQ water (MQ) as a control for 15 minutes. Following PAW exposure, the biofilms were stained with 150 µL of 20 µM DCFDA or 5 µM DAF-FM for 30 minutes. The levels of intracellular ROS and RNS were quantified in triplicate using a microplate reader at Ex/Em of 485-15 nm/545-15 nm and Ex/Em 495-15 nm/515-15 nm, respectively. The final fluorescent intensity was determined by subtracting the background intensity from the fluorescent intensity of the stained cell solution.

4.3.10 Statistical analysis

Experiments were performed 3 times and values are expressed as mean ± standard error of mean ($\mu \pm \sigma_{\bar{x}}$). A parametric, One-way ANOVA (with Tukeys multiple comparisons test, $p<0.05$) was performed where appropriate to identify significant differences in log reduction of each sample compared to the control. Two-way ANOVA (with Tukeys multiple comparison test, $p < 0.05$) was performed where appropriate to identify significant differences in bacterial membrane permeability and intracellular ROS and RNS level of each sample.

4.4 Results

4.4.1 Direct PAW treatment inactivates biofilm cells

The efficacy of PAW in inactivating biofilms of *E. coli* UTI89 and *S. aureus* NCTC 8325 bacterial strains was evaluated. A time-dependent inactivation of biofilm cells was observed upon direct PAW treatment. A complete reduction of CFU was achieved after 13 min of treatment for *E.coli* (6.76 ± 0.01 log CFU/mL) and after 11 min of treatment for *S. aureus* biofilms (6.82 ± 0.02 log CFU/mL) (Figure 4.2). PAW treatment for 5 min (5min-PAW) already resulted in a significant log reduction in both *E. coli* (3.06 ± 0.06 log CFU/mL) and *S. aureus* (3.78 ± 0.03 log CFU/mL), corresponding to over 99% reduction compared to the initial CFU. The biofilm populations of *E. coli* exhibited greater susceptibility than *S. aureus* biofilms within the first minute of PAW treatment. However, S. *aureus* biofilm cells were reduced to below the detection limit of 1.0 log10 at 11 min, while it took 13 min for *E. coli* biofilms to reach the same level. No significant difference was observed in the reduction of overall biofilm populations between these two bacterial species.

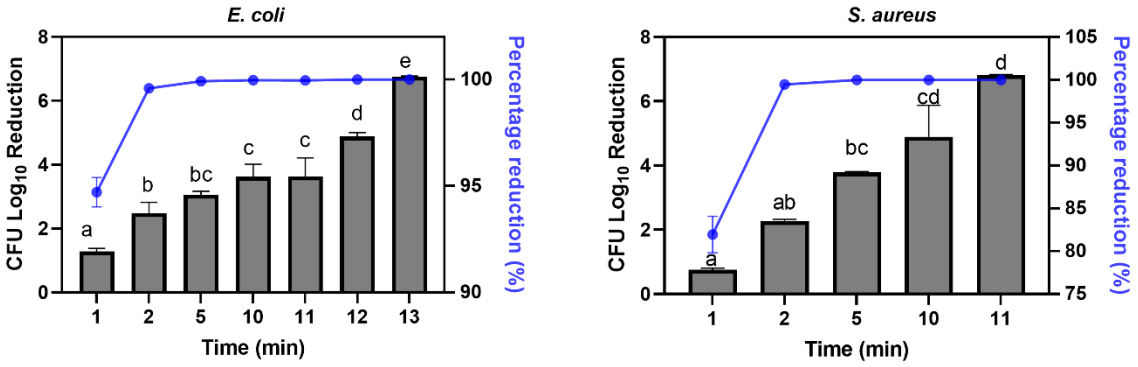

Figure 4.2 Inactivation efficacy of PAW with different plasma discharge time on 48h *E. coli UTI89* biofilm and *S. aureus NCTC8325* biofilms. Different letters indicate significant differences between groups ($p<0.05$). The data are represented as mean ± SEM (n=3).

4.4.2 Effect of PAW on biofilm biomass

The total biofilm biomass is another critical factor in studying inactivation efficiency. Biofilm biomass was assessed using the crystal violet staining assay. As shown in Figure 4.3, biofilms formed by both *E. coli* and *S. aureus* were reduced significantly after PAW treatment. More specifically, the biomass of *E. coli* biofilms decreased rapidly by 48.4% after 1 min of in-situ PAW treatment and reduced by up to 53.5% after 15 min of PAW treatment compared to the control (0-min treatment). Similarly, PAW-treated *S. aureus* biofilm biomass exhibited a time-dependent reduction, with reductions of 23.6% after 1 min of PAW treatment and 50.2% after 15 min of PAW treatment compared to the control (0 min- treatment). However, after the initial decrease in biomass detected by CV, no further reduction was observed and the absorbance numbers for the 15 min treatment are not significantly different to the 5 min treatment.

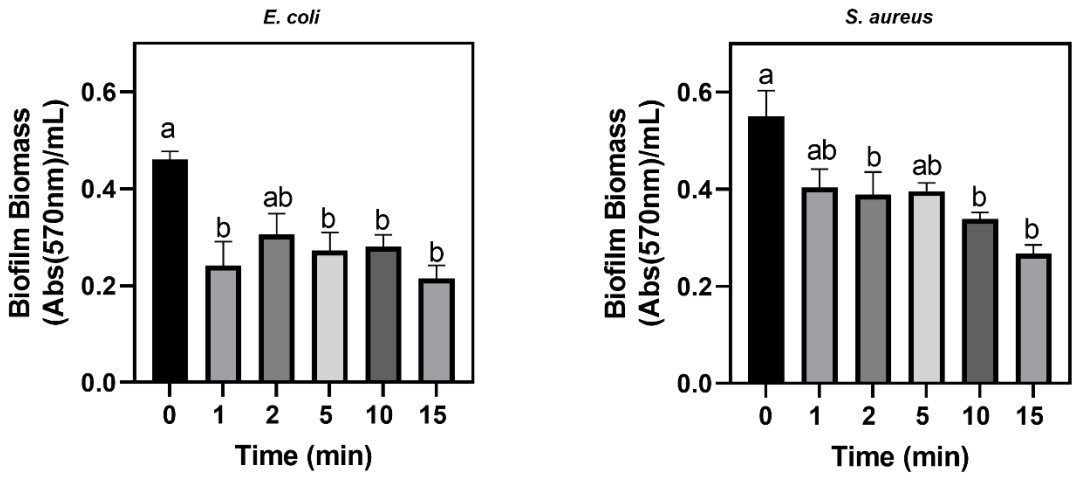

Figure 4.3 Change in biofilm biomass of *E. coli* UTI89 and *S. aureus* NCTC8325 biofilm challenged by 0 to 15 min of direct PAW treatment. Data represents mean ± SEM. Different letters indicate significant differences between groups ($p<0.05$); n =2 biological replicates, with 2 technical replicates each.

4.4.3 EPS matrix response to PAW treatment

To better understand the effect of PAW on the biofilm, the EPS matrix was assessed using a fluoroprobe, Con A Alexa Fluor 647, known for its reactivity with aldehydes in polysaccharides. As shown in Figure 4.4, PAW treatment notably reduced the EPS matrix in both *E. coli* and *S. aureus* biofilms in a time-dependent manner., significant differences in polysaccharides response to PAW treatment were observed and the EPS was reduced by 80.69% for E. coli and 79.08% for S. aureus after 15 min PAW treatment.

Polysaccharides are the predominant component of the biofilm matrix (Flemming & Wingender, 2010). One prominent exopolysaccharide is N-acetylglucosamine polymer found in the biofilms of *E. coli, S. aureus*, and *S. epidermidis* (Nguyen et al., 2020; Wang et al., 2004), with the ability to form a capsule on the cell surface, serving not only to bind cells to surfaces but also as an adhesin to stabilize the biofilm structure (Flemming & Wingender, 2010; Sharma et al., 2016). The significant removal of extracellular polysaccharides from the EPS matrix might contribute to the oxidative reaction between PAW RONS and the cells within the biofilm, leading to its destruction. For instance, the hydroxyl and carboxyl groups in polysaccharides may trap the plasma-generated OH radicals, resulting in hydrogen

abstraction and subsequent molecular damage to polysaccharides (Khosravian et al., 2014). This also helps to explain the reduction in biofilm biomass through PAW treatment.

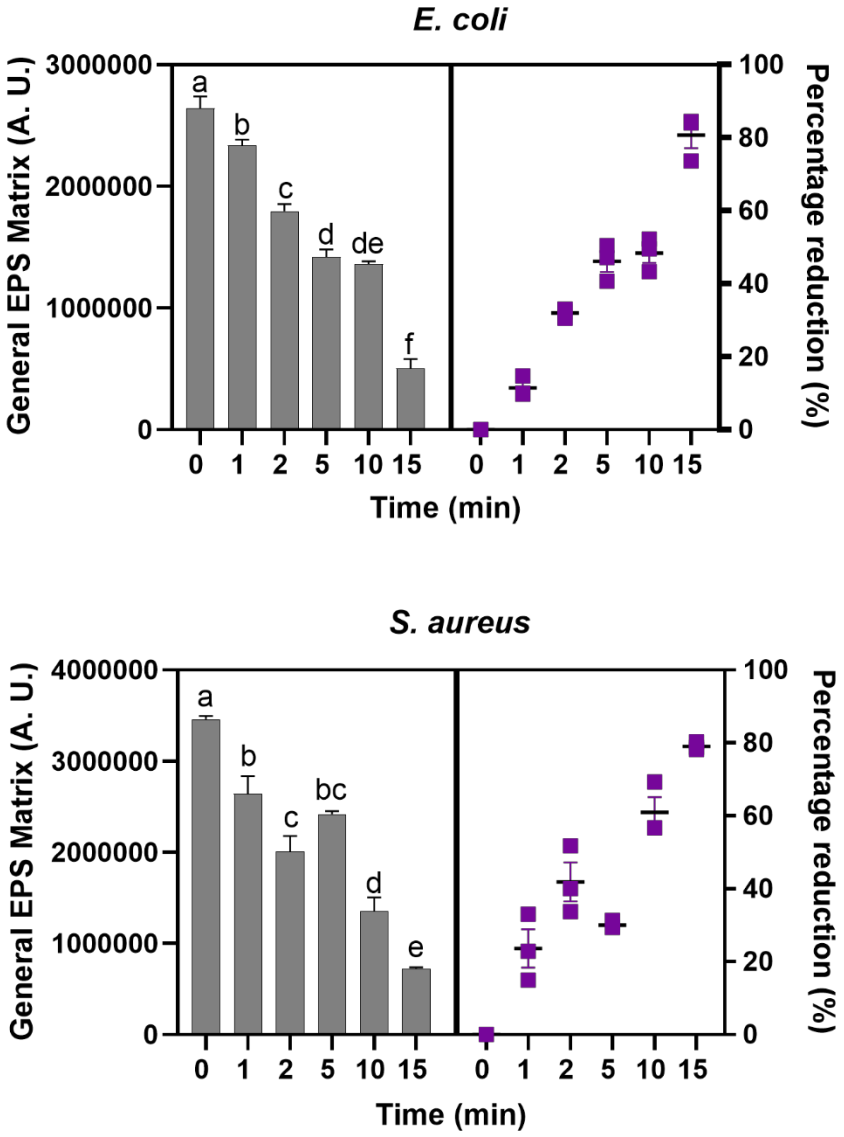

Figure 4.4 Time-dependant general EPS matrix deduction of *E. coli* UTI89 and *S. aureus* NCTC8325 biofilms challenged by 0 to 15 min of direct PAW treatment. Different letters indicate significant differences between groups (P<0.05). Data represents mean ± SEM; n = 3.

In addition to the quantitative polysaccharides assessment, the PAW treated biofilms were stained with fluorescent probes to visualize for polysaccharides, eDNA and protein components of the EPS matrix using a fluorescent microscope (Figure 4.5). The polysaccharides (*Con A* staining) of *E. coli* and *S. aureus* biofilms exhibited a significant decrease compared to the untreated biofilms after 1, 5 ,

and 15 min treatment. From the images, some polysaccharide debris was observed after PAW exposure, confirming the results of the quantitative EPS matrix evaluation above.

Sytox Blue, impermeable to live cells but able to stain the extracellular nucleic acid of dead cells or the matrix, was utilized for staining eDNA. The fluorescence intensity of the eDNA stain in *E. coli* and *S. aureus* decreased rapidly after 1 min of PAW treatment, followed by a notable increase in fluorescence intensity at 5 min-PAW treatment, after which its fluorescent signal significantly decreased. Alongside the log reduction results (Figure 4.2), the observed increase in blue fluorescence might be attributed to the DNA released by dead cells following PAW exposure. eDNA serves as a cohesive agent, binding the biofilm matrix with the cells, which is crucial for structural stability (Flemming & Wingender, 2010). Upon eDNA removal, the biofilm cells are more prone to detachment from the matrix, rendering them more susceptible to oxidative exposure from PAW (Patange et al., 2021). The observed changes in eDNA levels suggest that PAW initiates biofilm cell detachment as early as the first minute of treatment by removing eDNA, subsequently disrupting the bacterial cells to release intracellular DNA, thus facilitating the complete eradication of biofilm cells.

In contrast to the consistent reduction observed in exopolysaccharides and eDNA, the protein matrix in *E. coli* and *S. aureus* biofilms remained present even when cells were undetected. As shown in the images under red fluorescence in Figure 4.5, extracellular proteins were clustered and evenly spread across the steel surface. Following 1 min-PAW treatment, a significant portion of these protein clusters was removed, revealing an evenly distributed protein signal resembling the shape of cells. Subsequently, an increase in protein fluorescence was noted at the 5 min-PAW treatment point. One possible explanation could be the release of proteins by dead cells, akin to the eDNA dynamics mentioned earlier, as the cell wall comprises a significant proportion of glycoproteins. Oxidative agents in PAW (e.g., hydrogen peroxide, a long-lived ROS generated in PAW) have demonstrated the ability to oxidise proteins, disrupting protein and DNA (da Cruz Nizer et al., 2021). Additionally, the reactive species in PAW might inhibit the enzyme activity of producing catalase enzymes and superoxide dismutase which can convert harmful ROS within the cell before they induce damage (Finnegan et al., 2010).

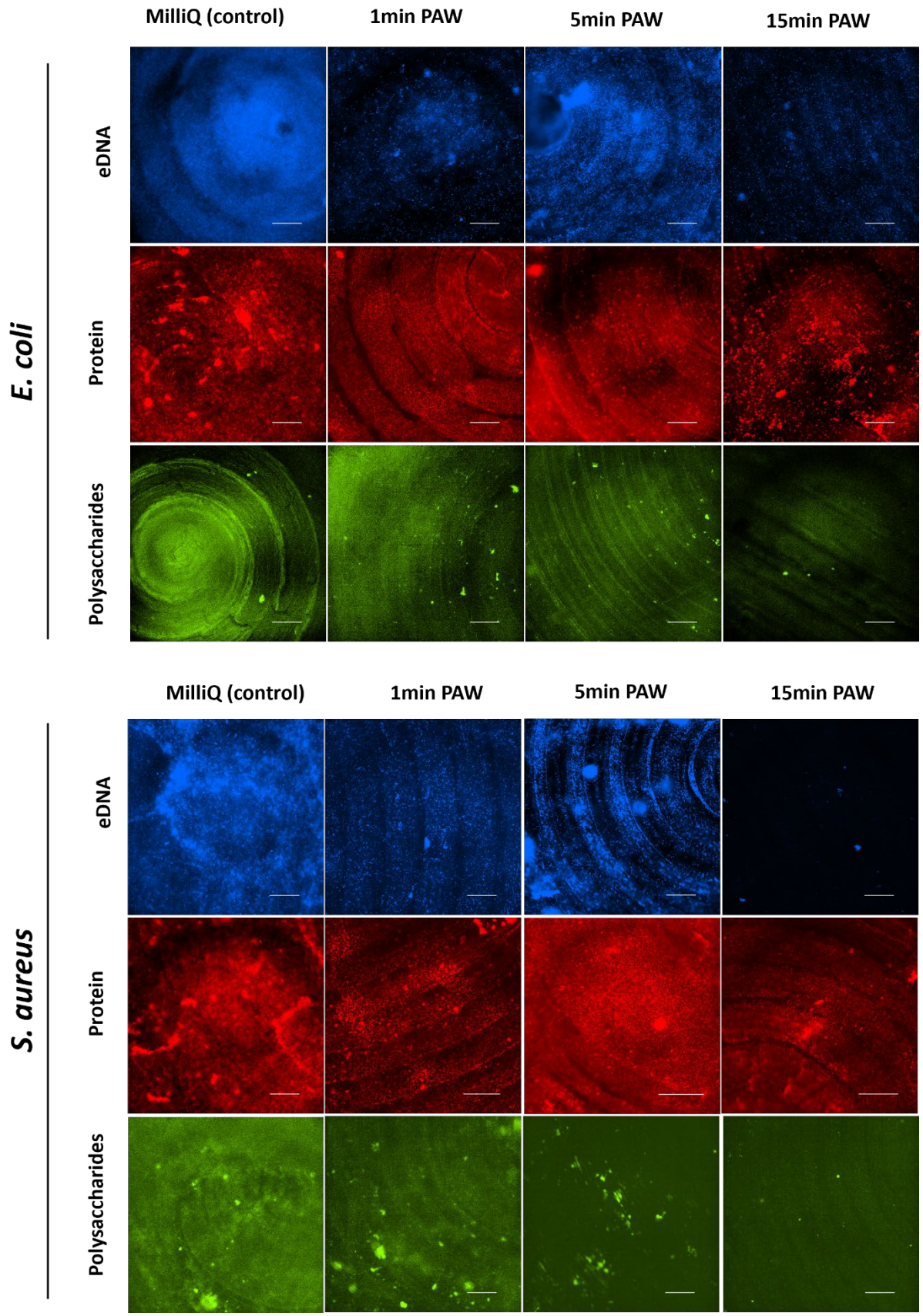

Figure 4.5 The EPS matrix fluorescent images of *E. coli* UTI89 and *S. aureus* NCTC8325 under non-treatment (control), 1 min, 5 min, and 15 min-PAW treatment. EPS matrix of extracellular DNA, protein, and polysaccharides

were stained using Sytox Blue, Sypro Ruby, and Con A Alexa fluo 647, respectively. Experiments were repeated in triplicates and random positions were taken. Scale bar = 100 µm.

4.4.4 Biofilm morphology changed after PAW treatment

To visualise the effects of direct PAW treatment on the biofilm and the cell structure, SEM imaging was conducted (Figure 4.6). As biofilm cells were completely removed after 15 min treatment, therefore, cells under 1 min and 5 min PAW treatment were imaged by SEM. Qualitative analysis demonstrates a discernible decrease in the number of physically adhered *E. coli* and *S. aureus* biofilm cells on the stainless-steel surface following both 1 min and 5 min PAW treatments, as compared to the MilliQ control. Additionally, PAW treatments induce morphological alterations in both *E. coli* and *S. aureus* biofilm cells, resulting in a flattened appearance that is particularly evident in *E. coli* cells.

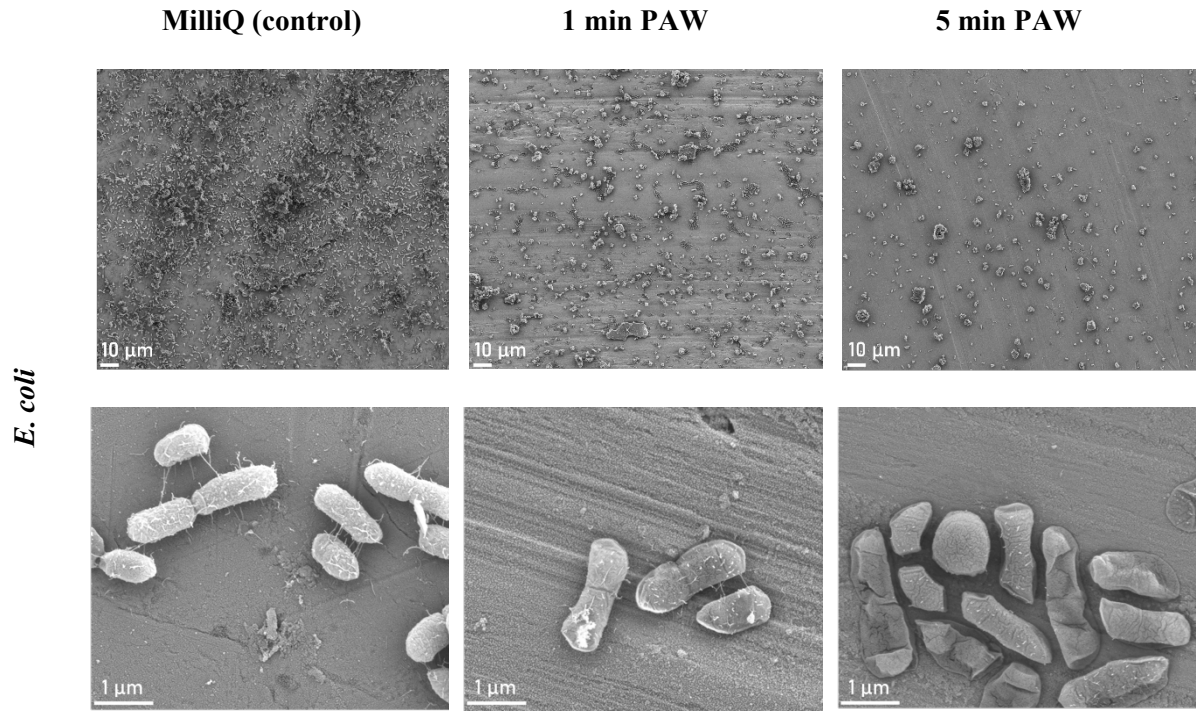

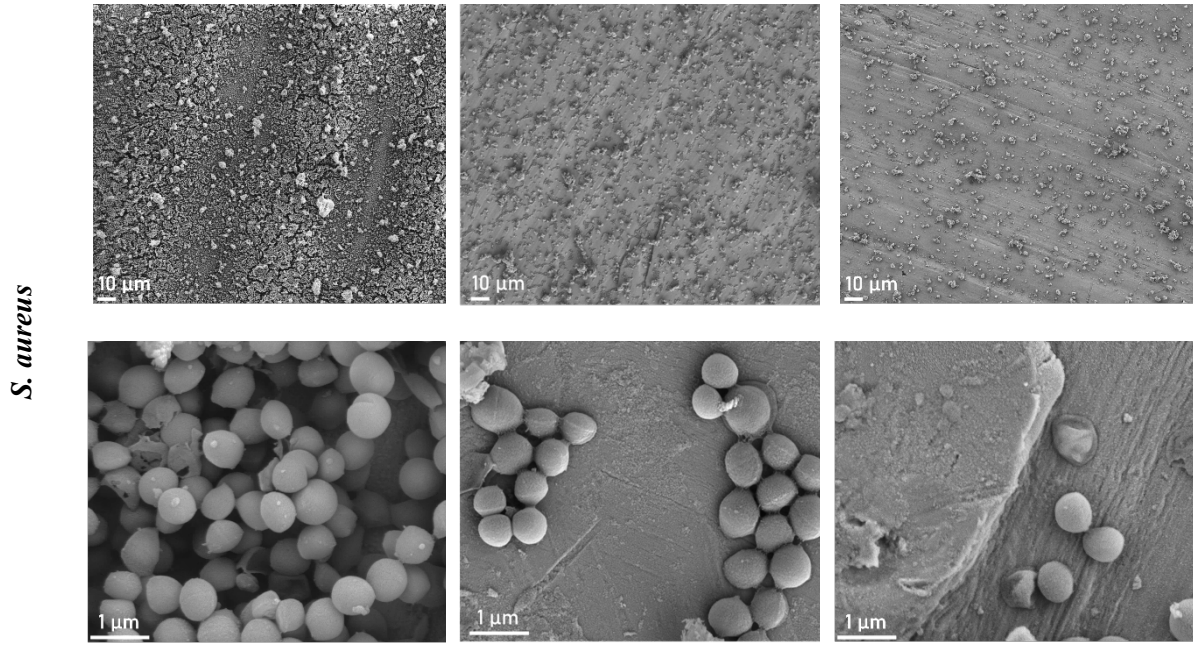

Figure 4.6 PAW treatment physically dislodges *E. coli* and *S. aureus* bacterial biofilm cells and is altering the bacterial cell morphology. SEM imaging was utilised to visualise the architectural and morphological changes induced by 1 and 5 min treatments. A MilliQ control was included for comparison. Both 1 and 5 min treatment time points resulted in significant bacterial cell removal from the stainless steel surface, with some cells exhibiting a flattened cell morphology.

4.4.5 Membrane response to PAW

The alterations in membrane permeability and extracellular membrane potential enable bacteria to respond to environmental stress by connecting intracellular reactions to external conditions (Mingeot-Leclercq & Décout, 2016). Following this principle, the NPN-based assay and $DiSC_3(5)$ stains were used to elucidate the mode of action of PAW on the membrane permeability and membrane depolarization of *E. coli* and *S. aureus* cells (Figure 4.7). NPN fluorescence increases as the dye enters the cell due to the disruption of the membrane that leads to an increase in permeability. In PAW-treated *E. coli* and *S. aureus* suspensions a time-dependent increase in the fluorescence of NPN was observed. Compared to the MilliQ control, the fluorescence of NPN of *E. coli* and *S. aureus* suspensions rapidly increased after approximately 1 min treatment. NPN uptake fluctuated but remained not significantly different until 30 min.

$DiSC_3(5)$ can evaluate the polarization state of cells, as it can penetrate the lipid bilayer of membrane and further accumulate in cells intracellularly (Buttress et al., 2022). An increased fluorescence of $DiSC_3(5)$ under PAW treatment was observed in both of *E. coli* and *S. aureus* cells (Figure 4.7). More specifically, the membrane of *S. aureus* cells exhibited significant depolarization at 1 min PAW

exposure (P≤0.0001). This effect gradually increased until 20 min and remained consistent until 30 min. Conversely, PAW induced a less pronounced depolarization of the *E. coli* cell membrane compared to *S. aureus*. The membrane of *E. coli* gradually depolarized until 15 min (P<0.05), with this effect remaining stably until 30 min compared to the MilliQ control.

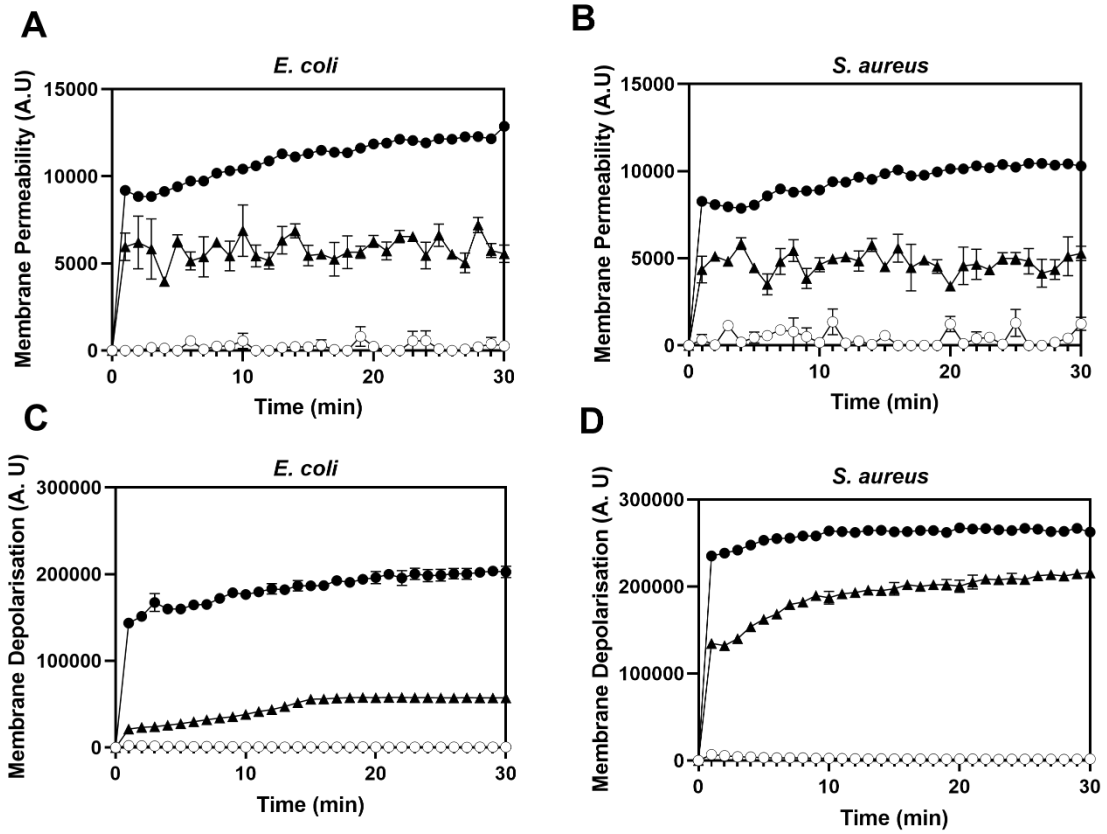

Figure 4.7 The response of bacterial *E. coli* UTI89 and *S. aureus* NCTC 8325) membrane permeability (A and B: assayed by NPN staining) and membrane depolarisation (C and D: assayed by DiSC3(5) staining) in the presence of control (negative control of Milli- Q water ○), PAW (▲), and CTAB (positive control, ●).

4.4.6 PAW induces an increase in intracellular RONS level

The accumulation of intracellular ROS and RNS within the PAW-treated *E. coli* and *S. aureus* biofilms was assessed using fluorescence probes DCFDA (ROS, Figure 4.8A) and DAF-FM (RNS, Figure 4.8B), respectively., A significant increase in DCFDA fluorescence (P ≤ 0.0001) was observed in both *E. coli* and *S. aureus* biofilm cells compared to the control, indicating that 15 min-PAW treatment induced the accumulation of ROS within both *E. coli* and *S. aureus* biofilms. However, the

amount of intracellular ROS increased even more significantly ($P \leq 0.01$) in *S. aureus* biofilms compared to *E. coli* biofilms. The fluorescence of DAF-FM-stained *E. coli* and *S. aureus* biofilms challenged by PAW treatment was also significantly increased ($P \leq 0.0001$), but there was no significant difference in intracellular RNS accumulation between *E. coli* and *S. aureus* biofilm.

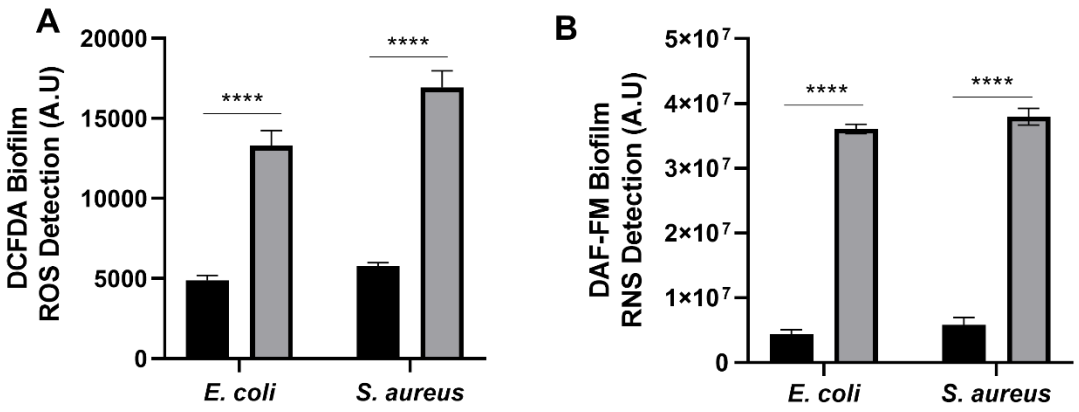

Figure 4.8 PAW induces the intracellular accumulation of ROS and RNS within bacterial (*E. coli* UTI89 and *S. aureus* NCTC8325) biofilm cells. (A) DCFDA staining assay and (B) DAF-FM staining assay was performed to detect the intracellular ROS and RNS under 15 min-PAW treatment (grey bar). Milli Q water was applied as the control (black bar). Data represents mean ± SEM, * (P<0.05), **(P<0.01), *(P<0.001), and ****(P<0.0001); n =3 biological replicates, with 3 technical replicates for each.**

4.5 Discussion

4.5.1 The viability of biofilm cells and biofilm biomass was significantly reduced by *in-situ* PAW treatment

The antibacterial efficacy of PAW varies among different bacterial strains. In this study, PAW was able to eradicate biofilm cells completely for both of *E. coli* and *S. aureus*. However, this process happened 2 min quicker in *S. aureus* than *E. coli*. Previous studies have indicated that Gram-negative bacteria (such as *E. coli* and *P. aeruginosa*) are generally less resistant to PAW treatments compared to Gram-positive bacteria (such as *Bacillus subtilis* and *Staphylococcus. epidermidis*) (Hozák et al., 2018; Mai-Prochnow et al., 2016; Ziuzina et al., 2015). However, non-selective activity of PAW on both *S. aure*us (Gram +) and *P. aeruginosa* (Gram -) has also been reported (Brun et al., 2018). In contrast to our findings, it has been observed that Gram-positive cells are more resistant to gaseous plasma treatment, likely due to the physical protection provided by the thicker peptidoglycan layer of

Gram-positive cells (Mai-Prochnow et al., 2021). The variations in antibacterial biofilm efficacy reported may be attributed to differences in the chemical reactive species present in PAW generated under different systems and the structural differences among bacterial cells.

Despite the absence of viable CFU cells of *E. coli* and *S. aureus* biofilms after 15 min-PAW treatment (Figure 2), approximately 50% of the biofilm biomass remained on the coupon surface. This suggests that while PAW treatment kills all biofilm cells, it may only remove a portion of the bacterial biofilm structure from the steel surface. Several studies have similarly found that the biofilm structure persists and biofilm biomass retained the same or even slightly increased after PAW treatment (Chen et al., 2017; Hozák et al., 2018). This phenomenon might be due to increased metabolic activities caused by a high concentration of NO_3^- in PAW used as nitrogen nutrition (Chen et al., 2017). Together, it could be hypothesized that the reactive stress from PAW may detach a portion of the biofilm biomass, exposing the biofilm cells, and allowing diffusion of reactive plasma species into biofilms through the protective matrix that then leads to the killing of the inner cells. However, the mechanisms of action of PAW on the bacterial biofilm EPS matrix remain unclear and warrant further investigation.

4.5.2 Antimicrobial mechanisms of PAW against bacterial biofilm

Mechanistically, the impact of PAW on the EPS matrix exhibits variability across different components. In this study, the interaction of PAW with the biofilm initiates the disruption of the extracellular polysaccharide structure, followed by the neutralization of extracellular proteins and removal of eDNA, weakening the biofilm structure and facilitating the release of planktonic cells (Mai-Prochnow et al., 2021). These released cells are subsequently more susceptible to the oxidative activity of PAW compared to the cells within biofilms (Fernández-Gómez et al., 2023). Regarding the remaining EPS matrix, the surplus RONS in PAW could further permeate the biofilm and react with biofilm cells (Chen et al., 2017). While the response of the EPS matrix of *E. coli* and *S. aureus* to PAW treatment was similar in this study, variations in the thickness, composition, and quantity of EPS may occur depending on the microorganism type, potentially influencing the efficacy of PAW inactivation.

PAW treatment involves physical dislodgement as well as flattening of the individual cells. These physical effects are likely due to the reactive oxygen species present in the PAW, with ROS known to disrupt the microbial membrane (Heema Kumari Nilesh et al., 2019; Rothwell et al., 2023). We have previously shown that within 1 min-PAW treatment, *E. coli* biofilm cell membranes are rapidly depolarised, and the outer membrane is significantly permeabilised (Vyas et al., 2023). Other research also found that the outer membrane of *S. aureus* cells was significantly damaged due to the oxidative stress created in cells during PAW treatment (Rathore et al., 2021a). However, as noted by Vyas et al., (2023) PAW that was applied post-generation did not physically remove biofilm, suggesting that the direct treatment utilised in this study has the additional benefits of physical forces that can weaken and disrupt biofilm structures. This highlights an advantage of direct treatment, as it may enhance biofilm susceptibility to subsequently applied antimicrobials (e.g., antiseptics, disinfectants).

The oxidative stress (ROS and RNS) created in cells during PAW results in cell death (Gunes et al., 2022). Plasma-induced membrane damage involves the cumulative impact of several long- and short-lived ROS, such as superoxide anion radicals, hydroxyl radicals, hydrogen peroxide, and ozone. These can act on membrane-associated proteins, further triggering oxidative stress within biofilm cells, and DNA damage within cells (Balcerczyk et al., 2005; Carpenter & Schoenfisch, 2012). We have previously shown that PAW generated with air (mixture of mostly nitrogen and oxygen, some argon) as an input gas source results in significant intracellular RONS accumulation for *E. coli* biofilms (Vyas et al., 2023), whilst ROS significantly predominate within biofilms treated with PAW that is generated with pure oxygen (Xia et al., 2023). Further studies should examine PAW generated with differing input gas sources (e.g., pure oxygen, nitrogen or argon) for their effects on intracellular RONS accumulation and how biofilm viability, biomass, and EPS may be impacted differently.

4.6 Conclusion

This study demonstrated that PAW treatment exhibits a generally non-selective inhibitory effect on pathogenic *S. aureus* NCTC8325 biofilms and *E. coli* UTI89 biofilms. The study also contributes novel insights into PAW's mechanisms of action, particularly its impact on the EPS matrix and the matrix components (i.e., exopolysaccharides, eDNA, and protein), enhanced membrane permeability

and depolarization, and intracellular RONS accumulation in both Gram-positive and Gram-negative biofilms. These findings highlight PAW's potential as a promising strategy for biofilm control across diverse microbial species. This is the first time a comparative and systematic investigation has been undertaken to uncover the anti-biofilm mechanisms of PAW against both Gram-positive and Gram-negative bacterial strains to in situ BSD-generated PAW treatment. Future research should extend this work by evaluating the efficacy of PAW against a broader range of species, including additional Gram-positive bacteria such as *Salmonella* and *Listeria*, as well as other Gram-negative pathogens like *Pseudomonas* and *Klebsiella*, particularly in the context of mixed-species biofilms. Moreover, further research into the specific interactions between PAW components and the EPS matrix will provide valuable insights for optimizing PAW-based treatments against biofilm-related challenges in antimicrobial development and water system decontamination.

4.7 Reference

Balcerczyk, A., Soszynski, M., & Bartosz, G. (2005). On the specificity of 4-amino-5-methylamino-2′,7′-difluorofluorescein as a probe for nitric oxide. *Free Radical Biology and Medicine, 39*(3), 327-335. https://doi.org/10.1016/j.freeradbiomed.2005.03.017

Billings, N., Birjiniuk, A., Samad, T. S., Doyle, P. S., & Ribbeck, K. (2015). Material properties of biofilms—a review of methods for understanding permeability and mechanics. *Reports on Progress in Physics, 78*(3), 036601. https://doi.org/10.1088/0034-4885/78/3/036601

Brun, P., Bernabè, G., Marchiori, C., Scarpa, M., Zuin, M., Cavazzana, R., Zaniol, B., & Martines, E. (2018). Antibacterial efficacy and mechanisms of action of low power atmospheric pressure cold plasma: membrane permeability, biofilm penetration and antimicrobial sensitization. *Journal of Applied Microbiology, 125*(2), 398-408. https://doi.org/10.1111/jam.13780

Buttress, J. A., Halte, M., te Winkel, J. D., Erhardt, M., Popp, P. F., & Strahl, H. (2022). A guide for membrane potential measurements in Gram-negative bacteria using voltage-sensitive dyes. *Microbiology, 168*(9). https://doi.org/https://doi.org/10.1099/mic.0.001227

Cámara, M., Green, W., MacPhee, C. E., Rakowska, P. D., Raval, R., Richardson, M. C., Slater-Jefferies, J., Steventon, K., & Webb, J. S. (2022). Economic significance of biofilms: a multidisciplinary and cross-sectoral challenge. *npj Biofilms and Microbiomes, 8*(1), 42. https://doi.org/10.1038/s41522-022-00306-y

Campoccia, D., Montanaro, L., & Arciola, C. R. (2021). Extracellular DNA (eDNA). A Major Ubiquitous Element of the Bacterial Biofilm Architecture. *International journal of molecular sciences, 22*(16), 9100. https://doi.org/10.3390/ijms22169100

Carpenter, A. W., & Schoenfisch, M. H. (2012). Nitric oxide release: Part II. Therapeutic applications. *Chemical Society Reviews, 41*(10), 3742-3752. https://www.ncbi.nlm.nih.gov/pmc/articles/PMC3341526/pdf/nihms-352469.pdf

Carrascosa, C., Raheem, D., Ramos, F., Saraiva, A., & Raposo, A. (2021). Microbial Biofilms in the Food Industry—A Comprehensive Review. *International Journal of Environmental Research and Public Health, 18*(4), 2014. https://doi.org/10.3390/ijerph18042014

Chen, T.-P., Liang, J., & Su, T.-L. (2018). Plasma-activated water: antibacterial activity and artifacts? *Environmental Science and Pollution Research, 25*(27), 26699-26706. https://doi.org/10.1007/s11356-017-9169-0

Chen, T.-P., Su, T.-L., & Liang, J. (2017). Plasma-Activated Solutions for Bacteria and Biofilm Inactivation. *Current Bioactive Compounds, 13*(1), 59-65. https://doi.org/10.2174/1573407212666160609082945

Costa Oliveira, B. E., Cury, J. A., & Ricomini Filho, A. P. (2017). Biofilm extracellular polysaccharides degradation during starvation and enamel demineralization. *PLOS ONE, 12*(7), e0181168. https://doi.org/10.1371/journal.pone.0181168

da Cruz Nizer, W. S., Inkovskiy, V., Versey, Z., Strempel, N., Cassol, E., & Overhage, J. (2021). Oxidative Stress Response in Pseudomonas aeruginosa. *Pathogens, 10*(9), 1187. https://doi.org/10.3390/pathogens10091187

Danese, P. N., Pratt, L. A., & Kolter, R. (2000). Exopolysaccharide Production Is Required for Development of Escherichia coli K-12 Biofilm Architecture. *Journal of bacteriology, 182*(12), 3593-3596. https://doi.org/doi:10.1128/JB.182.12.3593-3596.2000

Dula, S., Ajayeoba, T. A., & Ijabadeniyi, O. A. (2021). Bacterial biofilm formation on stainless steel in the food processing environment and its health implications. *Folia Microbiologica, 66*(3), 293-302. https://doi.org/10.1007/s12223-021-00864-2

Fernández-Gómez, P., Cobo-Díaz, J. F., Oliveira, M., González-Raurich, M., Alvarez-Ordóñez, A., Prieto, M., Walsh, J. L., Sivertsvik, M., Noriega-Fernández, E., & López, M. (2023). Susceptibility and transcriptomic response to plasma-activated water of Listeria monocytogenes planktonic and sessile cells. *Food Microbiology, 113*, 104252. https://doi.org/10.1016/j.fm.2023.104252

Finnegan, M., Linley, E., Denyer, S. P., McDonnell, G., Simons, C., & Maillard, J.-Y. (2010). Mode of action of hydrogen peroxide and other oxidizing agents: differences between liquid and gas forms. *Journal of Antimicrobial Chemotherapy, 65*(10), 2108-2115. https://doi.org/10.1093/jac/dkq308

Flemming, H.-C., & Wingender, J. (2010). The biofilm matrix. *Nature reviews microbiology, 8*(9), 623-633. https://doi.org/10.1038/nrmicro2415

Gunes, S., He, Z., Tsoukou, E., Ng, S. W., Boehm, D., Pinheiro Lopes, B., Bourke, P., Malone, R., Cullen, P. J., Wang, W., & Curtin, J. (2022). Cell death induced in glioblastoma cells by Plasma-Activated-Liquids (PAL) is primarily mediated by membrane lipid peroxidation and not ROS influx. *PLOS ONE, 17*(9), e0274524. https://doi.org/10.1371/journal.pone.0274524

Guo, D., Liu, H., Zhou, L., Xie, J., & He, C. (2021). Plasma‐activated water production and its application in agriculture. *Journal of the Science of Food and Agriculture, 101*(12), 4891-4899. https://doi.org/10.1002/jsfa.11258

Guo, L., Yang, L., Qi, Y., Niyazi, G., Huang, L., Gou, L., Wang, Z., Zhang, L., Liu, D., Wang, X., Chen, H., & Kong, M. G. (2021). Cold Atmospheric-Pressure Plasma Caused Protein Damage in Methicillin-Resistant Staphylococcus aureus Cells in Biofilms. *Microorganisms, 9*(5), 1072. https://doi.org/10.3390/microorganisms9051072

Halder, S., Yadav, K. K., Sarkar, R., Mukherjee, S., Saha, P., Haldar, S., Karmakar, S., & Sen, T. (2015, 2015/11/04). Alteration of Zeta potential and membrane permeability in bacteria: a study with cationic agents. *SpringerPlus, 4*(1), 672. https://doi.org/10.1186/s40064-015-1476-7

Handorf, O., Pauker, V. I., Weihe, T., Schäfer, J., Freund, E., Schnabel, U., Bekeschus, S., Riedel, K., & Ehlbeck, J. (2021). Plasma-Treated Water Affects Listeria monocytogenes Vitality and Biofilm Structure. *Frontiers in Microbiology, 12*, 652481. https://doi.org/10.3389/fmicb.2021.652481

Horvat, M., Pannuri, A., Romeo, T., Dogsa, I., & Stopar, D. (2019). Viscoelastic response of Escherichia coli biofilms to genetically altered expression of extracellular matrix components [10.1039/C9SM00297A]. *Soft Matter, 15*(25), 5042-5051. https://doi.org/10.1039/C9SM00297A

Hozák, P., Scholtz, V., Khun, J., Mertová, D., Vaňková, E., & Julák, J. (2018, 2018/09/01). Further Contribution to the Chemistry of Plasma-Activated Water: Influence on Bacteria in Planktonic and Biofilm Forms. *Plasma Physics Reports, 44*(9), 799-804. https://doi.org/10.1134/S1063780X18090040

Jenns, K., Sassi, H. P., Zhou, R., Cullen, P. J., Carter, D., & Mai-Prochnow, A. (2022). Inactivation of foodborne viruses: Opportunities for cold atmospheric plasma. *Trends in food science & technology*. https://doi.org/10.1016/j.tifs.2022.04.006

Karygianni, L., Ren, Z., Koo, H., & Thurnheer, T. (2020). Biofilm Matrixome: Extracellular Components in Structured Microbial Communities. *Trends in microbiology, 28*(8), 668-681. https://doi.org/10.1016/j.tim.2020.03.016

Khosravian, N., Bogaerts, A., Huygh, S., Yusupov, M., & Neyts, E. C. (2014). How do plasma-generated OH radicals react with biofilm components? Insights from atomic scale simulations. *Biointerphases, 10*(2). https://doi.org/10.1116/1.4904339

Limoli, D. H., Jones, C. J., & Wozniak, D. J. (2015). Bacterial Extracellular Polysaccharides in Biofilm Formation and Function. *Microbiology Spectrum, 3*(3), 3.3.29. https://doi.org/doi:10.1128/microbiolspec.MB-0011-2014

Mai-Prochnow, A., Clauson, M., Hong, J., & Murphy, A. B. (2016). Gram positive and Gram negative bacteria differ in their sensitivity to cold plasma. *Scientific Reports, 6*(1), 38610. https://doi.org/10.1038/srep38610

Mai-Prochnow, A., Zhou, R., Zhang, T., Ostrikov, K. K., Mugunthan, S., Rice, S. A., & Cullen, P. J. (2021). Interactions of plasma-activated water with biofilms: inactivation, dispersal effects and mechanisms of action. *npj Biofilms and Microbiomes, 7*(1), 1-12. https://doi.org/10.1038/s41522-020-00180-6

Mingeot-Leclercq, M.-P., & Décout, J.-L. (2016). Bacterial lipid membranes as promising targets to fight antimicrobial resistance, molecular foundations and illustration through the renewal of aminoglycoside antibiotics and emergence of amphiphilic aminoglycosides [10.1039/C5MD00503E]. *MedChemComm, 7*(4), 586-611. https://doi.org/10.1039/C5MD00503E

Muhammad, A. I., Liao, X., Cullen, P. J., Liu, D., Xiang, Q., Wang, J., Chen, S., Ye, X., & Ding, T. (2018). Effects of nonthermal plasma technology on functional food components. *Comprehensive Reviews in Food Science and Food Safety, 17*(5), 1379-1394. https://doi.org/10.1111/1541-4337.12379

Nguyen, H. T., Nguyen, T. H., & Otto, M. (2020). The staphylococcal exopolysaccharide PIA–Biosynthesis and role in biofilm formation, colonization, and infection. *Computational and Structural Biotechnology Journal, 18*, 3324-3334. https://doi.org/10.1016/j.csbj.2020.10.027

Patange, A. D., Simpson, J. C., Curtin, J. F., Burgess, C. M., Cullen, P. J., & Tiwari, B. K. (2021, 2021/01/27). Inactivation efficacy of atmospheric air plasma and airborne acoustic ultrasound against bacterial biofilms. *Scientific Reports, 11*(1), 2346. https://doi.org/10.1038/s41598-021-81977-z

Rathore, V., Patel, D., Butani, S., & Nema, S. K. (2021). Investigation of Physicochemical Properties of Plasma Activated Water and its Bactericidal Efficacy. *Plasma Chemistry and Plasma Processing, 41*(3), 871-902. https://doi.org/10.1007/s11090-021-10161-y

Rothwell, J. G., Hong, J., Morrison, S. J., Vyas, H. K. N., Xia, B., Mai-Prochnow, A., McConchie, R., Phan-Thien, K.-Y., Cullen, P. J., & Carter, D. A. (2023). An Effective Sanitizer for Fresh Produce Production: In Situ Plasma-Activated Water Treatment Inactivates Pathogenic Bacteria and Maintains the Quality of Cucurbit Fruit. *Microbiology Spectrum, 11*(4), e00034-00023. https://doi.org/10.1128/spectrum.00034-23

Sharma, G., Sharma, S., Sharma, P., Chandola, D., Dang, S., Gupta, S., & Gabrani, R. (2016). Escherichia coli biofilm: development and therapeutic strategies. *Journal of Applied Microbiology, 121*(2), 309-319. https://doi.org/10.1111/jam.13078

Shineh, G., Mobaraki, M., Perves Bappy, M. J., & Mills, D. K. (2023). Biofilm Formation, and Related Impacts on Healthcare, Food Processing and Packaging, Industrial Manufacturing, Marine Industries, and Sanitation–A Review. *Applied Microbiology, 3*(3), 629-665. https://doi.org/10.3390/applmicrobiol3030044

Vyas, H. K., Proctor, E.-J., McArthur, J., Gorman, J., & Sanderson-Smith, M. (2019). Current understanding of Group A Streptococcal biofilms. *Current Drug Targets, 20*(9), 982-993. https://doi.org/10.2174/1389450120666190405095712

Vyas, H. K. N., Indraratna, A. D., Everest-Dass, A., Packer, N. H., De Oliveira, D. M. P., Ranson, M., McArthur, J. D., & Sanderson-Smith, M. L. (2020). Assessing the Role of Pharyngeal Cell

Surface Glycans in Group A Streptococcus Biofilm Formation. *Antibiotics, 9*(11), 775. https://www.mdpi.com/2079-6382/9/11/775

Vyas, H. K. N., Xia, B., Alam, D., Gracie, N. P., Rothwell, J. G., Rice, S. A., Carter, D., Cullen, P. J., & Mai-Prochnow, A. (2023). Plasma activated water as a pre-treatment strategy in the context of biofilm-infected chronic wounds. *Biofilm, 6*, 100154. https://doi.org/10.1016/j.bioflm.2023.100154

Wang, X., Preston, J. F., & Romeo, T. (2004). The pgaABCD Locus of Escherichia coli Promotes the Synthesis of a Polysaccharide Adhesin Required for Biofilm Formation. *Journal of bacteriology, 186*(9), 2724-2734. https://doi.org/10.1128/jb.186.9.2724-2734.2004

Xia, B., Vyas, H. K. N., Zhou, R., Zhang, T., Hong, J., Rothwell, J. G., Rice, S. A., Carter, D., Ostrikov, K., Cullen, P. J., & Mai-Prochnow, A. (2023). The importance of superoxide anion for Escherichia coli biofilm removal using plasma-activated water. *Journal of Environmental Chemical Engineering, 11*(3), 109977. https://doi.org/10.1016/j.jece.2023.109977

Zhou, R., Zhou, R., Wang, P., Xian, Y., Mai-Prochnow, A., Lu, X., Cullen, P. J., Ostrikov, K., & Bazaka, K. (2020). Plasma-activated water: generation, origin of reactive species and biological applications. *Journal of Physics D: Applied Physics, 53*(30), 303001. https://doi.org/10.1088/1361-6463/ab81cf

Ziuzina, D., Boehm, D., Patil, S., Cullen, P. J., & Bourke, P. (2015). Cold Plasma Inactivation of Bacterial Biofilms and Reduction of Quorum Sensing Regulated Virulence Factors. *PLOS ONE, 10*(9), e0138209. https://doi.org/10.1371/journal.pone.0138209

5 Chapter 5 Proteomic analysis of pathogenic *Escherichia coli* and *Staphylococcus aureus* biofilms subjected to *in-situ* plasma activated water treatment

5.1 Abstract

Plasma-activated water (PAW), a new technology, has shown promise in killing both biofilm and non-biofilm bacteria due to its mix of reactive oxygen and nitrogen species (RONS). However, the specific proteomic mechanisms behind PAW's effectiveness, especially against biofilms, are not yet fully understood. Here, we examine *Escherichia coli* UTI89 biofilm and *Staphylococcus aureus* NCTC 8325 proteomic stress responses to direct 1 min PAW treatment and 5 min PAW treatment. A marked variation in protein regulation was observed of 5 min PAW treated biofilms when compared to 1 min PAW treatment and controls. Specifically, 5 min PAW treatment resulted in 78 upregulated genes (> 1.5 log2FC) in E. coli biofilm and 59 upregulated genes (> -1.5 log2FC) in S. aureus biofilm compared to control. Biological process enrichment analysis revealed significant upregulation of revealed i) cell adhesion, ii) negative regulation of translational elongation, iii) pilus, and iv) dimethyl sulfoxide reductase complex for *E. coli* biofilms treated with PAW compared to control, and metal ion binding and hydrolase activity for *S. aureus* biofilms treated with PAW compared to control. This study gives a detailed insight into how *E. coli* biofilms and *S. aureus* biofilms respond to stress induced by PAW via protein perspective. Overall, our findings shed light on the specific genes and pathways that help *E. coli* biofilms and *S. aureus* biofilms survive and respond to PAW treatment, offering a new understanding of plasma technology and its anti-biofilm mechanisms.

5.2 Introduction

Biofilms are complex microbial communities embedded within an extracellular polymeric substance (EPS) matrix that serves as a protective barrier, facilitating bacterial survival under hostile conditions. The EPS matrix is primarily composed of polysaccharides, proteins, lipids, and extracellular DNA, all of which play critical roles in biofilm formation, stability, and resistance to antimicrobial agents (McDougald et al., 2012). Among the components of the EPS matrix, proteins are of particular importance due to their involvement in cell-to-cell communication, structural integrity, and interactions with the environment (Flemming & Wingender, 2010). Proteins in the EPS matrix can also mediate adhesion to surfaces and the formation of microbial aggregates, contributing to the persistence and pathogenicity of biofilms (Sheng et al., 2010). As such, targeting these proteins within the EPS matrix is a promising strategy for disrupting biofilms and mitigating biofilm-associated infections.

Recent advancements in biofilm control have highlighted the potential of non-thermal plasmas, such as plasma-activated water (PAW), as effective antimicrobial agents. PAW, generated by exposing water to cold plasma, contains reactive oxygen and nitrogen species (RONS) such as hydrogen peroxide (H_2O_2), nitrate (NO_3-), and nitrite (NO_2-), which have been shown to exert strong bactericidal effects (Vyas et al., 2023; Xia et al., 2023)These reactive species are known to interact with various biomolecules, including proteins and lipids within the EPS matrix, leading to biofilm disruption. The effectiveness of PAW in biofilm removal is attributed to its ability to oxidize key components of the EPS, thereby weakening the structural integrity of the biofilm and enhancing the penetration of antimicrobial agents (Xu et al., 2020).

Studies have demonstrated the ability of PAW to reduce biofilm biomass and bacterial viability, particularly in pathogens such as Escherichia coli and Staphylococcus aureus. For instance, Xu et al.

(2020) observed that a 60 min treatment with PAW resulted in a significant reduction of biofilm formation by *S. aureus* achieving up to around 4.74-log reduction in viable cells. Furthermore, PAW was shown to inactivate *E. coli* O157:H7 grown on a stainless surface, which indicate a potential of real life application (Khan et al., 2016). These findings underscore the role of RONS in breaking down the EPS matrix and enhancing the accessibility of PAW to bacterial cells, contributing to its effectiveness in biofilm control.

Despite the promising results, the precise mechanisms by which PAW interacts with the EPS matrix remain an area of active investigation. Research has shown that PAW-induced oxidation of protein, polysaccharide and DNA components in the EPS matrix can lead to changes in biofilm architecture and a reduction in biofilm thickness (Khan et al., 2016). Additionally, the ability of PAW to modulate the levels of specific proteins involved in biofilm adhesion, such as outer membrane proteins (e.g., *OmpA* in *E. coli*), may further contribute to the disruption of biofilm integrity (Chowdhury et al., 2022). However, the full spectrum of interactions between PAW and the biofilm matrix, as well as the optimal conditions for its application, remains to be fully elucidated.

This study aims to investigate the effectiveness of PAW in biofilm removal and the role of PAW stress in modifying the EPS matrix, with a focus on protein-mediated interactions. Proteomics analysis will be applied to provide insights into understanding the molecular characteristics of bacteria, which contributes to developing useful strategies for controlling the pathogenic microbial biofilms. The effect of cold plasma on the proteomic profile of bacteria biofilms were addressed by some studies (L. Guo et al., 2021; Yau et al., 2018), but proteomic analysis of the response of them to bubble spark discharge (BSD) generated PAW treatments has not been described. This study aims to investigate the effects of PAW treatment on proteomic profile of *E. coli* UTI89 and *S. aureus* NCTC8325 biofilms, searching for possible mechanisms of biofilm removal and response to this treatment.

5.3 Methods

5.3.1 Bacterial strains and cultivation

Uropathogenic *Escherichia coli* UTI89 and pathogenic *Staphylococcus aureus* NCTC8325 were chosen as the Gram-negative and Gram-positive strains, respectively. *E. coli* and *S. aureus* were routinely cultured on Luria-Bertani (LB) agar, consisting of 10.0 g/L pancreatic digest of casein tryptone, 10.0 g/L sodium chloride, 5.0 g/L yeast extract, and 7.5 g/L agar powder. A single colony from a freshly streaked agar plate was inoculated into 5 mL of LB broth and incubated overnight at 37°C with agitation at 160 rpm. The *E. coli* UTI89 stain was from J. Moller-Jensen (University of Southern Denmark), with 5077 proteins identified in proteome (Chen et al., 2006). The *S. aureus* NCTC8325 strain was from NCTC, with 2889 proteins identified in proteome.

5.3.2 Biofilm formation

E. coli and *S. aureus* biofilms were formed on sterile stainless-steel coupons (Thickness = 3.8 mm, Diameter = 12.7mm; BioSurface Technologies, USA) placed in a 24-well plate. 1 mL of the diluted culture (~ $5x10^6$ CFU/mL) was inoculated into each well of the plate and then incubated for 48 hours at 37 °C without shaking to facilitate cell attachment and subsequent biofilm formation.

5.3.3 PAW generation and treatment

PAW was produced using a BSD reactor, following the procedure outlined in prior chapter 4. Even though PAW generated with O_2 showed the highest reduction of biofilms in Chapter 3, considering the balance of antibiofilm efficacy and the cost of real-life application, PAW generated with air was applied in this chapter. Briefly, the BSD reactor was immersed in 100 mL of sterile MilliQ water contained within a 250 mL Schott bottle, with coupons bearing attached biofilms (Figure 5.1). A high-voltage power source (Leap100, PlasmaLeap Technologies, Sydney) was utilized to discharge plasma into the water, employing an input voltage of 150 V, a discharge frequency of 1500 Hz, a resonance frequency of 60 kHz, and a duty cycle of 100 µs. Treatment durations ranged from 1 to 20 min with a compressed air gas flow of 1 standard liter per minute (slm). Coupons with biofilms were immersed in

100 mL of sterile MilliQ water and subjected to plasma treatment. As a control, coupons were submerged in 100 mL of sterile MilliQ water without plasma discharge.

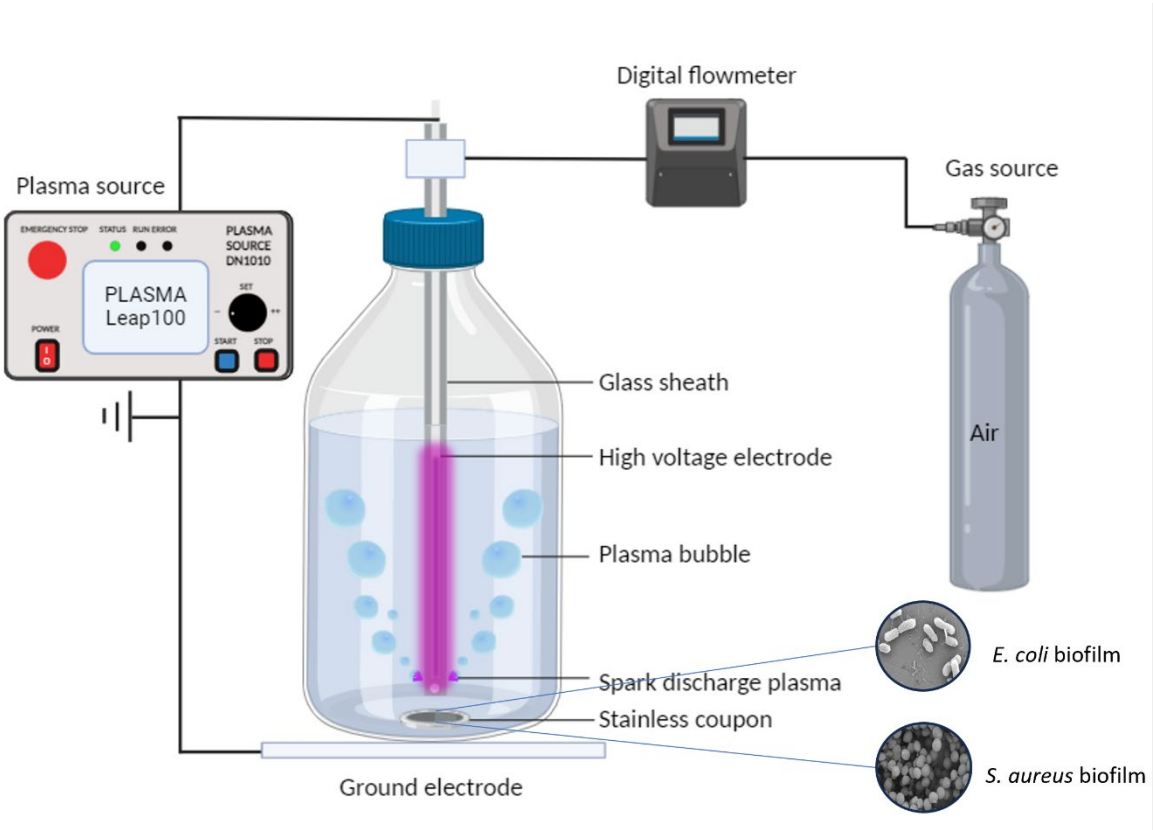

Figure 5.1 A schematic illustration of the in-situ biofilm treatment using plasma-activated water (PAW) generated by a bubble spark discharge (BSD) plasma reactor. *E. coli* UTI89 biofilm and *S. aureus* NCTC8325 biofilm were formed on stainless-steel coupons and positioned at the bottom of a Schott bottle containing 100 mL of MilliQ water. The BSD reactor comprises a high-voltage electrode and a glass sheath. To induce spark discharge plasma, a flow rate of 1 standard liter per minute (slm) of compressed air was utilized to bubble the water, while the high-voltage electrode was energized by the PlasmaLeap100 power source.

5.3.4 Biofilm cell viability

Immediately following the PAW treatment, coupons were retrieved from the treatment bottle and transferred into a Falcon tube containing 1 mL of 1x phosphate-buffered saline (PBS). The biofilm was detached from the coupon surface by gently scraping it with a sterile flat-end spatula. Subsequently, a 3 min water bath sonication at 45 kHz, followed by 10 s of vortexing, was employed to ensure complete dislodgment of biofilms. It is noteworthy that this procedure did not affect cell viability (data not shown). Serial dilutions were then drop-plated (10 µL) onto LB agar in triplicates. The plates were subsequently incubated overnight at 37 °C before determining the colony-forming units (CFU).

5.3.5 Quantitative proteomics of data-independent acquisition (DIA)

1min PAW treatment showed 1log reduction. To ensure sufficient protein samples for proteomic analysis, 5 individual samples under 1min and 5 min PAW-treated *E. coli* and *S. aureus* biofilm were collected to study the mechanism of PAW on protein perspective. The biofilm immersed in sterile water was used as the control group.

(1) Protein extraction and quantitation

PAW-treated biofilm cells were collected at 10,000 xg for 20 min at 4 °C. Then the supernatant was collected and added with 200 µL lysis buffer (containing 6 M urea, 2 M thiourea, and 100 mM HEPES at pH 7.5), followed by 10 s sonication with tip probe sonicator at 30% output with 10 s ice between sonication for triplicates. The cell debris were removed via 10 min centrifuge at 10,000xg, 4 °C. The supernatant was kept, and the protein was quantitated via BCA assay (Pierce™ BCA Protein Assay Kits, 23225) followed by the manufacture instruction.

(2) Protein digestion

The supernatant was kept and precipitated protein with 800 µL ice-cold acetone overnight at -30°C. The acetone was removed by 10 min centrifuge at 10,000 xg 4 °C, and the reasonable sized protein pellet was kept. The protein was resuspended in 100 µL of lysis buffer (6 M urea, 2 M thiourea, and 100 mM HEPES at pH 7.5), followed by 30 min reduction with 10 µL 100 mM DTT (10 mM DTT final conc.) and 30 min alkylation with 10 µL 250 mM IAA (25 mM IAA final conc.) in the dark.

The alkylated samples were performed qubit. Briefly, 30 µg of each sample were taken for digestion and made sample volume up to 63 µL. Samples were diluted by 4 volumes (252 µL) 100 mM HEPES at pH 7.5 followed by 16 h digestion at 37 °C shaking at 700 rpm on Thermomix with 1.2 µg trypsin (1:25 ratio; added 6 µL of trypsin resuspended at 20 µg in 100 µL 100 mM HEPES at pH 7.5). The samples were stored at 4 °C after digestion. Samples were then acidified with 10% TFA to 1 % final concentration (adding 31.5 µL 10% TFA) and centrifuged at 16,000x g for 5 min. A HLB was used to clean up the sample. In short, the HLB was equilibrated with 500 µL of pure methanol. Second equilibration was rinsed with 500 µL of pure acetonitrile. The HLB was then washed by 500 µL of 0.1% of TFA for three times. The washed HLB was then loaded with samples and further washed

with 500 µL of 0.1% of TFA for three times. After that, the samples were eluted with 200 µL of 50% ACN/0.1% TFA. The samples were dry to completion overnight.

(3) DIA and protein identification

Among LC-MS/MS-based quantitative proteomics strategies, data-independent acquisition (DIA) is a recent-developed technique that is believed to have the strengths of both high sensitivity, reproducibility and broad protein coverage (Li et al., 2021).

The dried samples were resuspended in 90 µL of 3% ACN and 1% FA followed by 5 min of vortex and bath sonication. 5 µL of samples were added into 195 µL of Qubit buffer followed by 5 min of centrifuge at 16,000 x g. Approx. 0.5 µg of peptide for each sample was transferred to a 96 well plate, and the volume was made up to 20 µL for each sample. 2 µL of sample (~50 ng) was injected into with a 90 min DIA method.

PD2.6 and Mascot 2.8 were used to analyzed the LC-MS/MS data for label-free quantitation. Peptides and proteins were accepted with a false discovery rate < 0.01. Identified proteins were filtered using at least 2 of the identified peptides. Data analysis and gene ontology (GO) analysis was performed on the PC Omoikane on Spectronaut version 19.0.240606.

5.3.6 Statistical analysis

Experiments were performed 3 times and values are expressed as mean ± standard error of mean ($\mu \pm \sigma_{\bar{x}}$). A parametric, One-way ANOVA (with Tukeys multiple comparisons test, $p<0.05$) was performed where appropriate to identify significant differences in log reduction of each sample compared to the control.

5.4 Results

5.4.1 PAW antibiofilm activities

Previous chapter has determined that 10 min PAW generated with air is rich in ROS, crucial for its antimicrobial effectiveness against biofilms. In this study, we examine the proteomic response of *E. coli* biofilms and *S. aureus* biofilms to PAW. 1 min of direct PAW treatment was deemed sub-lethal,

achieving around 1 log reduction of biofilm cell death compared to the MQ control (Figure 5.2 and Figure 5.3). Biofilms treated for 5 min with PAW achieved around 50% of both of the *E. coli* biofilm and *S. aureus* biofilm cell death.

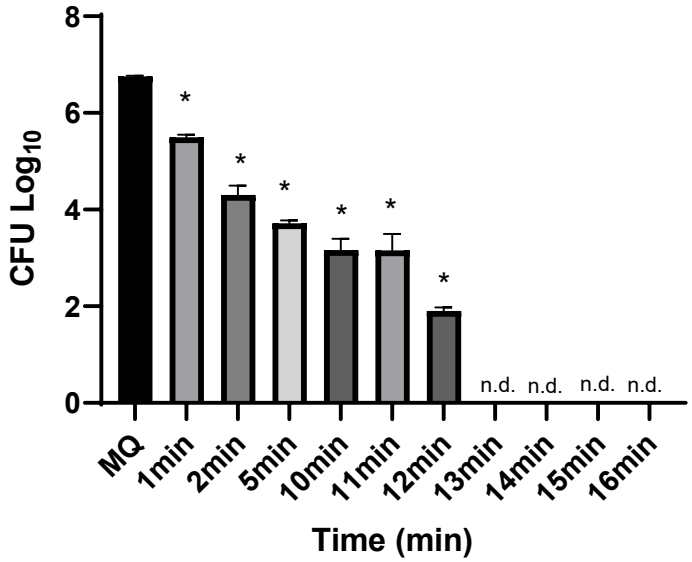

Figure 5.2 E. coli biofilm viability under 1-16 min direct PAW treatment compared to MQ control. Data represents mean ± SEM, *(P < 0.05); n = 3 biological replicates, with 2 technical replicates each.

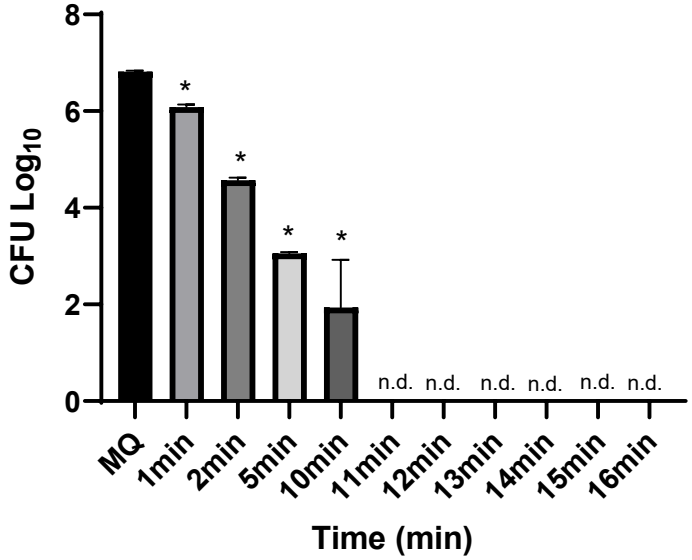

Figure 5.3 S. aureus biofilm viability under 1-16 min in direct PAW treatment compared to MQ control. Data represents mean ± SEM, *(P < 0.05); n = 3 biological replicates, with 2 technical replicates each.

5.4.2 Protein differentiation on the PAW-treated biofilm cells

Analysis revealed only a few difference in protein expression in *E. coli* (Figure 5.4) and *S. aureus* (Figure 5.5) biofilms formed on steel surfaces when exposed direct to 5 min PAW treatment as depicted by volcano plot. 5 min PAW treatment resulted in 78 upregulated proteins (> 1.5 log2FC) and 47 downregulated proteins (< -1.5 log2FC) compared to MQ control treated *E. coli* biofilm cells, while 92 upregulated proteins (> 1.5 log2FC) and 54 downregulated proteins (< -1.5 log2FC) compared to 1 min PAW treated *E. coli* biofilm cells (Figure 5.4). 5 min PAW treatment also resulted in 59 upregulated protein (> 1.5 log2FC) and 50 downregulated genes (< -1.5 log2FC) compared to MQ control treated *E. coli* biofilm cells, while 53 upregulated protein (> 1.5 log2FC) and 30 downregulated genes (< -1.5 log2FC) compared to 1 min PAW treated *E. coli* biofilm cells (Figure 5.4). While 1 min PAW treatment resulted in a relatively fewer regulation in protein expression on both of *E. coli* biofilm and *S. aureus* biofilm.

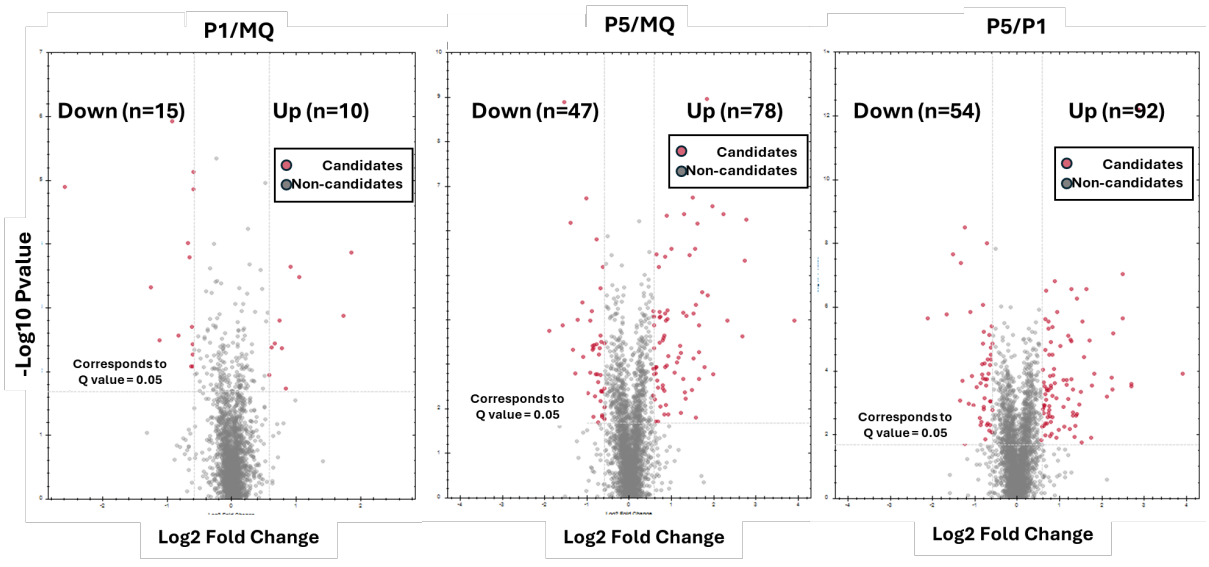

Figure 5.4 Differential protein expression analysis of *E. coli* biofilm during 1 min and 5 min direct treatment with PAW and bubbling MQ water. Volcano plot compared to 1min PAW and control bubble, 5 min PAW and control bubble, 1min PAW and 5 min PAW. The log-fold (base 2) change is plotted on the x-axis and the negative log of P-value (base 10) is plotted on the y-axis. Data shows individual Log FC changes in expression between pooled *E. coli* biofilms (each comprising 3 pooled replicates). Up- and down- regulated proteins are represented by red circles, while non-significant proteins are represented by grey circles.

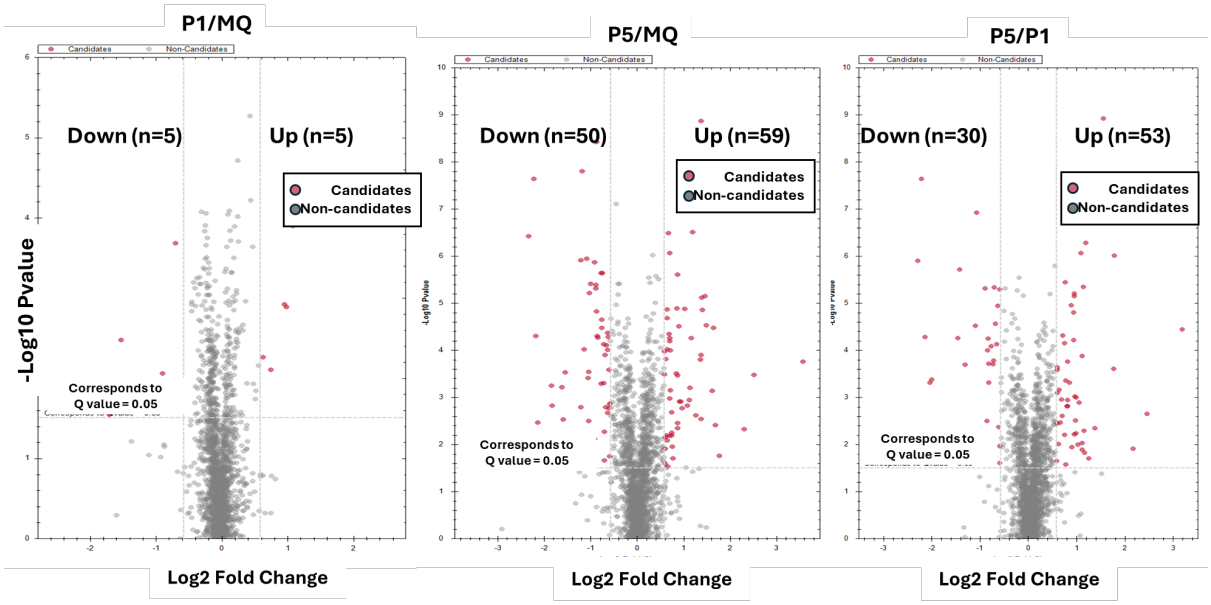

Figure 5.5 Differential protein expression analysis of *S. aureus* biofilm during 1 min and 5 min direct treatment with PAW and bubbling MQ water. Volcano plot compared to 1min PAW and control bubble, 5 min PAW and control bubble, 1min PAW and 5 min PAW. The log-fold (base 2) change is plotted on the x-axis and the negative log of P-value (base 10) is plotted on the y-axis. Data shows individual Log FC changes in expression between pooled *S. aureus* biofilms (each comprising 3 pooled replicates). Up- and down- regulated proteins are represented by red circles, while non-significant proteins are represented by grey circles.

5.4.3 GO enrichment analysis of the upregulated protein

Given that the *E. coli* and *S. aureus* biofilm viability data (Figure 5.2 and Figure 5.3), differential gene expression analysis (Figure 5.4 and Figure 5.5), and heatmap (Supporting Information) revealed a few regulations between PAW and MQ control, these were combined and used for comparison to PAW treatment in pathway enrichment and biological process enrichment analysis (Figure 5.6 and Figure 5.7).

In *E. coli* biofilms treated with 5-min PAW vs control (MQ) (Figure 5.6), cell adhesion involved in single-species biofilm formation (GO ID: 0043709) rich factor (0.62) was the highest compared to any other pathway. Similarly, genes involved in negative regulation of translational elongation/pilus/dimethyl sulfoxide reductase complex were relatively upregulated (fold enrichment values ranging 0.05-0.16). Notably, in *E. coli* biofilms treated 5-min PAW vs 1-min PAW, the defence response to bacterium (GO ID: 0042742) also shows a high upregulated enrichment.

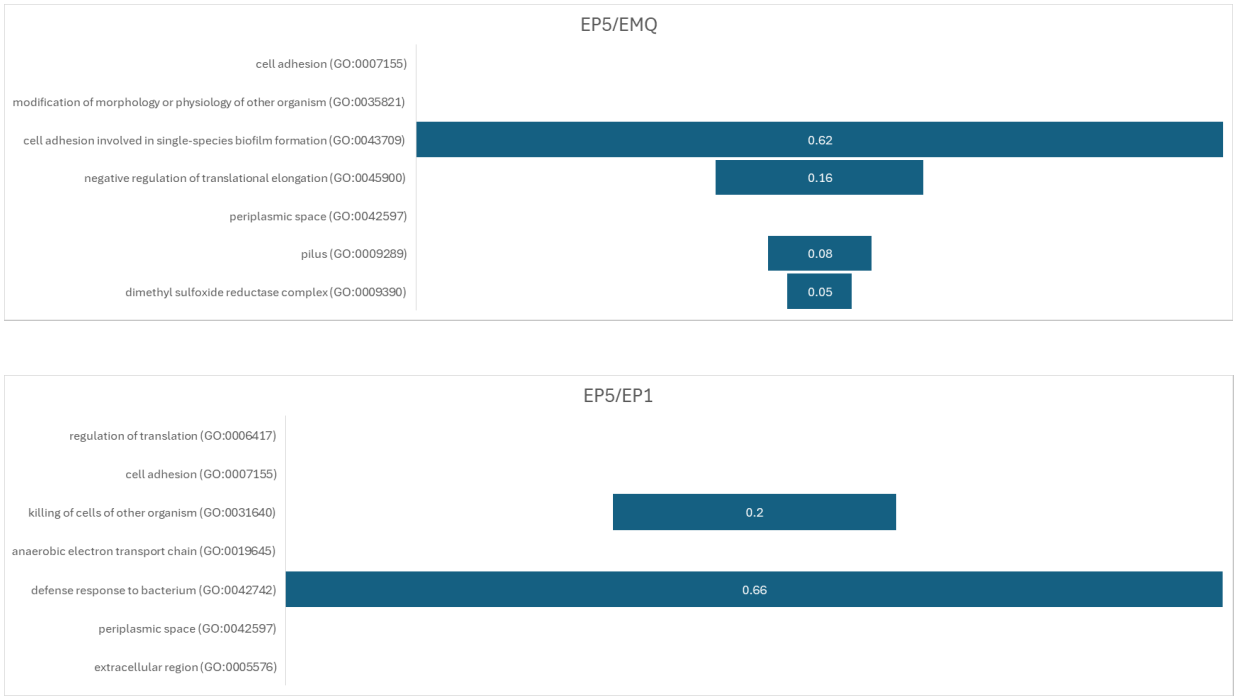

Figure 5.6 GO enrichment analysis of the upregulated differentially expressed genes of PAW-treated *E. coli*. The top GO terms annotated in the biological process category for the upregulated genes are selected based on their dispensability values. Color bar representing dispensability ratio. EP5 represents *E. coli* under 5 min PAW treatment group; EP1 represents *E. coli* under 1 min PAW treatment group; and EMQ represents *E. coli* under MQ control group.

Unlike the active upregulation pathway, the upregulation pathway of *S. aureus* showed only a few changes via GO enrichment. The highest enrichment occurs in metal ion binding (GO ID: 0046872) when 5-min PAW treated *S. aureus* compared to control, as well as 5-min PAW treated *S. aureus* compared to 1-min PAW treated *S. aureus* (rich factor: 0.26) (Figure 5.7). A hydrolase activity (GO ID: 0016787) was also observed under GO enrichment when 5-min PAW vs 1-min PAW.

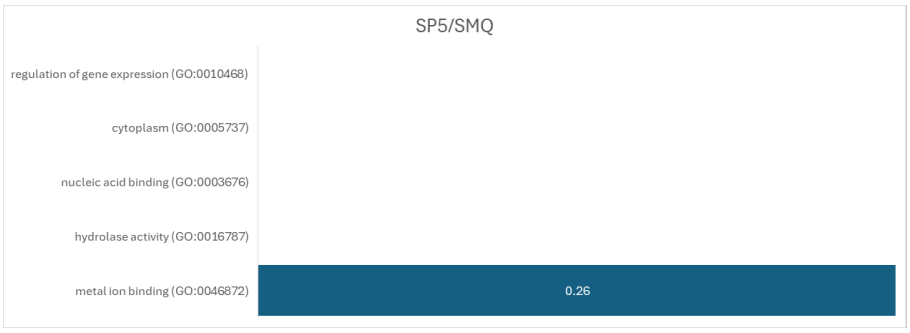

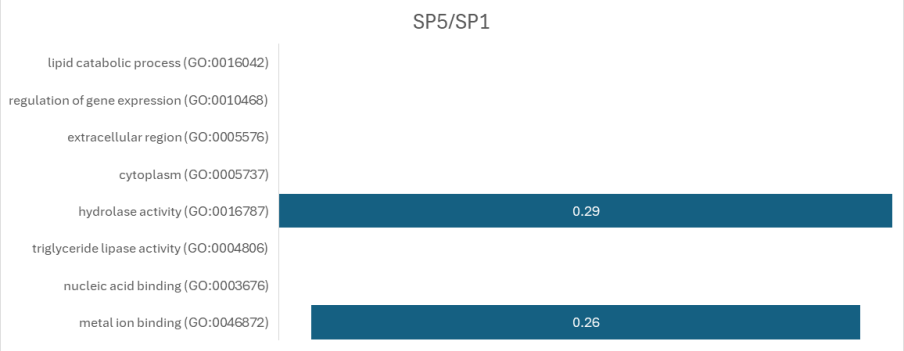

Figure 5.7 GO enrichment analysis of the upregulated differentially expressed genes of PAW treated *S. aureus*. The top GO terms annotated in the biological process category for the upregulated genes are selected based on their dispensability values. Color bar representing dispensability ratio. SP5 represents *S. aureus* under 5 min PAW treatment group; SP1 represents *S. aureus* under 1 min PAW treatment group; and SMQ represents *S. aureus* under MQ control group.

5.5 Discussion

In this study, we show that a 1 min direct PAW treatment is a sub-lethal dose and reduces biofilm viability by 1-log reduction and 5 min direct PAW induced 50% reduction of biofilm viability of both of *E. coli* and *S. aureus*. PAW's highly oxidising environment, rich in potent ROS can cause disastrous biological effects on microbial membranes, lipids, enzymes, proteins, and nucleic acids(Patange et al., 2019). As found in Chapter 3 and Chapter 4, superoxide (and its by-products hydrogen peroxide and hydroxyl radicals) cause membrane disruption leading to an increase of intracellular ROS levels. Other research found PAW treatment is able to reduce quorum sensing related virulence genes expression in *E. faecalis* biofilm development (Li et al., 2019), reduce the gene expression of early stage of biofilm formation (*csgD*, *agfA*, *fimA*, *lpfE*, and *rpoS*) in *S. enteritidis* planktonic cells (Basiri et al., 2023), inhibit the activities of antioxidant enzymes including superoxide dismutase (SOD), catalase (CAT), and nitrite reductase (NiR) of *P. aeruginosa* (Cai et al., 2025). However, the finding of regulated protein is very limited.

Our proteomic analysis revealed i) cell adhesion, ii) negative regulation of translational elongation, iii) pilus, and iv) dimethyl sulfoxide reductase complex as some of the major pathways to be significantly upregulated for *E. coli* biofilm cells exposed to 5 min direct PAW treatment. While for *S. aureus* biofilm, the major pathways to be upregulated is metal ion binding and hydrolase activity. Gene *OmpA* has been recognized as a highly conserved and immunogenic antigen, playing a crucial

role in the adhesion phenotype of *E. coli* O157:H7 and promoting bacterial aggregation (Monteiro et al., 2023), due to the genes *ompA*, *ompC*, *ompD*, and *ompF*, is responsible for encoding porins on the outer membrane(Chowdhury et al., 2022). A recent study found PAW stress can upregulated the expression of *OmpA* in *Salmonella Newport* (Sun et al., 2024), which is corresponding to our finding.

5.6 Conclusion

This study presents, for the first time, new insights into PAW's mechanisms of action. Providing novel knowledge of the proteomic stress responses *E. coli* biofilms and *S. aureus* biofilm under BSD-generated PAW stress conditions. Within just 1 min direct PAW treatment, biofilm viability is significantly decreased. In 5 min direct PAW treatment, a complex cellular response is prompted by upregulating 78 proteins and 59 proteins for *E. coli* and *S. aureus* biofilms, respectively. These results underscore PAW's utility as an anti-biofilm agent. Further work is warranted to better understand long-term effects over multiple generations of *E. coli* and *S. aureus* biofilm bacteria.

5.7 Supporting information

5.7.1 Cell sample protein quantification and SDS page gel blotting

The bacterial pellets were resuspended in lysis buffer (50 mM Tris-HCl, 150 mM NaCl, 1% Triton X-100, pH 8.0) supplemented with protease inhibitors (e.g., PMSF, EDTA). The suspension was incubated on ice for 30 minutes, followed by sonication (3 cycles of 30 seconds with a 30-second rest) to break the cells. The lysates were clarified by centrifugation at 12,000 × g for 15 minutes at 4°C, and the supernatant was collected for protein analysis. Protein concentration was determined using the Bradford assay (Bio-Rad, Hercules, CA, USA) following the manufacturer's instructions. Bovine serum albumin (BSA) was used as a standard.

The protein samples were mixed with 2× SDS-PAGE loading buffer (containing 100 mM Tris-HCl, pH 6.8, 200 mM DTT, 4% SDS, 0.2% bromophenol blue, 20% glycerol) and boiled at 95°C for 5 minutes to denature the proteins. Equal amounts of protein (15 uL per lane, equal to approximately 10 ug) were loaded onto a 12% SDS-PAGE gel. Equal amount of protein ladder was loaded as control (PageRuler™ Prestained Protein Ladder, 10 to 180 kDa, 26616). Electrophoresis was performed at

120 V for 90 minutes in running buffer (25 mM Tris, 192 mM glycine, 0.1% SDS) until the dye front reached the bottom of the gel. The gel was stained with Coomassie Brilliant Blue R-250 or silver stain for protein visualization if required. Protein bands were detected using Bio-rad universal hood imaging system according to the manufacturer's instructions.

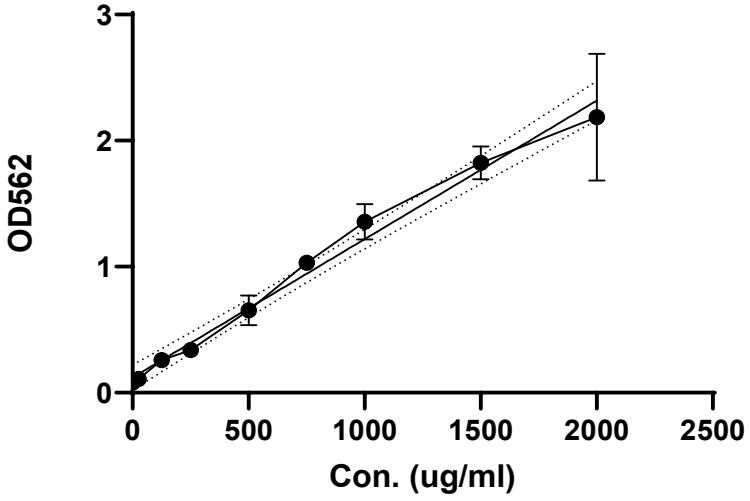

Figure S5.1 BCA standard curve of BSA.

Table S5.1 Protein quantification via BCA assya of E. coli and S. aureus biofilm cells after PAW treatment.

Bacteria strain	Treatment*	Mass of protein/μg†	No. coupon‡
***E. coli* UTI89**	Control	50.23±0.11	12
	PAW-1	74.31±4.01	12
	PAW-5	27.56±1.38	24
***S. aureus* NCTC8325**	Control	44.53±3.07	12
	PAW-1	78.16±1.99	12
	PAW-5	54.04±18.45	24

*Treatment of control is MQ treatment without any plasma discharge; PAW-1 is *In-situ* PAW treatment of 1 min; PAW-5 is *In-situ* PAW treatment of 5 min.

†Mass of protein is quantified by BCA assay (n=3, standard error of mean).

‡The no. of coupon is the no. of samples that combinates to concentrate more protein.

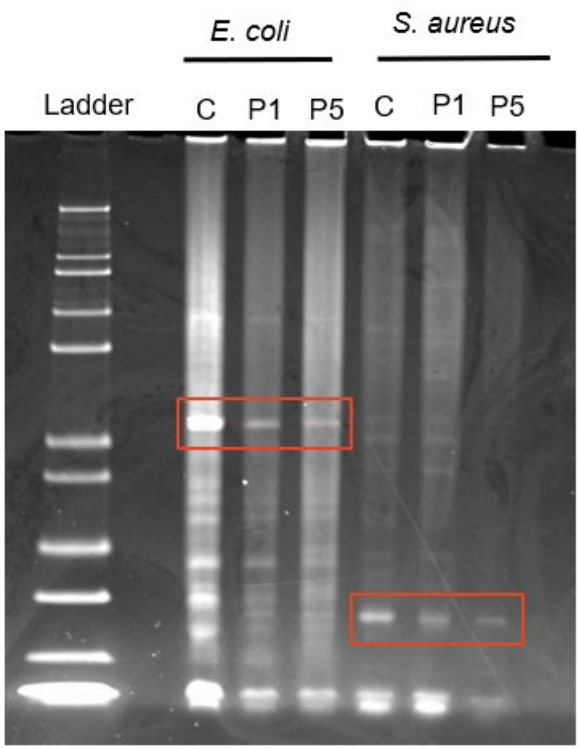

Figure S5.2 SDS page gel blotting image of lysed *E. coli* and *S. aureus*. Treatment of C is MQ treatment without any plasma discharge; P1 is In-situ PAW treatment of 1 min; P5 is In-situ PAW treatment of 5 min.

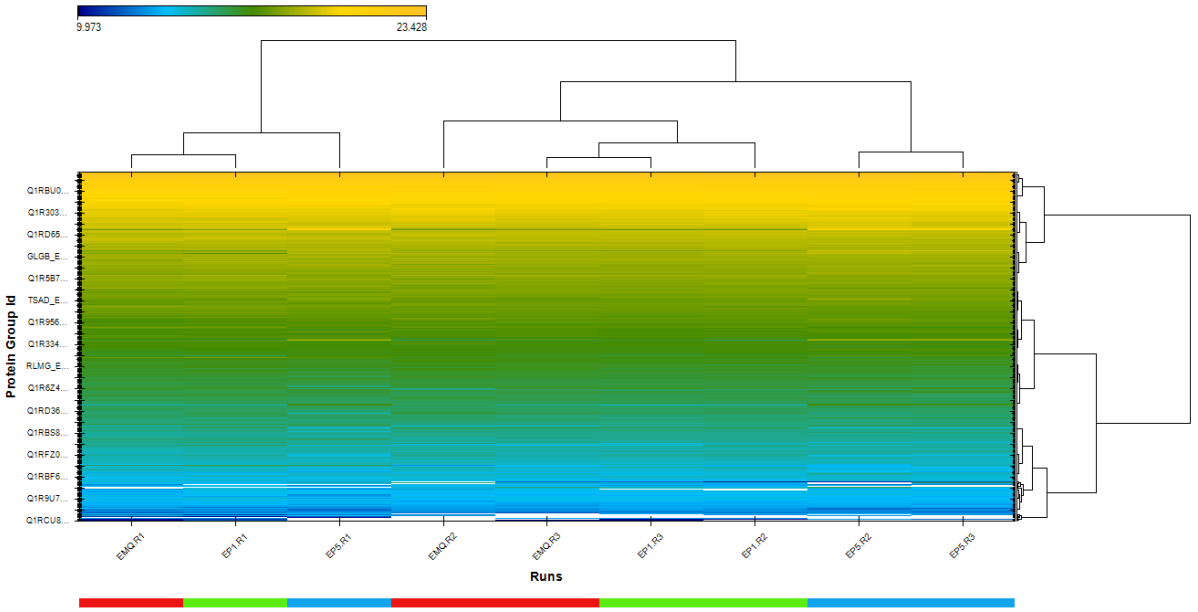

Figure S5.3 Heatmap of LCMS data showing all differentially expressed proteins in *E. coli* biofilms treated with PAW vs MQ control. Data represents mean-centred log2 transformed expression values measured in RPKM units.

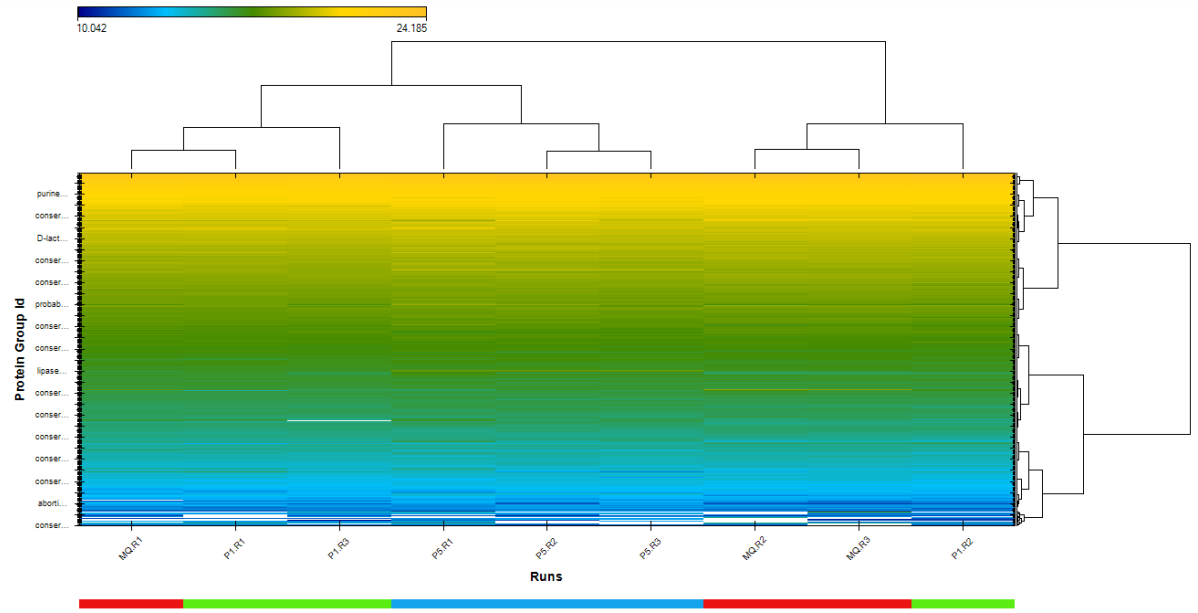

Figure S5.4 Heatmap of LCMS data showing all differentially expressed proteins in *S. aureus* biofilms treated with PAW vs MQ control. Data represents mean-centred log2 transformed expression values measured in RPKM units.

5.8 Reference

Basiri, N., Zarei, M., Kargar, M., & Kafilzadeh, F. (2023). Effect of plasma-activated water on the biofilm-forming ability of Salmonella enterica serovar Enteritidis and expression of the related genes. *International Journal of Food Microbiology, 406*, 110419. https://doi.org/10.1016/j.ijfoodmicro.2023.110419

Cai, Z., Zhang, W., Liao, G., Huang, C., Wang, J., & Zhang, J. (2025). Inhibiting mechanism of Pseudomonas aeruginosa biofilm formation-An innovational reagent of plasma-activated lactic acid. *Journal of Water Process Engineering, 69*, 106613. https://doi.org/10.1016/j.jwpe.2024.106613

Chen, S. L., Hung, C.-S., Xu, J., Reigstad, C. S., Magrini, V., Sabo, A., Blasiar, D., Bieri, T., Meyer, R. R., Ozersky, P., Armstrong, J. R., Fulton, R. S., Latreille, J. P., Spieth, J., Hooton, T. M., Mardis, E. R., Hultgren, S. J., & Gordon, J. I. (2006). Identification of genes subject to positive selection in uropathogenic strains of Escherichia coli: A comparative genomics approach. *Proceedings of the National Academy of Sciences, 103*(15), 5977-5982. https://doi.org/doi:10.1073/pnas.0600938103

Chowdhury, A. R., Mukherjee, D., Singh, A. K., & Chakravortty, D. (2022). Loss of outer membrane protein A (OmpA) impairs the survival of Salmonella Typhimurium by inducing membrane damage in the presence of ceftazidime and meropenem. *Journal of Antimicrobial Chemotherapy, 77*(12), 3376-3389. https://doi.org/10.1093/jac/dkac327

Flemming, H.-C., & Wingender, J. (2010). The biofilm matrix. *Nature reviews microbiology, 8*(9), 623-633. https://doi.org/10.1038/nrmicro2415

Khan, M. S. I., Lee, E.-J., & Kim, Y.-J. (2016). A submerged dielectric barrier discharge plasma inactivation mechanism of biofilms produced by Escherichia coli O157: H7, Cronobacter sakazakii, and Staphylococcus aureus. *Scientific Reports, 6*(1), 37072. https://doi.org/10.1038/srep37072

Li, J., Smith, L. S., & Zhu, H.-J. (2021). Data-independent acquisition (DIA): An emerging proteomics technology for analysis of drug-metabolizing enzymes and transporters. *Drug Discovery Today: Technologies, 39*, 49-56. https://doi.org/10.1016/j.ddtec.2021.06.006

Li, Y., Pan, J., Wu, D., Tian, Y., Zhang, J., & Fang, J. (2019). Regulation of Enterococcus faecalis biofilm formation and quorum sensing related virulence factors with ultra-low dose reactive species produced by plasma activated water. *Plasma Chemistry and Plasma Processing, 39*, 35-49. https://doi.org/10.1007/s11090-018-9930-2

McDougald, D., Rice, S. A., Barraud, N., Steinberg, P. D., & Kjelleberg, S. (2012). Should we stay or should we go: mechanisms and ecological consequences for biofilm dispersal. *Nature reviews microbiology, 10*(1), 39-50. https://doi.org/10.1038/nrmicro2695

Monteiro, R., Chafsey, I., Caccia, N., Ageorges, V., Leroy, S., Viala, D., Hébraud, M., Livrelli, V., Pizza, M., & Pezzicoli, A. (2023). Specific Proteomic Identification of Collagen-Binding Proteins in Escherichia coli O157: H7: Characterisation of OmpA as a Potent Vaccine Antigen. *Cells, 12*(12), 1634. https://doi.org/10.3390/cells12121634

Patange, A., O'Byrne, C., Boehm, D., Cullen, P., Keener, K., & Bourke, P. (2019). The effect of atmospheric cold plasma on bacterial stress responses and virulence using Listeria monocytogenes knockout mutants. *Frontiers in Microbiology, 10*, 2841. https://doi.org/10.3389/fmicb.2019.02841

Sheng, G.-P., Yu, H.-Q., & Li, X.-Y. (2010). Extracellular polymeric substances (EPS) of microbial aggregates in biological wastewater treatment systems: a review. *Biotechnology advances, 28*(6), 882-894. https://doi.org/10.1016/j.biotechadv.2010.08.001

Sun, Y., Gao, R., Liao, X., Shen, M., Chen, X., Feng, J., & Ding, T. (2024). Stress response of Salmonella Newport with various sequence types toward plasma-activated water: Viable but nonculturable state formation and outer membrane vesicle production. *Current Research in Food Science, 8*, 100764. https://doi.org/10.1016/j.crfs.2024.100764

Vyas, H. K. N., Xia, B., Alam, D., Gracie, N. P., Rothwell, J. G., Rice, S. A., Carter, D., Cullen, P. J., & Mai-Prochnow, A. (2023). Plasma activated water as a pre-treatment strategy in the context of biofilm-infected chronic wounds. *Biofilm, 6*, 100154. https://doi.org/10.1016/j.bioflm.2023.100154

Xia, B., Vyas, H. K. N., Zhou, R., Zhang, T., Hong, J., Rothwell, J. G., Rice, S. A., Carter, D., Ostrikov, K., Cullen, P. J., & Mai-Prochnow, A. (2023). The importance of superoxide anion for Escherichia coli biofilm removal using plasma-activated water. *Journal of Environmental Chemical Engineering, 11*(3), 109977. https://doi.org/10.1016/j.jece.2023.109977

Xu, Z., Zhou, X., Yang, W., Zhang, Y., Ye, Z., Hu, S., Ye, C., Li, Y., Lan, Y., & Shen, J. (2020). In vitro antimicrobial effects and mechanism of air plasma‐activated water on Staphylococcus aureus biofilm. *Plasma Processes and Polymers, 17*(8), 1900270. https://doi.org/10.1002/ppap.201900270

6 Chapter 6 Conclusions and Future Directions

6.1 Overview and conclusions

The primary objective of this thesis is to investigate and improve the efficacy of biofilm removal with bubble spark discharge generated plasma-activated water. The PAW is a green method that only requires water, air gas, and electricity to reach the antibiofilm activity, which does not generate toxic residues. By addressing the specific aims outlined in the introduction and discussed in the following sections, the findings of this thesis may contribute to green and clean water treatment to help reduce the contamination of bacterial biofilm.

In chapter 2, we investigated and compared direct and indirect PAW treatment to Escherichia coli (ATCC 25922) biofilms, assessing cell viability, reactive oxygen and nitrogen species (RONS) levels, and PAW stability during storage. Results showed that a 10-minute direct PAW treatment using air was most effective in removing *E. coli* biofilms on stainless steel. PAW retained stable RONS levels, including H_2O_2, NO_3^-, and NO_2^-, for up to 24 hours at 4°C and continued to effectively inactivate biofilms post-storage. The findings emphasize the importance of optimizing PAW treatments to enhance biofilm removal in practical, real-world conditions.

Following this work, a more detailed investigation of directPAW on biofilm removal was undertaken in chapter 3. In this study, various PAWs were generated from argon, nitrogen, air, and oxygen using a plasma bubble spark discharge (BSD) reactor to treat *Escherichia coli* (ATCC 25922) biofilms. PAW-O_2 was found to be the most effective in completely removing biofilms on stainless steel surfaces. Confocal microscopy revealed that PAW treatment removed most biofilm cells, leaving only a few dead cells. Intracellular ROS levels significantly increased in PAW-O_2^-treated biofilms, and superoxide anion radicals ($\bullet O_2^-$) were identified as key contributors to biofilm inactivation. The study highlights the importance of optimizing input gases and plasma conditions to enhance biofilm removal efficiency.

In chapter 4, a detailed insight into antibiofilm mechanisms of PAW-O_2 was investigated to EPS matrix. This study evaluated the effectiveness of plasma-activated water (PAW) in inactivating *Escherichia coli* UTI89 and *Staphylococcus aureus* NCTC8325 biofilms. PAW was generated by discharging atmospheric pressure cold plasma into sterile distilled water. The treatment completely killed biofilm cells of both bacteria (6.76 ± 0.01 log CFU/mL for E. coli and 6.82 ± 0.02 log CFU/mL for S. aureus), with faster inactivation in *S. aureus*. PAW disrupted the biofilm structure, reducing biomass and EPS. The treatment increased membrane permeability and caused significant intracellular reactive oxygen and nitrogen species accumulation, demonstrating PAW's potential for biofilm control.

Last but not least, a further investigation was conducted on proteomic stress responses of *Escherichia coli* and *Staphylococcus aureus* biofilms to 1 min and 5 min plasma-activated water (PAW) treatments. The 5 min PAW treatment caused significant protein regulation changes, with 78 upregulated genes in *E. coli* and 59 in *S. aureus* compared to controls. Biological process enrichment analysis showed that *E. coli* biofilms upregulated genes related to cell adhesion, translational elongation, pilus formation, and dimethyl sulfoxide reductase complex, while S. aureus biofilms upregulated genes for metal ion binding and hydrolase activity. These findings provide insight into the genes and pathways involved in biofilm survival and stress response to PAW.

6.2 Future work

Despite the recent considerable progress in the development and optimization of PAW for biofilm removal, more fundamental issues should be addressed.

1. **Optimization of PAW Treatment Parameters for Biofilm Removal**

Future studies should focus on identifying the optimal parameters for PAW generation and application, including the effects of gas composition, treatment time, and storage conditions. Investigating the influence of different factors on the efficacy of PAW in biofilm removal will help to refine its use for various industrial and clinical applications.

2. Mechanistic Studies on Biofilm Disruption by PAW

Further research is needed to elucidate the specific mechanisms by which PAW disrupts biofilms. Understanding how reactive species, such as H_2O_2, NO_3-, and NO_2-, interact with the extracellular matrix and microbial cells will provide insights into the molecular targets and pathways responsible for biofilm inactivation.

3. Evaluation of PAW Efficacy Against Mixed-Species Biofilms

While many studies have focused on single-species biofilms, future work should investigate the effectiveness of PAW in removing mixed-species biofilms, which are more representative of real-world environments. This would include testing on biofilms formed by both pathogenic and non-pathogenic organisms to assess the broad-spectrum potential of PAW.

4. Long-Term Stability and Reusability of Stored PAW

Investigating the long-term stability of PAW's antimicrobial properties after multiple storage cycles is crucial for practical applications. Studies should focus on the potential for reusing stored PAW in multiple treatment rounds and its effectiveness over time, especially in large-scale industrial settings.

5. Integration of PAW with Other Biofilm Control Methods

Combining PAW with other biofilm control techniques, such as enzymatic treatments or conventional cleaning agents, could enhance its effectiveness and broaden its application scope. Future research should explore synergistic effects and the development of combined treatment strategies that can be implemented in medical and industrial settings to tackle biofilm-related issues more efficiently.